國立臺灣大學理學院物理學研究所

碩士論文

Department of Physics

College of Science

National Taiwan University

Master Thesis

以單光子方法量測 LYSO 光產率及其延伸研究

Measuring Light Yield of LYSO With Single Photon Method and Its Extended Study

陶鎮宇

Chen-Yu Tao

指導教授: 王名儒 教授

Advisor: Min-Zu Wang, Prof.

中華民國 112 年 6 月

June, 2023

doi:10.6342/NTU202300991

doi:10.6342/NTU202300991

國立臺灣大學碩士學位論文
口試委員會審定書

MASTER'S THESIS ACCEPTANCE CERTIFICATE
NATIONAL TAIWAN UNIVERSITY

以單光子方法量測 LYSO 光產率及其延伸研究

Measuring Light Yield of LYSO With Single Photon Method and Its Extended Study

本論文係陶鎮宇君(R09222024)在國立臺灣大學物理學研究所完成之碩士學位論文，於民國 112 年 6 月 5 日承下列考試委員審查通過及口試及格，特此證明。

The undersigned, appointed by the Department of Physics on 5 / 6 / 2023 have examined a Master's thesis entitled above presented by Chen-Yu Tao (R09222024) candidate and hereby certify that it is worthy of acceptance.

口試委員 Oral examination committee:

王名儒　　郭家銘

（指導教授 Advisor）

張壁祥　　徐靜戈

系主任/所長 Director:

doi:10.6342/NTU202300991

誌謝

在台大物理所的研究生涯中，我想首先感謝我所參與的 LYSO project 的三位指導老師：王名儒教授、呂榮祥教授、徐靜戈研究員。王名儒老師與呂榮祥老師在會議時能了解我的問題並提出研究方向，並且王名儒老師也在我需要時，作為指導教授提供許多實質的建議與幫助。徐靜戈老師會與我積極討論實驗細節，甚至有時親自參予實驗。老師們的指導，讓我得以完成一個渺小的學術研究並得到成果。

再來我想感謝的是一起共事的同學與研究助理。碩士畢業生郭晉嘉與碩士生沈昀臻皆有協助改善實驗架設或分析，並讓我在每次交流中可以逐步完善我的實驗結果。研究助理周建宏先生、劉建宏先生、籃德暐先生在儀器加工、網路、電子等方面給予很多技術協助。

然後是來自同實驗室學長們的提攜。博士後研究員黃坤賢與博士生陳昱潭是我剛開啟研究之路時的指引者，也在我研究遇到瓶頸時提供我經驗與可能解決方案。此外還有其他學長姐或同學們大大小小的關心，使我能在良好的實驗室氛圍下努力不懈。

最後要感謝的是我的父母，謝謝他們的耐心與支持，我才能堅持並完成我的碩士學業，為我的研究生涯畫上一個美好的句點。

doi:10.6342/NTU202300991

doi:10.6342/NTU202300991

Abstract

Lutetium-Yttrium Oxyorthosilicate, $Lu_{2(1-x)}Y_{2x}SiO_5 : Ce$, also called "LYSO", is one of the modern commonly used scintillation crystals. It offers several benefits compared to many common scintillation crystals, such as short attenuation length, fast decay time, non-hygroscopic, and comparable light yield. These benefits have advantages for the detection of 511 keV annihilation photons, so it is a good candidate for the photodetector in the positron emission tomography (PET) system.

To study the light yield of LYSO, we need to know the exact photon counting method. I use photomultiplier tube (PMT) as the light sensor and use light-emitting diode (LED) as the adjustable light source to calibrate the single photoelectron of PMT. I confirm the LYSO intrinsic spectrum and also use Sodium-22 as a radioactive source to study the light yield of LYSO for 511 keV incident photons. I also use my experience in single photoelectron calibration to conduct an extended study of polarized single photon.

With these results so far, we know the combination of a controllable light source and light sensor can quickly test single photoelectron. This is very useful for future scientific research, such as the calibration of arbitrary light amounts and the manufacture of single photon sources with different requirements.

Keywords: Single Photon, Scintillator, LYSO, Light Yield, Polarization

doi:10.6342/NTU202300991

doi:10.6342/NTU202300991

摘要

Lutetium-Yttrium Oxyorthosilicate，$Lu_{2(1-x)}Y_{2x}SiO_5:Ce$，又稱"LYSO"，是現代常用的閃爍體之一。與其他常見的閃爍晶體相比，它具有多項優勢，例如短衰減距離、快速衰減時間、非吸濕性和良好的光產率。這些優點對於檢測 511 keV 湮滅光子具有優勢，因此成為正電子發射斷層掃描（PET）系統中光電探測的良好候選者。

為了研究 LYSO 的光產率，我們需要知道準確的光量計算方法。我使用光電倍增管（PMT）作為光感測器，並使用發光二極管（LED）作為可調整光源校准 PMT 的單光電子。我檢查了 LYSO 的本徵光譜，並以鈉 22 為放射源來研究 LYSO 對 511 keV 入射光子的光產率。我還利用在單光電子校正實驗中的經驗，對偏振單光子進行延伸研究。

到目前為止，我們根據這些結果知道可控光源和適當光感測器的組合可以快速測試單個光電子。這對以後的科學研究非常有用，比如任意光量的校正，以及製造不同要求下的單光子源。

關鍵字：單光子、閃爍體、LYSO、光產率、偏振

doi:10.6342/NTU202300991

doi:10.6342/NTU202300991

Contents

doi:10.6342/NTU202300991

doi:10.6342/NTU202300991

doi:10.6342/NTU202300991

doi:10.6342/NTU202300991

List of Figures

doi:10.6342/NTU202300991

doi:10.6342/NTU202300991

doi:10.6342/NTU202300991

doi:10.6342/NTU202300991

doi:10.6342/NTU202300991

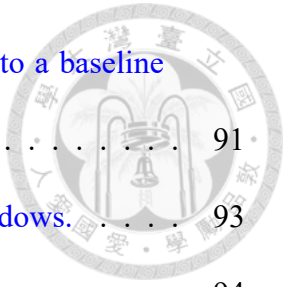

doi:10.6342/NTU202300991

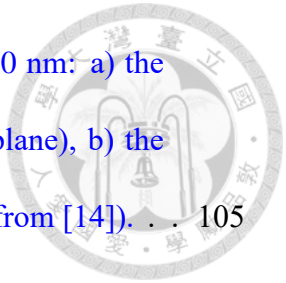

doi:10.6342/NTU202300991

doi:10.6342/NTU202300991

List of Tables

doi:10.6342/NTU202300991

doi:10.6342/NTU202300991

Chapter 1

Introduction

1.1 Inorganic scintillator

Scintillators can convert radiation such as gamma-ray to scintillation lights that are visible or near visible. It is often coupled to photodetectors to achieve radiation study, which is to convert the outcoming light from scintillator to electrical signals. According to the scintillator material, it can be divided into two categories: organic and inorganic, and their principles are completely different. Since the scintillator we want to study, LYSO, is an inorganic scintillator, the following will briefly introduce the scintillation mechanism of the inorganic scintillator.

The scintillation mechanism depends on the structure of the crystal lattice [1]. In pure crystal, the absorption of energy can elevate electrons from the valence band to the conduction band (Fig. 1.1(a)). However, the return of an electron to valence band with the emission of a photon is an inefficient process, and also the band gap widths in pure crystals make the resulting emitted photon energies too high to lie within the visible range. Therefore, small amounts of impurities, called activators, are added to the crystal. They

doi:10.6342/NTU202300991

create special sites in the lattice at which the band gap structure (Fig. 1.1(b)), so the photons emitted by the electron transitions from upper to lower activator states will be lower energy. That makes the light emission spectrum to be shifted to the visible light range. The timing of the light output is dependent on the half-lifetime of these states, which typical lifetimes of such excited states are at the order of 30 to 500 ns.

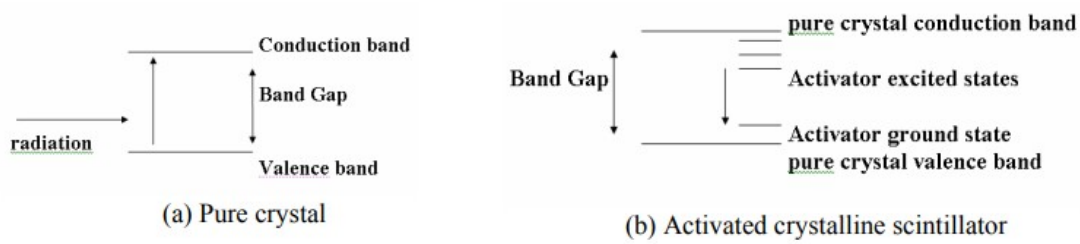

Figure 1.1: The energy band structure of a pure crystal and an activated crystalline scintillator [1].

1.2 LYSO and its intrinsic spectrum

LYSO is a scintillation crystal that has physical properties including comparable light output (about 30 number of photons per keV), fast decay time (about 40 ns), and short attenuation length (about 1.2 cm at 511 keV). It is a convenient scintillator for the detection of 511 keV annihilation photons and is widely used in positron emission imaging systems to become photodetectors (Append. A.1).

In addition to being excited by external radioactive sources, LYSO also has self-radiation and its intrinsic radioactive spectrum [2]. Natural lutetium contains about 2.6% of ^{176}Lu, which decays by beta-emission followed by one or more prompt gamma-ray emissions with different associated probabilities to the excited states of ^{176}Hf (Fig. 1.2). The beta spectrum here is simplified and the peak is close to zero due to the Coulomb

doi:10.6342/NTU202300991

attraction between the emitted electrons and heavy nucleus. The simultaneous combinations of beta-particle and gamma-ray self-detection in the crystal makes LYSO intrinsic spectrum characteristic that the beta-particle energy spectrum of ^{176}Lu is shifted from zero to the corresponding gamma-ray energy value, and the probability of each energy combinations is associated with the size of the crystal [2]. This intrinsic spectrum can be used to study light yield, while it is also a constant neutral background signal to affect the energy spectrum of the external radioactive source with similar activity levels.

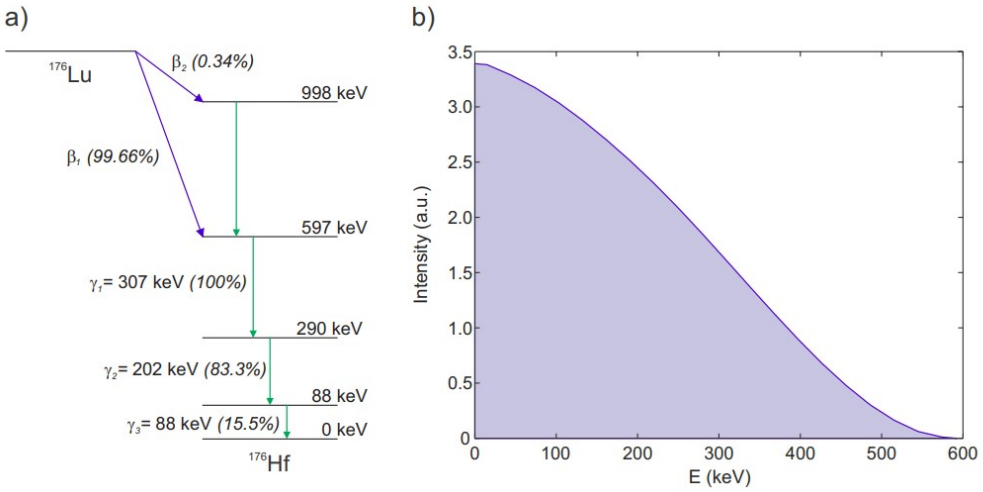

Figure 1.2: The simplified ^{176}Lu decay scheme and beta-particle energy spectrum (from [2]).

1.3 From the single photon measurement to the extension

To study the light yield of LYSO, we choose to study the absolute light output in the number of photons, which means I need to carry out the single photon method. I use PMT as the light sensor to observe different light level results produced by LED, and through the spectrum to PMT to obtain single photoelectron.

In Chap. 2, I explain the structure and working principle of PMT, its physics pro-

doi:10.6342/NTU202300991

cesses, response, and how to get the single photoelectron and high voltage factor by approximate models finally. In Chap. 3, I conduct the LED calibration study, including each component and their details in setup, and the calibration results under different light level intensities. In Chap. 4, I introduce light yield measurement setup, LYSO intrinsic spectrum, radioactive source Sodium-22 spectrum, systematic studies, and finally the standard process to measure the light yield of our LYSO sample. In Chap. 5, I combine polarizers with PMT and LED and show an extension study of polarized single photon.

doi:10.6342/NTU202300991

Chapter 2

Photon counting by PMT

2.1 Introduction

The normal light sensor is not useful for scintillation counting because the scintillation light intensity, usually $10^3 \sim 10^4$ photons, is too weak to convert the scintillation light pulse into a usable electrical signal by the normal light sensor. PMT can convert low light intensity into a usable current pulse without adding a large amount of random noise to the electrical signal. This feature allows us to study light yield in the number of photons.

In this Chapter, I start with the structure of a typical PMT and introduce how it goes from the light collection to the amplified electrical signal output. Then, how the physical process in each step will affect our signal (distribution), and its theoretical response. Finally, I made some approximations under my circumstance to determine the fitting model on low light level results and high light level results respectively. Low light level results allow us to quantify the single photoelectron. High light level results allow us to make a light intensity reference and calculate the high voltage factor.

doi:10.6342/NTU202300991

2.2 The structure and working principle

The simplified structure of a typical photomultiplier tube is illustrated in Fig. 2.1 [3]. It has the basic elements of a photocathode, focusing electrodes, several dynodes, and finally anode. All of them are enveloped with a secure boundary (usually glass) to sustain vacuum conditions and make all electrons accelerated well by the internal electric fields. The working process of PMT can be divided into two major parts. The first part is photoelectron conversion, and the second part is the electron multiplication.

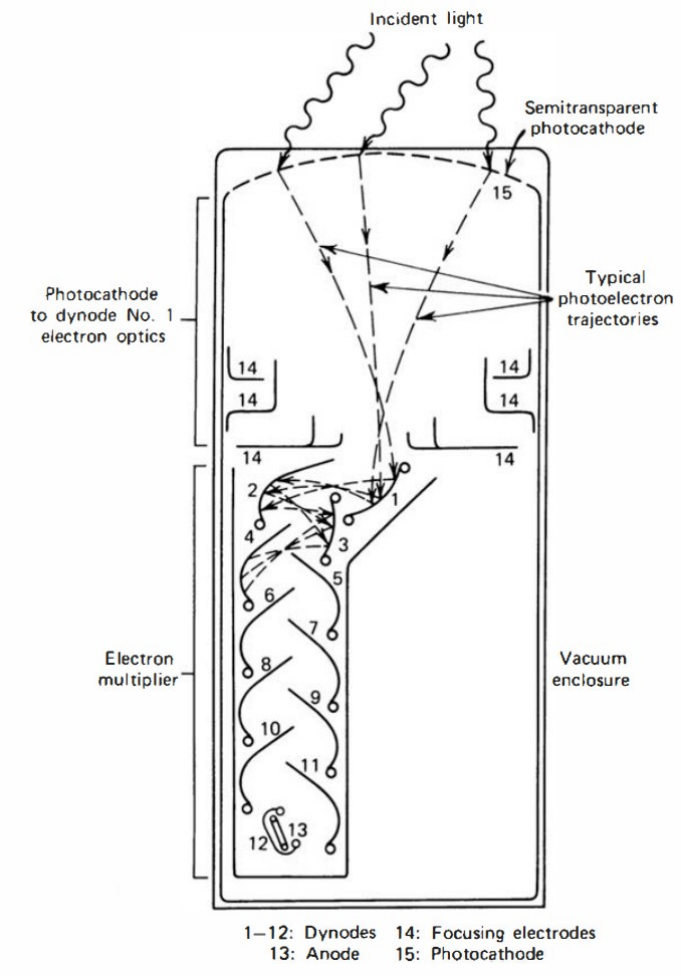

Figure 2.1: Basic elements of a PMT (from [3]).

In photoelectron conversion, PMT converts incident photons into low energy elec-

doi:10.6342/NTU202300991

trons via the photoelectric effect. The escape of the electron from the opposite of the light incident surface can be accelerated by the focusing electrodes to reach the first dynode. The ideal situation is the number of incident photons equal to the number of emitted photoelectrons. However, some processes such as electron-electron collisions in migration, or incident photon energies do not match the escape depth perfectly, making it impossible to achieve this ideal situation. The sensitivity of photocathodes is usually simply defined as

$$QE = \frac{\text{number of photoelectrons emitted}}{\text{number of incident photons}} \tag{2.1}$$

. The maximum quantum efficiency is about 20 to 30% for common photocathodes. It strongly depends on the wavelength (quantum energy) of the incident light, so it is best to choose the PMT with the maximum quantum efficiency that matches the wavelength of measured objects in the experiment.

After photoelectron conversion, electron multiplication amplifies the electrical signal. It is based on the secondary electron emission, in which electrons are accelerated by the internal electric field and strike the surface of the next electrode, called a dynode, then the transferred energy can kick out more than one electron on the same surface. The secondary electron yield is a function of incident energy, and we can quote an overall multiplication factor δ for a single dynode:

$$\delta = \frac{\text{number of secondary emitted electrons}}{\text{primary incident electron}} \tag{2.2}$$

. To achieve electron gains on the order of $10^5 \sim 10^6$, all PMTs use multiple stages. If N stages are provided, then the overall gain G for the PMT is

$$G = \alpha\delta^N \tag{2.3}$$

doi:10.6342/NTU202300991

, where α is the fraction of all photoelectrons collected by the multiple structures. The typical value of $\delta = 5$ and $\alpha \sim 1$ is for conventional dynode materials and well-designed tubes. This makes the gain of a common PMT with ten stages $G = 5^{10}$, or about 10^7. After amplification, a typical light pulse with $10^0 \sim 10^3$ photons, will give rise to $10^7 \sim 10^{10}$ electrons that are finally collected by anode and output. The current magnitude of this electric signal is enough to be read by a general DAQ for analysis.

2.3 The physics processes and response

In photoelectron conversion, we assume the number of photons emitted by LED follows Poisson distribution [4]. The probability that x number of photons will arrive when N is the average number of photons arriving:

$$P_1(x;N) = \frac{N^x}{x!}e^{-N} \tag{2.4}$$

. We assume the condition that N number of photons hit on photocathode and quantum efficiency of photocathode is p. Each photon has a probability p to become a photoelectron and probability $1-p$ to disappear, and this consists with Binomial distribution. The probability of x number of photons falling on the photocathode and producing n number of photoelectrons:

$$P_2(n;x,p,N) = P_1(x;N)\frac{x!}{n!(x-n)!}p^n(1-p)^{x-n}, \quad x \geq n \tag{2.5}$$

doi:10.6342/NTU202300991

. Thus, the probability of n number of photoelectrons produced by an average of N number of photons fall on the photocathode:

$$\begin{aligned} P_3(n;p,N) &= \sum_{x=n}^{\infty} P_2(n;x,p,N) = \sum_{x=n}^{\infty} \frac{N^x}{x!} e^{-N} \frac{x!}{n!(x-n)!} p^n (1-p)^{x-n} \\ &= \frac{e^{-N}}{n!} p^n \sum_{j=0}^{\infty} \frac{N^{j+N}}{j!} (1-p)^j, \quad \text{where } j = x-n \\ &= \frac{e^{-N}}{n!} (Np)^n \sum_{j=0}^{\infty} \frac{(N-Np)^j}{j!} = \frac{e^{-N}}{n!} (Np)^n e^{N-Np} \\ &= \frac{(Np)^n}{n!} e^{-Np} = \frac{\mu^n}{n!} e^{-\mu} \end{aligned} \tag{2.6}$$

, where $\mu = Np$ means the average number of photoelectrons. The response of photoelectron conversion is Poisson distribution.

In electron multiplication, the simplest model assumes the production of secondary electrons at a single dynode follows Poisson distribution about the average yield. If δ is the mean gain per stage, the response to a single photoelectron should be Gaussian when $\delta \gg 1$. The detailed response is derived by reference [5]. Therefore, the response of a multiple dynode system to a single photoelectron can be approximated by a Gaussian distribution:

$$G_1(x) = \frac{1}{\sigma_1 \sqrt{2\pi}} e^{-\frac{(x-Q_1)^2}{2\sigma_1^2}} \tag{2.7}$$

, where x is the variable charge, Q_1 is the average charge output when one photoelectron is collected by the first dynode, and σ_1 is the corresponding standard deviation of the charge distribution. Q_1 means single photoelectron at this working voltage, and it can also be expressed by $Q_1 = eg$, where e is the elementary charge and g is the gain of PMT. If we assume the amplification processes from different photoelectrons are independent [6], then the PMT output charge distribution initiated by n number of photoelectrons is a

doi:10.6342/NTU202300991

convolution of n one-electron cases:

$$G_n(x) = \frac{1}{\sigma_1\sqrt{2\pi n}} e^{-\frac{(x-nQ_1)^2}{2n\sigma_1^2}}, \quad n > 0 \wedge n \in \mathbb{N} \tag{2.8}$$

. The response of an ideal PMT is a convolution of photoelectron conversion and electron multiplication:

$$S_{ideal}(x) = P(n;\mu) \bigotimes G_n(x) = \sum_{n=1}^{\infty} \frac{\mu^n}{n!} e^{-\mu} \frac{1}{\sigma_1\sqrt{2\pi n}} e^{-\frac{(x-nQ_1)^2}{2n\sigma_1^2}} \tag{2.9}$$

. But in a real PMT, various background processes will generate some additional noise and modify the output charge spectrum. The background processes can be mainly divided into two types [6]. The first type is the low charge processes contributing nonzero width of the signal when no photoelectron was emitted from the photocathode, also called "pedestal", and can be described by a Gaussian. The second type is the processes accompanied with measured signals, such as thermal emission or light noise in amplification, and can be described by an exponential decay function. If we call w as the probability of the second type background, then the background signal:

$$B(x) = \frac{1-w}{\sigma_0\sqrt{2\pi}} e^{-\frac{(x-Q_0)^2}{2\sigma_0^2}} + w\theta(x-Q_0)e^{-\alpha(x-Q_0)} \tag{2.10}$$

, where Q_0 is the pedestal, σ_0 is the standard deviation of the first type background distribution, α is the coefficient of exponential decay of second type background, and

$$\theta(x') = \begin{cases} 0, & x' < 0 \\ 1, & x' \geq 0 \end{cases} \tag{2.11}$$

doi:10.6342/NTU202300991

is the step function.

The realistic PMT response will be combined with the ideal PMT response and the background:

$$S_{real}(x) = \int S_{ideal}(x')B(x-x')dx' \tag{2.12}$$

, and for low noise intensity ($\frac{1}{\alpha} \ll Q_1$) we can treat the background function by

$$B(x) = \frac{1}{\sigma_0\sqrt{2\pi}} e^{-\frac{(x-Q_0-\frac{w}{\alpha})^2}{2\sigma_0^2}} \tag{2.13}$$

. Thus, the realistic PMT response function can be approximated as following:

$$\begin{aligned} S_{real}(x) \sim & [\frac{1-w}{\sigma_0\sqrt{2\pi}} e^{-\frac{(x-Q_0)^2}{2\sigma_0^2}} + w\theta(x-Q_0)e^{-\alpha(x-Q_0)}]e^{-\mu} \\ & + \sum_{n=1}^{\infty} \frac{\mu^n}{n!} e^{-\mu} \frac{1}{\sigma_1\sqrt{2\pi n}} e^{-\frac{(x-Q_0-\frac{w}{\alpha}-nQ_1)^2}{2n\sigma_1^2}} \end{aligned} \tag{2.14}$$

. For a large μ case, the Poisson distribution goes over to the Gaussian with standard deviation $\sqrt{\mu}$. For all G_n functions, only those with $\mu - \sqrt{\mu} < n < \sqrt{\mu} + \sqrt{\mu}$ will effectively contribute. Therefore, approximate the standard deviation of G_n by $\sigma_1\sqrt{n}$ and replacing $\sum_n$ to $\int dn$, we will find the limit spectrum for large μ:

$$S_{large}(x) = \frac{1}{\sqrt{2\pi\sigma_{large}^2}} e^{-\frac{(x-Q_0-\frac{w}{\alpha}-Q_{large})^2}{2\sigma_{large}^2}} \tag{2.15}$$

, where $Q_{large} = \mu Q_1$ and $\sigma_{large} = \sqrt{\mu(\sigma_1^2 + Q_1^2)}$. We can find that in this limit, μ, Q_{large} and σ_{large} are not independent, so we cannot separate the light intensity (μ) from the PMT amplification (Q_1).

doi:10.6342/NTU202300991

2.4 The approximated model on photon counting

Sec. 2.3 introduces the PMT response functions in theory, but the experimental spectrum cannot directly match it. I divide all LED calibration results, which will be mentioned in Chap 3, into two types: low light level and high light level. I will describe the approximate model in my analysis to each of them, and introduce their roles in the results.

The low light level result has the following features:

For incident light intensity, it corresponds to the small μ case, which μ means the average number of photoelectrons same as Sec. 2.3. Visually, the spectrum concludes pedestal and first photoelectron peak. It can also contain more photoelectron peaks, but the first peak must still be distinguishable.

As mentioned in Sec. 2.3, the standard relationship of $\sigma_n = \sigma_1\sqrt{n}$ is based on the assumption that "the amplification processes of the charges initiated by different photoelectrons are mutually independent". However, several photoelectrons cannot have no interference during electron multiplication in reality. Therefore, I cancel the restriction but still make some constraints. First, I fit the spectrum with four Gaussians where the fitting range is from $0.5Q_1$ to $4.5Q_1$. The mean of the nth Gaussian Q_n will be $n \pm 4\%$ times the mean of the first Gaussian (Q_1). The upper limit of the standard deviation of the nth Gaussian σ_n will be set to $\sqrt{n}$ times the standard deviation of the first Gaussian σ_1 to avoid the width becoming excessive. This fitting process will continuously tune Q_1 and σ_1 up and down to get the most suitable fitting result. Finally, I take out (Q_1, Q_2) obtained from four Gaussians fitting to perform linear fitting $(y = ax)$ to get the single photoelectron of this PMT.

doi:10.6342/NTU202300991

Follow this fitting method, the low light level result mainly allows us to get "single photoelectron" on the PMT that "spectrum resolution is enough to identify single photoelectron peak". I will select the spectrum that meets the condition of "second photoelectron peak appears obviously, but the height is still dominated by first photoelectron peak" as the "standard low light level spectrum of single photoelectron calibration". The analysis of the low light level results can be seen in Sec. 3.3.1.

The high light level result has the following features:

For the incident light intensity, it corresponds to large μ cases. Visually, it does not conclude pedestal and is impossible to distinguish the structure of any photoelectron peaks or to say all of them are assembled into an envelope.

According to the above description, the first idea is only consider the contribution by photoelectron conversion [7], then we can use a Poisson distribution to fit:

$$P_\mu(x) = A \times \frac{\mu^n}{n!} e^{-\mu} = A \times \frac{\mu^{\frac{x}{Q_1}}}{\Gamma(\frac{x}{Q_1}+1)} e^{-\mu} \tag{2.16}$$

, where A is amplitude, and x is measured ADC. The mean value $Q_{large} = \mu Q_1$ and standard deviation $\sigma_{large} = \sqrt{\mu} Q_1$ will allow us to get the light intensity factor μ and gain factor Q_1. This fitting function does not decouple the gain factor and light intensity factor as in theory, while the standard deviation is different. Unfortunately, we found this fitting function is self-inconsistent in the results A.4.

Therefore, I use another perspective to represent the "relative light intensity" of the high light level result, that is a pure Gaussian fit to get the peak value of the high light level spectrum. This fitting can be seen in Sec. 3.3.2. The high light level result mainly allows us to get a "high voltage factor", that is make the same light condition at two

doi:10.6342/NTU202300991

working voltages, then get the ratio between their peak. This magnification refers to the light yield of LYSO needs to be measured at a lower working voltage since it will saturate the digitizer range at higher working voltage will saturation, while single photoelectron needs to be measured at a higher working voltage since a lower working voltage cannot distinguish the standard low light level spectrum. The high voltage factor calculation can be seen in Sec. 3.3.2.

doi:10.6342/NTU202300991

Chapter 3

Setup & Measurements on LED calibration

3.1 Introduction

This chapter will first introduce my LED calibration setup, then the measurements including low light level and high light level. The low light level results help us to get single photoelectron, which allows us to perform calibration before light yield measurement every time. The comparison between signal integral and peak of signal in the high light level results helps us understand the light-emitting behavior of LED as a light source.

3.2 Setup

Fig 3.1 shows the LED calibration setup. From left to right in the figure above, they are the light source-LED, two types of light attenuators, and finally, the light sensor-PMT to receive the incident light. The above components are all installed in a black box. The

doi:10.6342/NTU202300991

operations and usages of these several main components will be explained in the following subsections.

Figure 3.1: The LED calibration setup, from different perspectives.

3.2.1 Light sensor-Hamamatsu R329-02

To achieve a good measurement of light output, the chosen PMT needs to have the following key properties. The first is to have enough resolution that can distinguish double photoelectron to help us meet the condition of ”standard low-light level spectrum”. Secondly, its maximum quantum efficiency region should match the maximum emission wavelength of measured samples to have better photoelectron conversion. Finally, it is necessary to conveniently couple with the sample in geometry.

doi:10.6342/NTU202300991

Hamamatsu PMT assembly H7195, which is built in Hamamatsu R329-02, fits well with the key properties mentioned above. The basic size and appearance information of R329-02 is shown in Fig. 3.2. The flat faceplate and the 46 mm diameter of photocathode window satisfies our requirement for optical coupling with our LYSO samples, which is roughly a cuboid crystal. The gain is $10^6 \sim 4 \times 10^7$ at the high voltage 1500 $\sim$ 2500 V (Fig. 3.3) is sufficient to convert a few of photons signal into an identifiable voltage signal on our ADC. The maximum quantum efficiency is at about 400 nm incident wavelength (Fig. 3.3), which is consistent with the maximum emission wavelength of LYSO scintillation light. The results in Sec. 3.3.1 shows it has enough resolution to distinguish double photoelectrons. Therefore, I choose R329-02 as the light sensor for our light yield measurement.

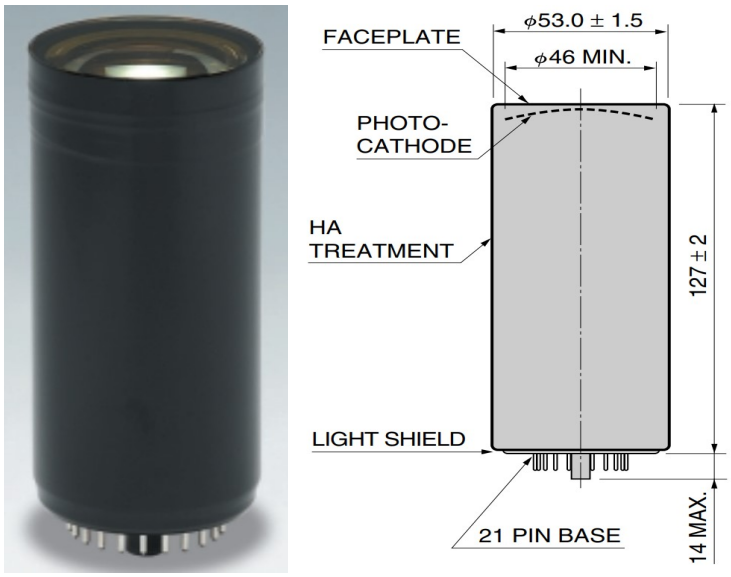

Figure 3.2: The appearance and dimensional outline of R329-02 (Unit: mm).

I use high voltage power supply module DT-5533E (Fig. 3.4) to make PMT operation. Using the built-in General Control Software for CAEN HV Power Supplies (Fig. 3.4) to control high voltage output, monitor, and record voltage and current.

doi:10.6342/NTU202300991

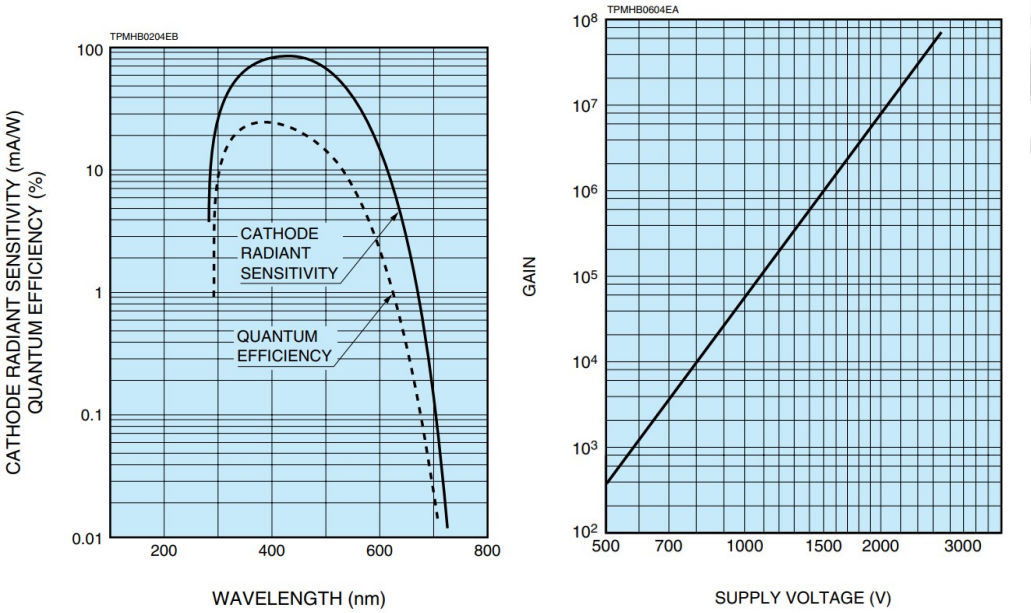

Figure 3.3: The spectral response to wavelength and gain to supply voltage of R329-02.

Figure 3.4: The high voltage power supply module DT-5533E from CAEN and its control software GECO.

doi:10.6342/NTU202300991

3.2.2 Black box, light source-LED, and attenuators

The black box must be well-light-shielded and fit with the assembly H7195, which has a 60 mm outer diameter. The black box size is 120 mm × 60 mm × 59 mm, just enough to place the PMT and leave enough space to place the other components (Fig.3.5(a)). The black box was made of cardboard, wrapped with several layers of black clothes and black tape both inside and outside, to better reduce the outside background light and inside reflection light. There is an irregular-shaped hole on the backside that makes the high voltage supply cable and signal output cable can pass through (Fig. 3.5(b)). An additional external black cloth is applied to block the external background light into this hole (Fig. 3.5(c)). On the front side, a fixed BNC connector is soldered together with a small resistor (10 Ω) and a round head LED on a general-purpose PCB in series (Fig. 3.5(d)), and I will use this LED as my controllable light source (Fig. 3.6).

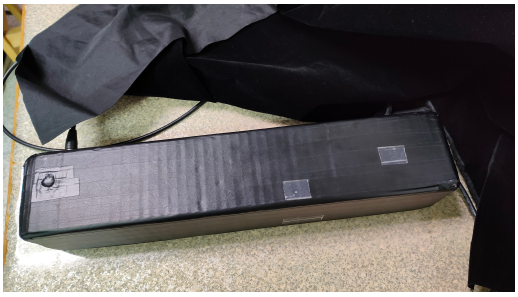

(a) The black box.

(b) The hole to pass cables.

(c) The black box cover with black cloth

(d) The BNC connector to receive signal input.

Figure 3.5: Instructions for use of the black box.

doi:10.6342/NTU202300991

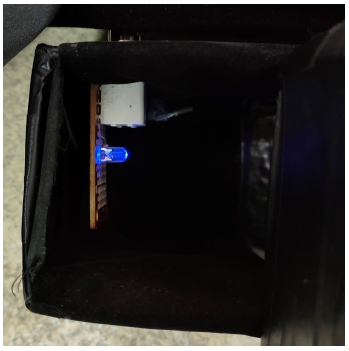

Figure 3.6: The example of LED lighting (not the case during the experiment).

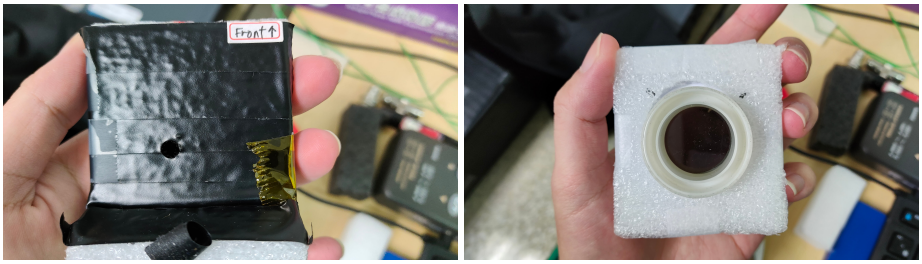

Figure 3.7: The two attenuators use in the LED calibration setup. The left figure is the first attenuator, and the right figure is the second attenuator.

Since the distance between the LED and the PMT window is only about 10 cm, I add two light attenuators between them during the LED calibration measurement (Fig. 3.7). The first attenuator is a small foam wrapped with several layers of interlaced black tape and aluminum foil, and a 5 mm diameter small hole is opened near the center. The second attenuator is a combination of two polarizers and can rotate the angle between them. These two light attenuators make the light received by the PMT weaken and adjustable.

3.2.3 The trigger system and digitizer

There are two methods for common signal triggering. The first one is called internal-trigger or self-trigger. It means we set a threshold (in voltage or ADC), and the event will be recorded when the input signal to DAQ exceeds this threshold. This trigger method is used for light yield measurement, delete events that are smaller than the target ADC.

doi:10.6342/NTU202300991

However, when the incident light is extremely weak, the generated photoelectric signal may be much smaller than the settable threshold value. It is also mentioned in Sec. 2.3 that we need to know the background spectrum of PMT when no light signal is generated. We need to use the other method, called external trigger. While sending a driven signal to the LED, send a synchronized trigger signal to the DAQ. We choose a function generator (Fig. 3.8), which can send pulses to LED and TTL signal to digitizer at the same time, to help us perform LED calibration measurement by external trigger method. How the different pulse parameters will affect the light-emitting behavior of LED will be discussed in Sec. 3.3.3 and Sec. 3.3.3.

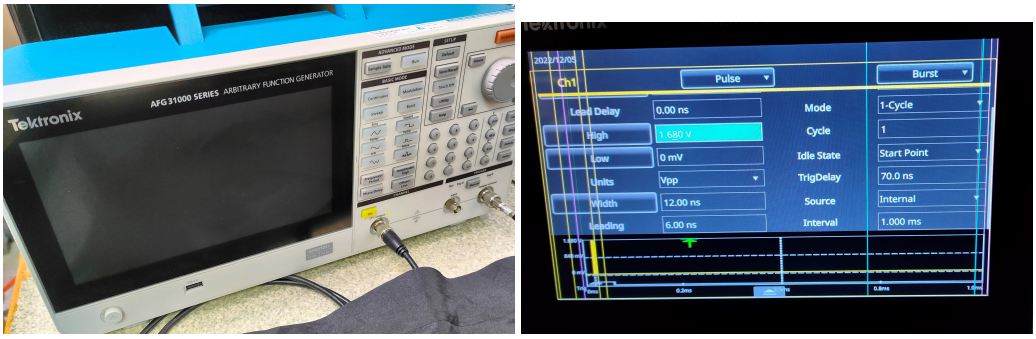

Figure 3.8: The function generator appearance and its working (not the case during the experiment).

Even through PMT can amplify a single photoelectron to 10^6 electrons level, the voltage signal that can be observed on the DAQ is still very small. I choose the CAEN N6730 digitizer as our DAQ (Fig. 3.9), which is a NIM module housing 8-channel, 14-bit, $V_{pp} = 2$ V input range, 500 MS/s Digitizer on single ended MCX coaxial connectors. Both its voltage and sample time resolution are good for us to deal with the details of a single photoelectron spectrum. I use a USB cable to connect the PC and N6730 digitizer, send control commands and receive signal waveforms in real time. The control part uses built-in software WaveDump, and the result processing is by software ROOT for analysis and graphing.

doi:10.6342/NTU202300991

Figure 3.9: The digitizer N6730 from CAEN.

3.3 Results of LED calibration

In general use, the light emitted by LED under DC operating voltage is not only too large for PMT, but also the continuous light emission makes us cannot process the results event by event. We found that pulse squared signals can meet our needs. When the pulse signal input to the LED is far below the rated working voltage (Ex: 1.5 V compared to 3.0 V) and has a very short width (Ex: about 10 ns order), LED will behave like a weak and fast switch light source. Through this method, I have successfully generated signals less to several photons, and divided them into two parts: low light level and high light level, for discussion.

3.3.1 Low light level

How it can be used as the low light level result has been explained in Sec. 2.4. Both reducing the voltage and width of the pulse signal to LED can reduce the light intensity

doi:10.6342/NTU202300991

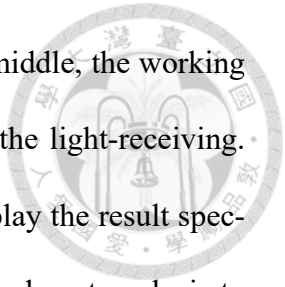

in the low light level results. Since the attenuators are placed in the middle, the working conditions of LED and PMT, and many other situations will affect the light-receiving. It is recommended to have a real-time waveform calculation and display the result spectrum immediately, or continuously doing short-time measurements and post-analysis to approach the desired low light level spectrum.

The following diagrams are used to demonstrate how the low light level spectrum changes with voltage or width. They are all tested successively at high voltage = 2500 V. Fig. 3.10 are the same pulse width = 10 ns while changing pulse voltage = 1550 mV to 1620 mV per 10 mV. The obvious bulge on the left side of each figure is the pedestal mentioned in Sec. 2.2, which is the events without incident light that allows us to determine the achievement of low light level results. The number of pedestal events will decrease as light intensity increases, and will disappear completely in the high light level results. Because in my results, all the pedestal value are close to 0 ADC, and the details of pedestal distribution are not needed, all of the following low light level spectrum will ignore pedestal. Fig. 3.11 is the plot of Fig. 3.10 while ignoring the pedestal. As pulse voltage increases, the second peak in the spectrum becomes more and more obvious, and the height exceeds first peak when above 1600 mV. Fig. 3.12 are the same pulse voltage = 1500 mV while changing pulse width = 10 ns to 12 ns per 0.5 ns. The change of pulse width can also adjust the light intensity. The spectrum at 12.0 ns and 12.5 ns has no characteristic peaks of the low light level spectrum, which means their light intensity is approaching the high light level result.

Fig. 3.11(e) is a spectrum that fits the condition of ”standard spectrum of single photoelectron calibration” as mentioned in Sec. 2.4. I can use this spectrum to perform single photoelectron calibration of PMT R329-02 working at high voltage = 2500 V. The

doi:10.6342/NTU202300991

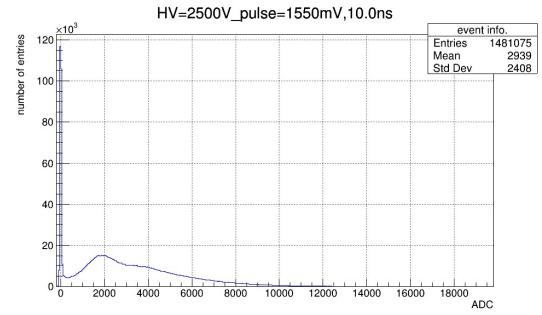

(a) pulse voltage = 1550 mV

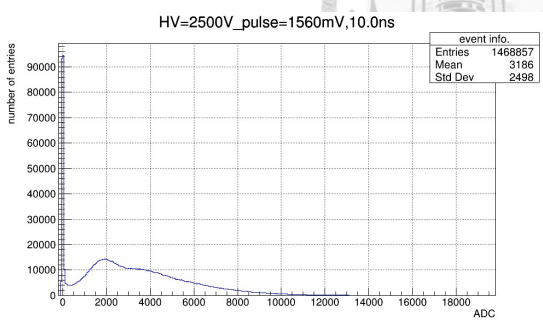

(b) pulse voltage = 1560 mV

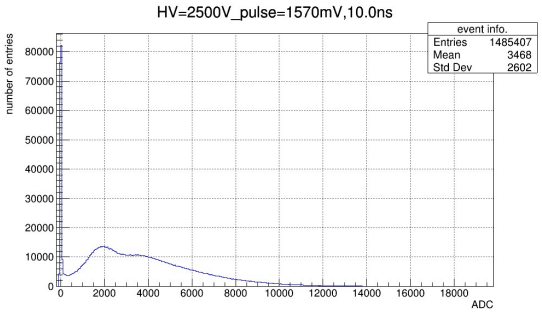

(c) pulse voltage = 1570 mV

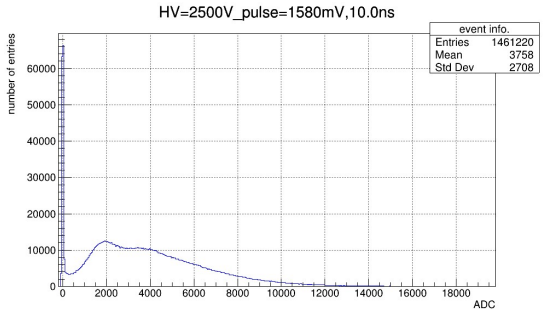

(d) pulse voltage = 1580 mV

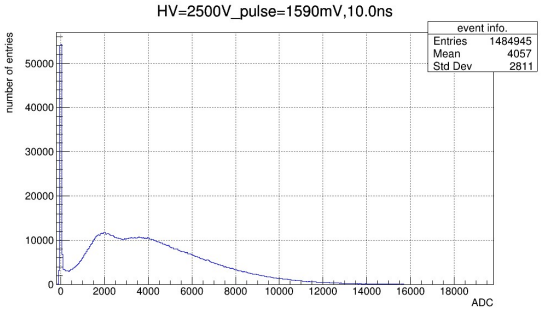

(e) pulse voltage = 1590 mV

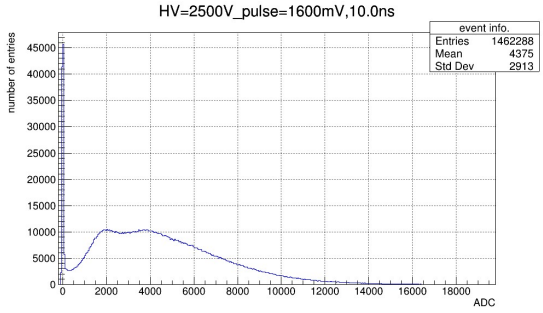

(f) pulse voltage = 1600 mV

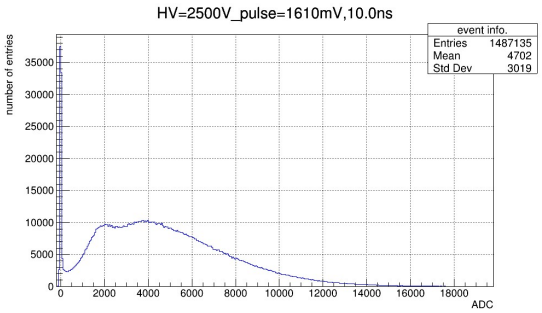

(g) pulse voltage = 1610 mV

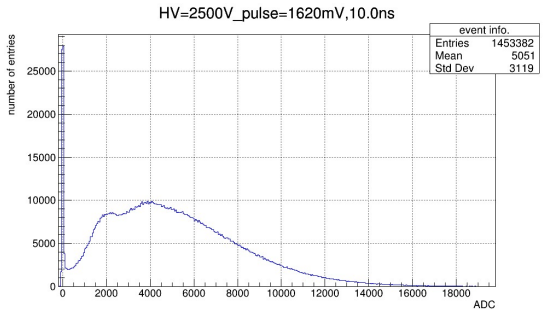

(h) pulse voltage = 1620 mV

Figure 3.10: Examples of low light level spectrum include pedestal by fixing pulse width 10 ns and changing pulse voltage at high voltage = 2500 V

doi:10.6342/NTU202300991

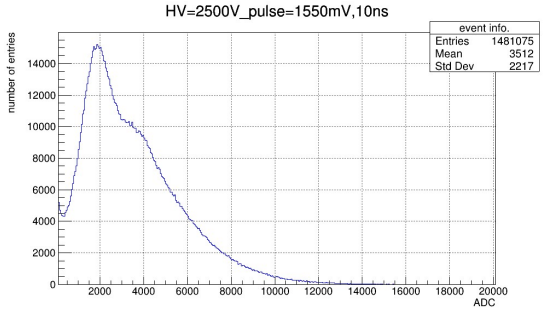

(a) pulse voltage = 1550 mV

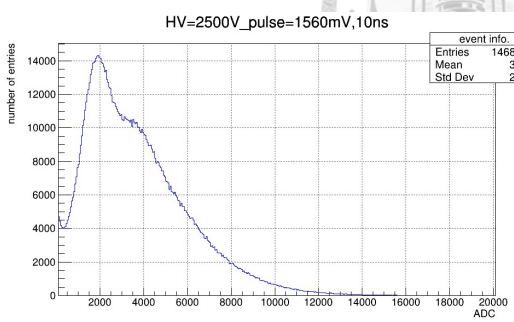

(b) pulse voltage = 1560 mV

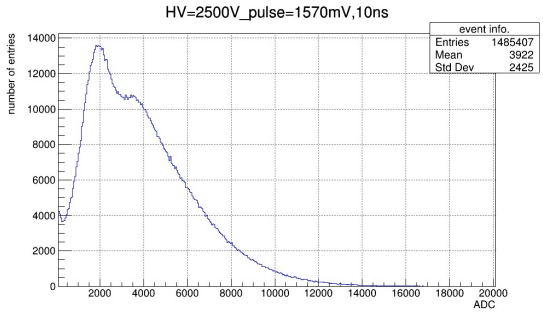

(c) pulse voltage = 1570 mV

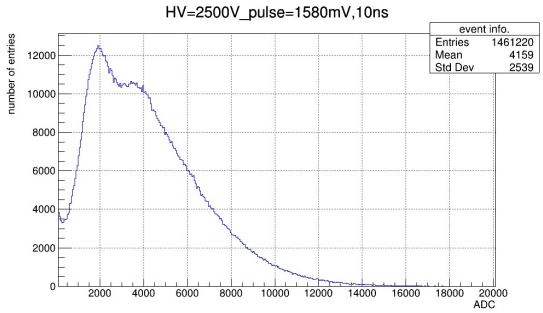

(d) pulse voltage = 1580 mV

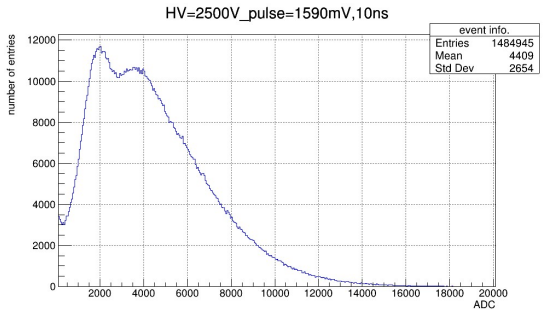

(e) pulse voltage = 1590 mV

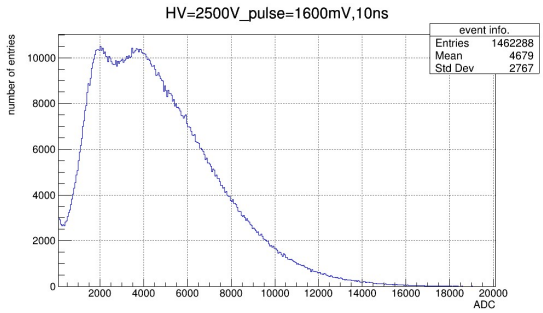

(f) pulse voltage = 1600 mV

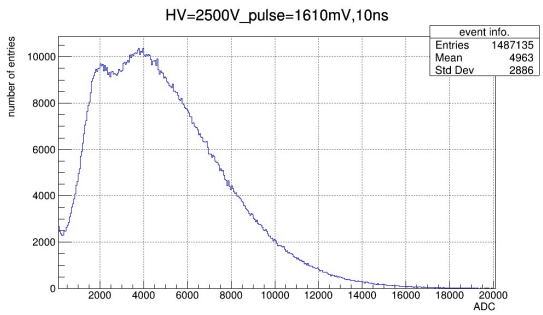

(g) pulse voltage = 1610 mV

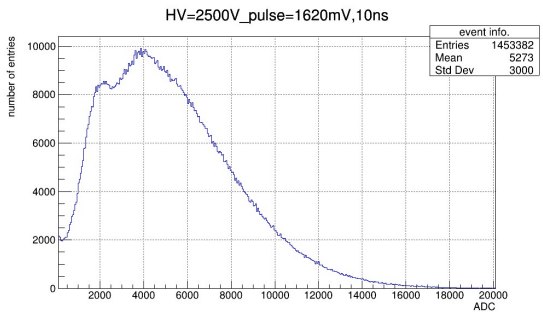

(h) pulse voltage = 1620 mV

Figure 3.11: Examples of low light level spectrum by fixing pulse width (10 ns) and changing pulse voltage at high voltage = 2500 V

doi:10.6342/NTU202300991

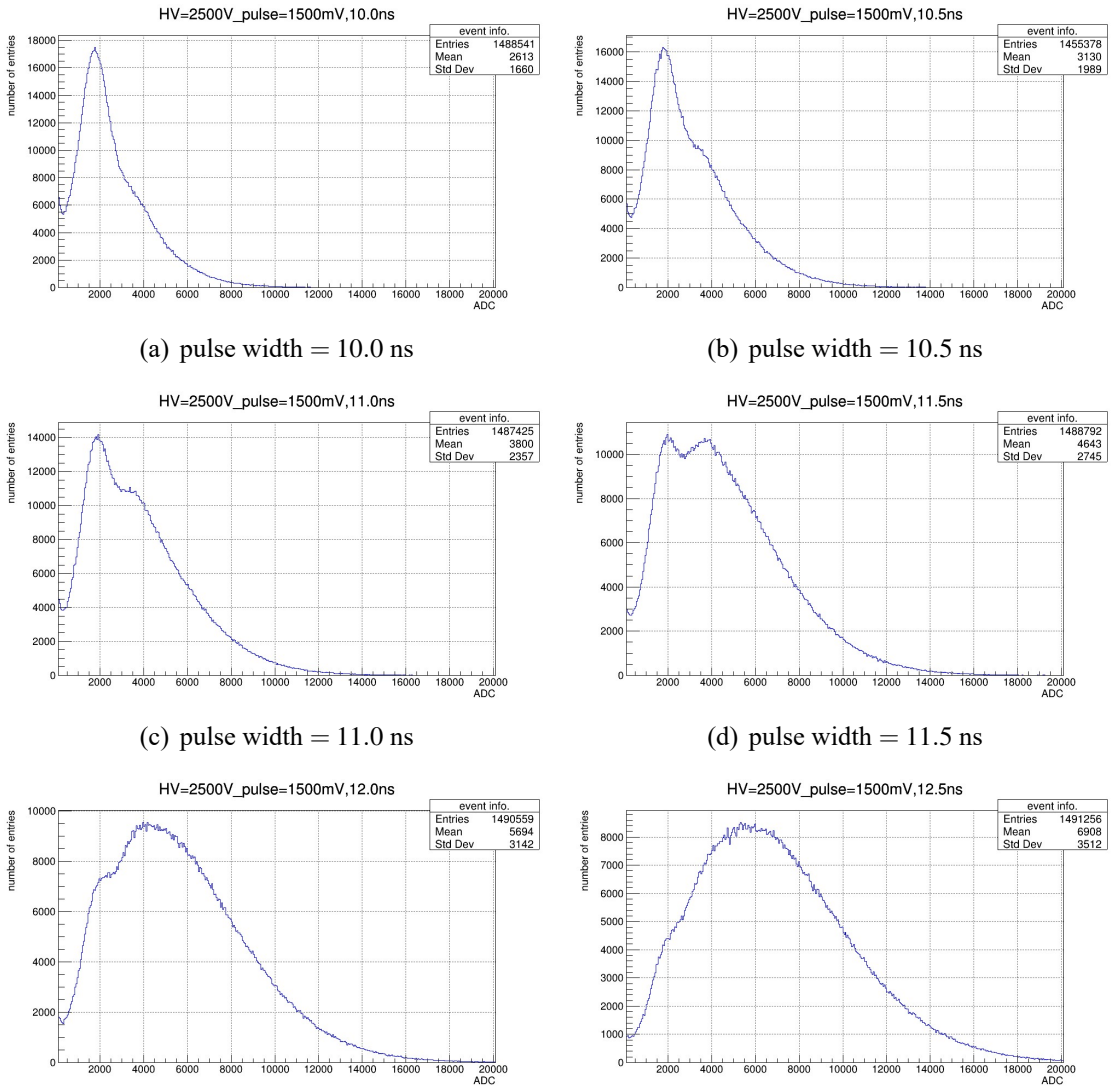

(a) pulse width = 10.0 ns

(b) pulse width = 10.5 ns

(c) pulse width = 11.0 ns

(d) pulse width = 11.5 ns

(e) pulse width = 12.0 ns

(f) pulse width = 12.5 ns

Figure 3.12: Examples of low light level spectrum by fixing pulse voltage (1500 mV) and changing pulse width at high voltage = 2500 V.

doi:10.6342/NTU202300991

fitting result of four Gaussians is shown in Fig. 3.13, and the linear fitting of Q_1 and Q_2 is shown in Fig. 3.14. The obtain single photoelectron mean $= 1735 \pm 5.6$ ADC at high voltage $= 2500$ V. This demonstrates how to obtain single photoelectron before each light yield measurement.

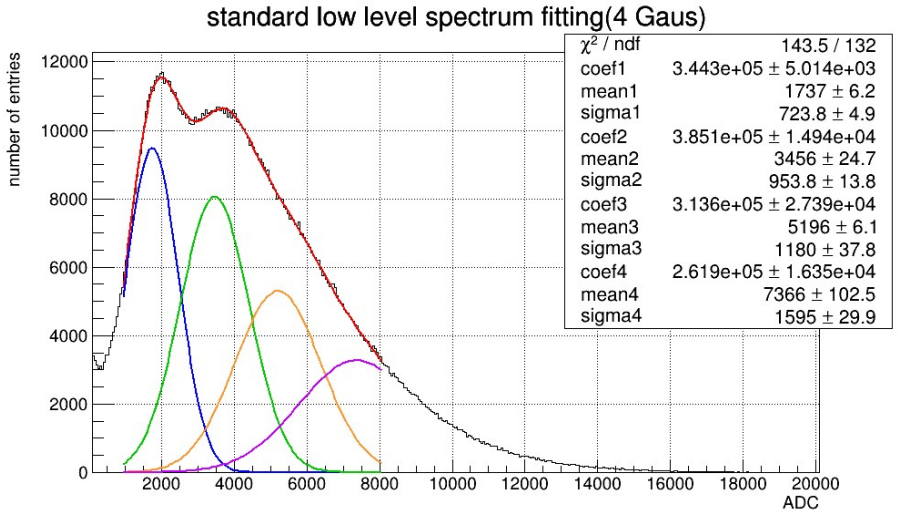

Figure 3.13: The example of the four Gaussians fitting of standard low light level spectrum.

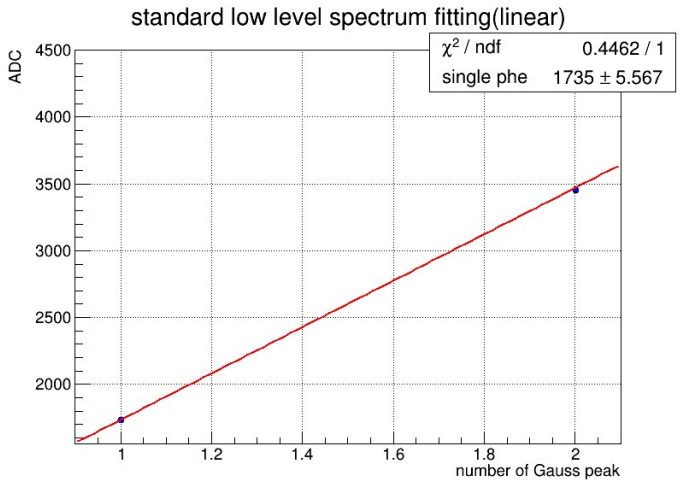

Figure 3.14: The example of the linear fitting of the first two Gaussians means to get single photoelectron.

doi:10.6342/NTU202300991

3.3.2 High light level

How it can be used as the high light level result has been explained in Sec. 2.4. The way to produce a high light level result is similar to the low light level result in Sec. 3.3.1, just rising the pulse parameters until it consists of the high light level spectrum (Fig. 3.15). As mentioned in Sec. 2.4, I make a pure Gaussian fitting:

$$p_0 \times e^{-\frac{(x-p_1)^2}{2p_2^2}} \tag{3.1}$$

, where p_0 is the scale coefficient, p_1 is thw mean, and p_2 is thw standard deviation, to collect the peak value by the Gaussian mean, such as $p_1 = 14940$ ADC in Fig. 3.15 as relative light intensity. Fig. 3.16 is one of the cases to show how to get the high voltage factor between high voltage = 1500 V and 2500 V, that is (p_1 at 2500 V)/(p_1 at 1500 V) and is $19820/269.3 = 73.60$ in this case.

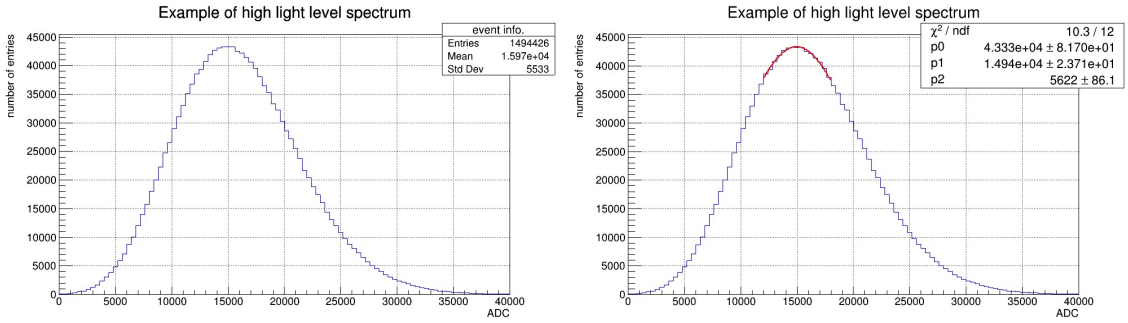

Figure 3.15: The example of high light level spectrum of (left figure) and its pure Gaussian fitting (right figure).

To make the study on light intensity comparison, I introduce another kind of spectrum here. The origin kind is "signal integral" (Fig. 3.15), which means the spectrum is statistics of the integral of the voltage signal. This is the correct method since the voltage integral to time is proportional to the charge. Another kind is the "peak of signal" (Fig. 3.17),

doi:10.6342/NTU202300991

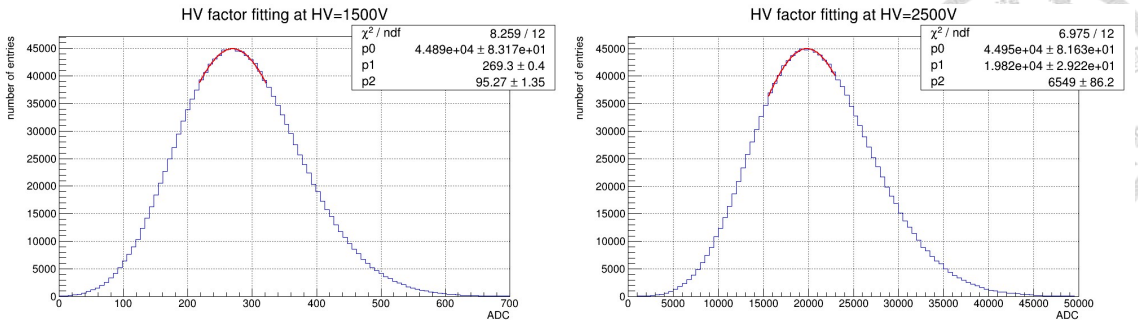

Figure 3.16: The example of high light level spectrum fitting to obtain high voltage factor between high voltage = 1500 V and 2500 V.

which means the spectrum is the statistics of a maximum of voltage signal. This method is incorrect and only used in this subsection to help me explain high light level results. I will adjust the pulse voltage or pulse width to create different high light level results, then compare the change of peak value both of ”signal integral” and ”peak of signal” to understand the light-emitting behavior of LED.

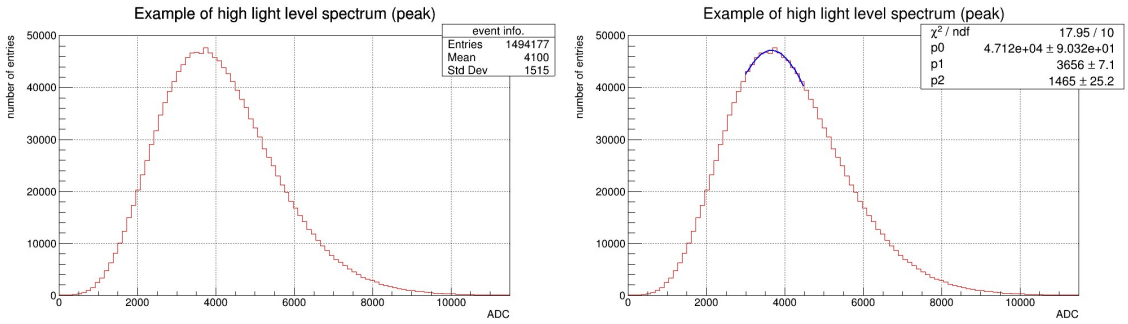

Figure 3.17: The example of high light level spectrum of the peak of signal (left figure) and its pure Gaussian fitting (right figure).

Fig. 3.18 is used to demonstrate how the high light level results change with voltage or width. The two figures in each column are from the same experimental results, while the left figure is the peak value of ”signal integral”, and the right figure is the peak value of ”peak of signal”. Fig. 3.18(a) is the same pulse width = 10 ns, change pulse voltage = 1820 mV to 1920 mV per 20 mV, and Fig. 3.18(b) is the same pulse voltage = 1500 mV, change pulse width = 15 ns to 18 ns per 0.5 ns. These two group results are measured

doi:10.6342/NTU202300991

at working voltage = 2500 V, and they represent the relatively small light intensity in the high light level results. It can be seen that the peak value of both signal integral and peak of signal have a nearly linear relationship with pulse voltage or pulse width. Fig. 3.18(c) is the same pulse width = 15 ns, change pulse voltage = 1750 mV to 1900 mV per 50 mV, and Fig. 3.18(d) is the same pulse voltage = 1500 mV, change pulse width = 20 ns to 34 ns per 2 ns. These two group results are measured at working voltage = 2000 V, and they represent the relatively high light intensity in the high light level results. It can be seen that the peak value of both signal integral and peak of signal still have a nearly linear relationship with pulse voltage or pulse width. However, if it is the same pulse voltage = 2000 mV, change pulse width = 20 ns to 100 ns per 10 ns, and measured at working voltage = 1500 V. That is very strong light intensity in high light level results, and results are shown in Fig. 3.18(e). The peak value of signal integral still maintains a nearly linear relationship, but peak of signal is obviously a monotonically decreasing nonlinear relationship. This result shows that changing the pulse voltage and changing the pulse width have different mechanisms for changing the LED luminosity. It will combine the content in Sec. 3.3.3 to let us understand the light-emitting behavior of LED.

3.3.3 The control and light-emitting behavior of LED

The following is the signal waveform recorded in some tests using another Digitizer, National Instrument PXI 5154, which also has an oscilloscope function. These records are not from any experimental results mentioned in Sec. 3.3.1 and Sec. 3.3.2, but the experimental situation is similar. I use them to help illustrate my understanding of the light-emitting behavior of LED driven by pulse signal.

Fig. 3.19 is the waveform recorded when the pulse voltage is slightly increased dur-

doi:10.6342/NTU202300991

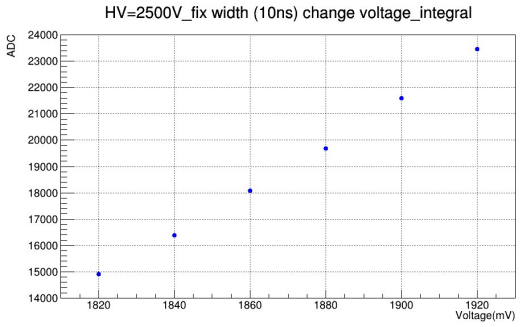

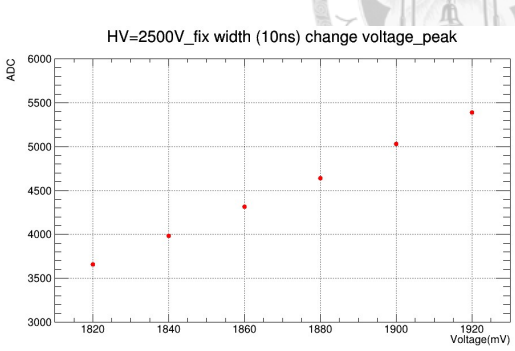

(a) Fix pulse width (10 ns) and change pulse voltage at high voltage = 2500 V.

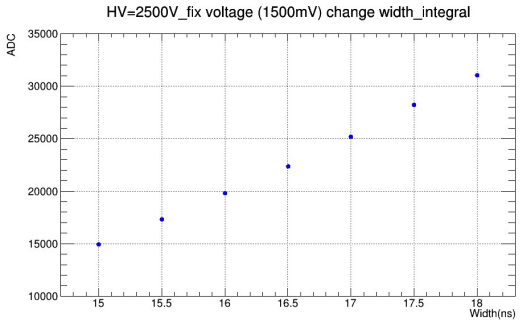

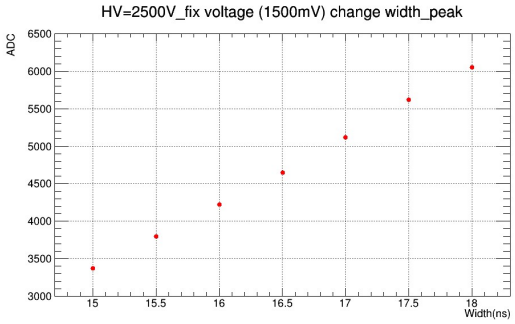

(b) Fix pulse voltage (1500 mV) and change pulse width at high voltage = 2500 V.

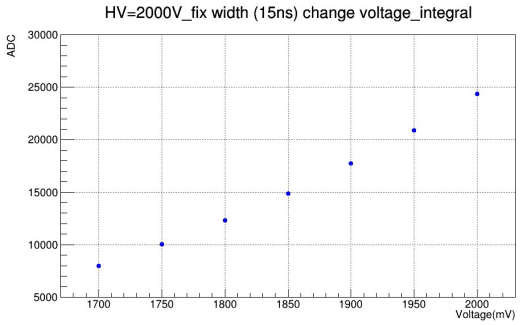

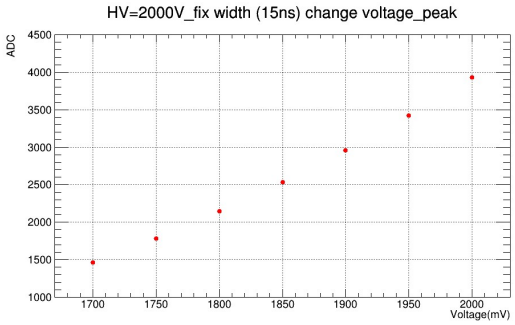

(c) Fix pulse width (15 ns) and change pulse voltage at high voltage = 2000 V.

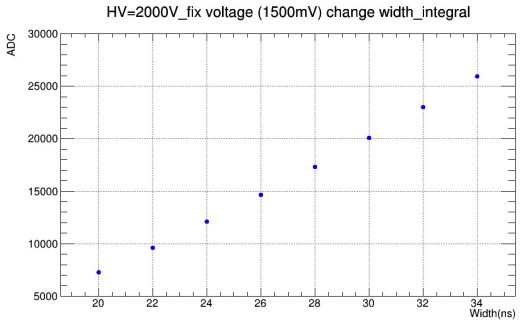

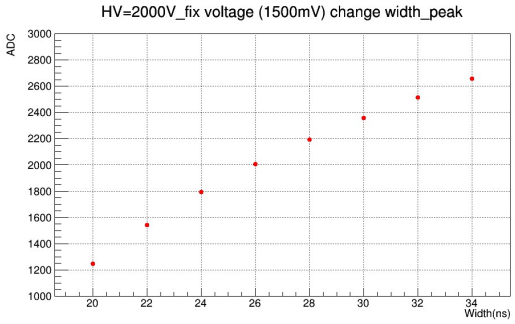

(d) Fix pulse voltage (1500 mV) and change pulse width at high voltage = 2000 V.

doi:10.6342/NTU202300991

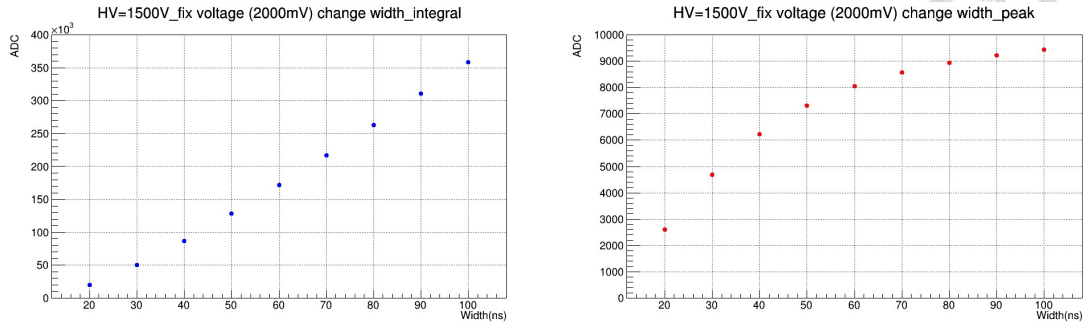

(e) Fix pulse voltage (1500 mV) and change pulse width at high voltage = 1500 V.

Figure 3.18: The peak value of high light level results in changes with voltage or width as PMT works at different high voltages. The left figure (blue dot) of each column is the signal integral, and the right figure (red dot) is the peak of signal.

ing a low light level test. It shows two kinds of short signals with obvious height difference, which are likely to be the candidates of the single photoelectron signal and double photoelectrons signal respectively. Fig 3.20 is the waveform recorded when the pulse width is slightly increased during a low light level test. There is a group of wider but similar in height to the lower signal, which is likely to be the candidate of several single photoelectron signals. Fig. 3.21 are recorded signal waveforms from a high light level test with pulse width = 20, 30, 40, 50 ns. We can find that while the source signal is widened, the waveform is separated into several peaks.

So far, I can simply summarize the light-emitting behavior of LED driven by pulse signal. Both increasing the pulse voltage and pulse width can make the light stronger, but their effects are different. The effect of increasing the pulse voltage is ”increasing the output light amount (photon number) within the same luminous time”. The photons incident to PMT will be stacked within the same time interval, so the signal integral and peak of signal will have a nearly linear relationship for different pulse voltage settings. The effect of increasing pulse width is to ”extend the luminescence time under the same output light amount (photon number)”. The photons incident to PMT will not be stacked

doi:10.6342/NTU202300991

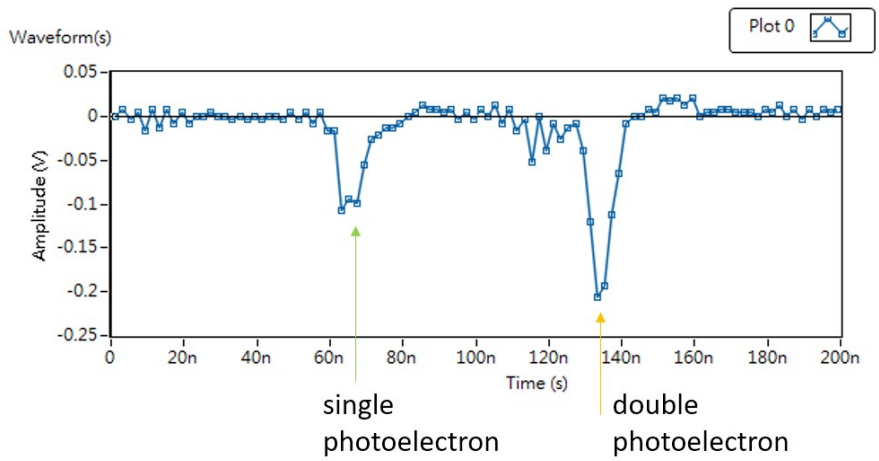

Figure 3.19: A waveform record that I think has single photoelectron and double photoelectron candidates.

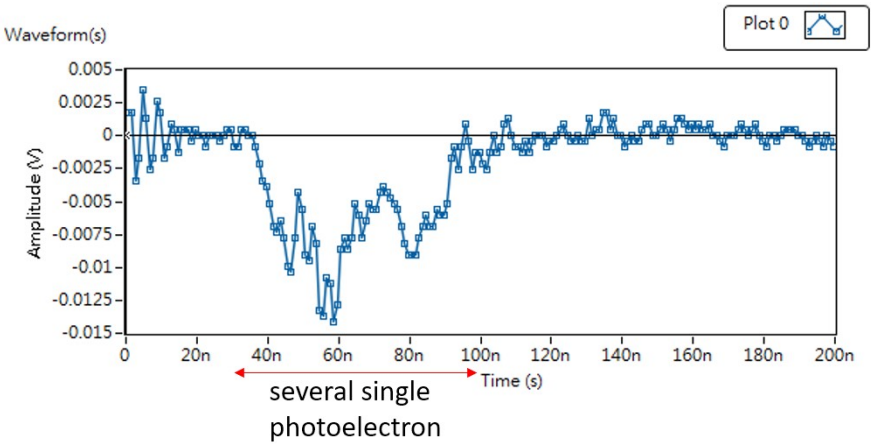

Figure 3.20: A waveform record that I think has several single photoelectron candidates.

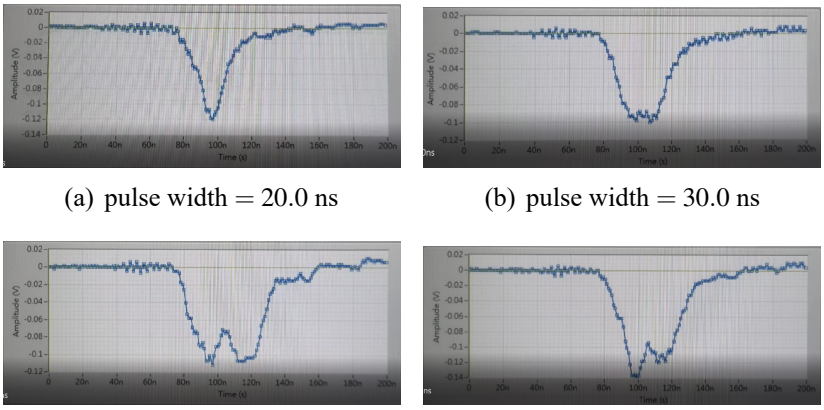

(a) pulse width = 20.0 ns (b) pulse width = 30.0 ns

(c) pulse width = 40.0 ns (d) pulse width = 50.0 ns

Figure 3.21: A few screenshots of the waveform recording when I changed the pulse width.

doi:10.6342/NTU202300991

within the same time interval, so the signal integral will have a nearly linear relationship, but the peak of the signal will not have a linear relationship for a widened pulse width, which is above a few ten nanoseconds order in this example. The signal waveform shape is likely to come from the fluctuation of the photons incident to the photocathode at different time, so the peak of waveform will not increase linearly but will oscillate violently or even split into two or three or more peaks.

Therefore, I use signal integral to obtain the light intensity. Comparing the light output by measured sample with the combination of single photoelectron and high voltage factor from the LED calibration, I can get the light yield of sample in the number of photoelectrons.

doi:10.6342/NTU202300991

Chapter 4

Light yield measurements of LYSO

4.1 Introduction

This chapter will mainly discuss the light yield measurement of LYSO. First is the introduction of setup, and then the demonstration of LYSO intrinsic spectrum and radioactive spectrum by Sodium-22. After that, I will discuss some systematic items that can be improved or need attention in my system. Finally, the standard measurement process I identified, and the light yield of our LYSO samples.

4.2 Setup

Fig. 4.1 is the light yield measurement setup. It removes the two attenuators in the LED calibration setup to place platforms that hold the radioactive source and LYSO. The digitizer is the same. The operations and usages of several main components will be explained in the following subsections.

doi:10.6342/NTU202300991

Figure 4.1: The light yield measurement setup.

4.2.1 LYSO samples

As mentioned in Sec. 1.2, the LYSO intrinsic spectrum is associated with its size. I use a large-size LYSO and a small-size LYSO as examples, and the small-size one is also what I use for the light yield measurement. These two crystals are from a group of LYSO samples provided by Taiwan Applied Crystal Company [8].

Fig. 4.2 shows the large size LYSO, which is a cuboid of size = 35.5 mm × 35.5 mm × 12.0 mm. The two sides of the square face are polished, while the other four sides do not look completely transparent. All surfaces are flat.

Fig. 4.3 shows the small size LYSO, which is a cuboid of size = 3.0 mm × 3.0 mm × 20.0 mm. All surfaces are flat, polished, and transparent.

4.2.2 Optical grease and seal tape

Since scintillation light can be emitted from any surface of the crystal, I need a good covering material to help me reflect scintillation light to the output cross-section. I choose

doi:10.6342/NTU202300991

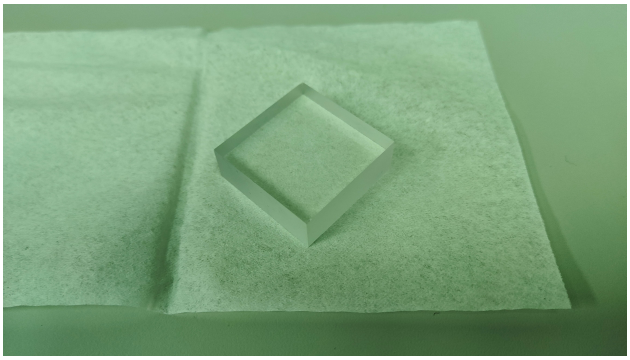

Figure 4.2: The large size LYSO sample.

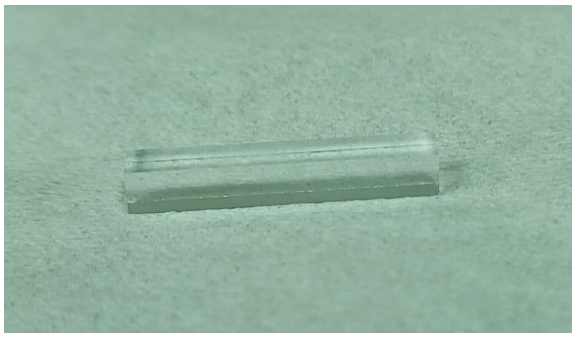

Figure 4.3: The small size LYSO sample.

commercially available seal tape, which is easy to wind and tightly attached to the object, and its main component is polytetrafluoroethylene (PTFE), which has high reflectivity at 400 nm. LYSO samples will be wrapped with seal tape in five cross sections except for the one contact with PMT. Some references on the reflection conditions, the appearance of seal tapes, and the method I use seal tape will be explained in Sec. 4.4.2.

Although I put the light-emitting surface of the crystal in direct contact with the PMT window, the air gap and high refractive index of LYSO (about 1.7) make the scintillation light very easy to lose. I use optical grease to optical couple crystal and PMT, eliminate the air gap and make the crystal surface better attached to the PMT window. The optical grease is EJ-550 optical grade silicone grease (Fig. 4.4) from ELJEN TECHNOLOGY, and its refractive index is about 1.46 according to its datasheet. The difference caused by optical grease is mentioned in Sec. 4.4.3.

doi:10.6342/NTU202300991

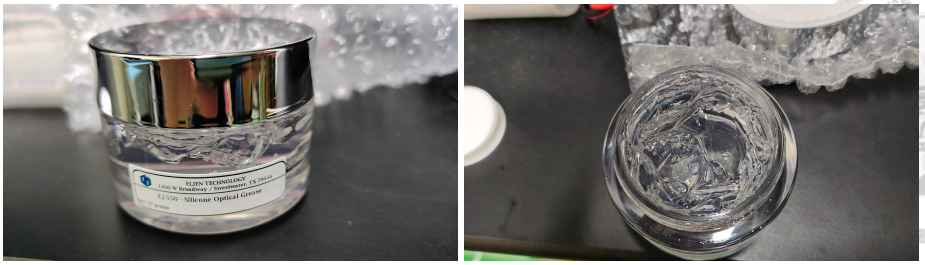

Figure 4.4: The optical grease EJ-550.

4.2.3 Radioactive source-Sodium-22

Because the gamma-ray in the PET system comes from positron-electron annihilation, whose energy = 511 keV. One of the radioactive sources Sodium-22 can emit 511 keV gamma-ray, and it also comes from its internal positron-electron annihilation. I use Sodium-22 as the radioactive source and use the 511 keV peak in the energy spectrum to study light yield.

We have two Sodium-22 sources as Fig. 4.5. The old Sodium-22 source is a cylinder with a diameter = 12.0 mm and length = 85.0 mm. The new Sodium-22 source is coin-shaped with a diameter = 21.0 mm and thickness = 3.5 mm. According to the record in the NTUHEP group, the radioactivity of the old Sodium-22 is about 0.07 μCi, and the new Sodium-22 is about 7.68 μCi at now. It can be seen that the activity of these two sources is very different, and the difference in their radioactive spectrum will be demonstrated in Sec. 4.3.2.

4.3 The scintillation light spectrum

In this section, I will demonstrate the scintillation light spectrum of the LYSO samples by its self-radiation or two Sodium-22 sources. I will compare whether the experimental

doi:10.6342/NTU202300991

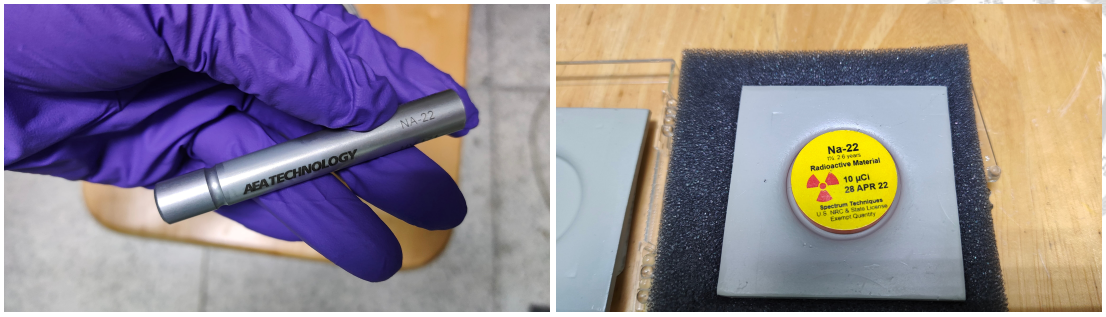

Figure 4.5: The two Sodium-22 radioactive sources we have. The left figure is the old one, and the right figure is the new one.

spectrum is consistent with the theory, and describe their characteristic energy peaks, to obtain the light yield of LYSO sample at 511 keV.

4.3.1 LYSO intrinsic spectrum

Sec. 1.2 first introduced that LYSO contains ^{176}Lu, which has a beta-particle energy spectrum and shifts to several dominant energies of gamma-ray. The four dominant deposited energy by gamma-ray are 88 keV, 290 keV ($88+202$), 395 keV ($88+307$), and 597 keV ($88+202+307$). Their probability, that is peak height in the spectrum, will be strongly associated with crystal size. [2] gives out two sizes of LYSO for example, and Fig. 4.6 is their spectrum distribution. The height of 290 keV, 395 keV, and 597 keV peaks are relatively similar in the intrinsic spectrum of small-size LYSO, while the height of 597 keV peak is highest in the intrinsic spectrum of large-size LYSO.

Fig. 4.7 shows the intrinsic spectrum of the large-size LYSO I measured. It has a three-layer stepped distribution. The ADC ratio at the three features (circled places) is about $3:4:6$, which are likely to represent 290, 395, and 597 keV peaks in LYSO intrinsic spectrum respectively, and the 597 keV peak is the highest. Fig. 4.8 shows the intrinsic spectrum of the small-size LYSO I measured. The ADC ratio at the four features (circled

doi:10.6342/NTU202300991

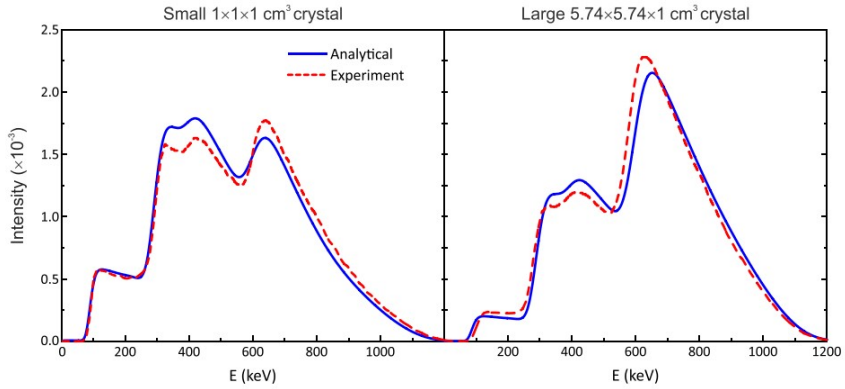

Figure 4.6: LYSO intrinsic spectrum of different size crystal (from [2]).

places) in this spectrum is about 1 : 3 : 4 : 6, which are likely to represent 88, 290, 395, and 597 keV peaks in LYSO intrinsic spectrum respectively, and 290, 395 keV peaks are higher than 597 keV peak. The ADC value of the several featured energy peaks in small-size LYSO is larger than large-size LYSO since I use optical grease to make sure the 88 keV peak can exceed the threshold.

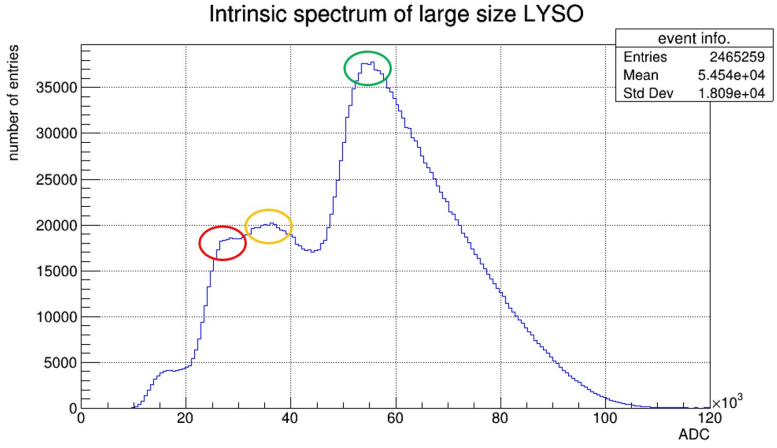

Figure 4.7: The intrinsic spectrum of our large-size LYSO sample.

There is also a subsequent simulation result from [2] and shown in Fig. 4.9. It shows when crystal size increases, the probability of 88, 290, 395 keV self-detection decreases, and the probability of 597 keV self-detection increases. This translates into a decline in relative intensity for the low energy peaks and a growth in relativity intensity for the high energy peak.

doi:10.6342/NTU202300991

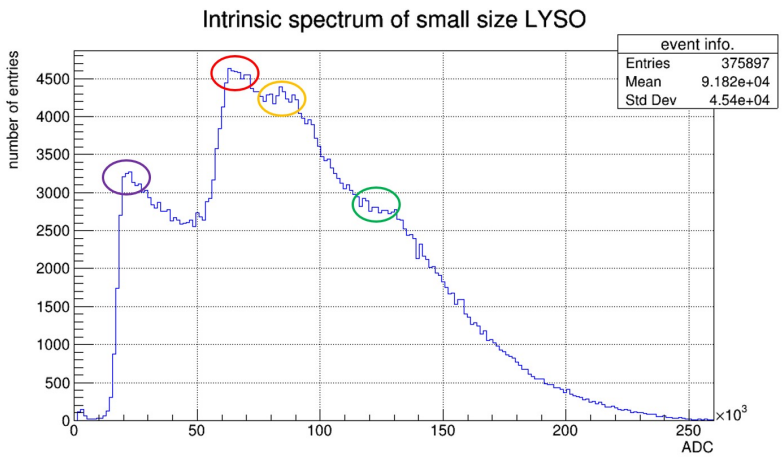

Figure 4.8: The intrinsic spectrum of our small-size LYSO sample.

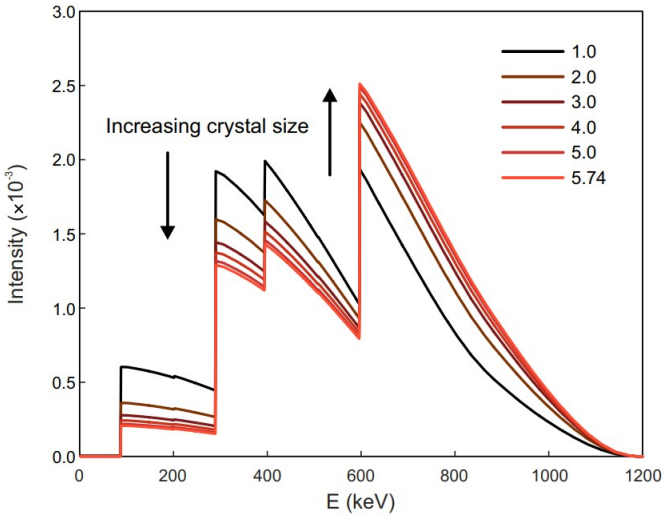

Figure 4.9: The simulation of the LYSO intrinsic spectrum changing with the size (from [2].)

doi:10.6342/NTU202300991

Therefore, the LYSO intrinsic spectrum of my measurements consists with the theory. However, the featured energy peaks are the combination of beta spectrum shift to corresponding gamma energy, and it is difficult to determine the ADC value by fitting. I will not use LYSO intrinsic spectrum to study light yield, but only as a reference in the initial tests. The high event rate of large-size LYSO will exist as the background when using an external radioactive source, and it also has significant self-absorption, which will be mentioned in Sec. 4.4.1. Thus, I will use small-size LYSO as the sample for the light yield measurement.

4.3.2 Sodium-22 spectrum

Sodium-22 is a man-made isotope with a half-life of about 2.6 years [9]. It decays into an excited state neon-22 mainly by emitting a positron (β^+-decay). The emitted positrons react with the electrons of surrounding matter and lead to annihilation radiation at 511 keV. The excited neon state passes into the ground state whereby a 1275 keV γ-ray is emitted. The standard Sodium-22 energy spectrum is shown in Fig. 4.10, which shows obvious gamma-ray energy peaks at 511 keV and 1275 keV. 511 keV peak is mainly used in the light yield study, while 1275 keV peak will not participate in any results in this thesis.

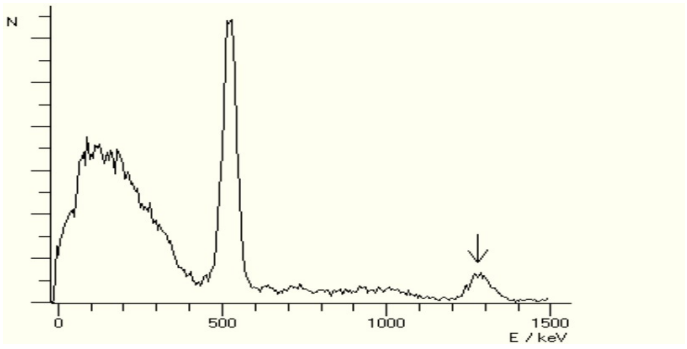

Figure 4.10: The example of Sodium-22 energy spectrum [9].

The left figure of Fig. 4.11 shows the scintillation spectrum of LYSO radiated by

doi:10.6342/NTU202300991

old Sodium-22. It can be seen that LYSO intrinsic spectrum exists obviously as the background since the activity of old Sodium-22 and small-size LYSO are similar. Fortunately, the 511 keV peak can still be distinguished. The right figure of Fig. 4.11 shows the fitting to get the light yield of LYSO at 511 keV by old Sodium-22, and it is 87180 ± 238 ADC in this example. The left figure of Fig. 4.12 shows the scintillation spectrum of LYSO under the radiation by new Sodium-22 source. This time LYSO intrinsic spectrum is negligible since the activity of new Sodium-22 is much higher than small-size LYSO, so the spectrum is close to the standard Sodium-22 energy spectrum. The right figure of Fig. 4.12 shows the fitting to get the light yield of LYSO at 511 keV by new Sodium-22, and it is 87120 ± 29.9 ADC in this example.

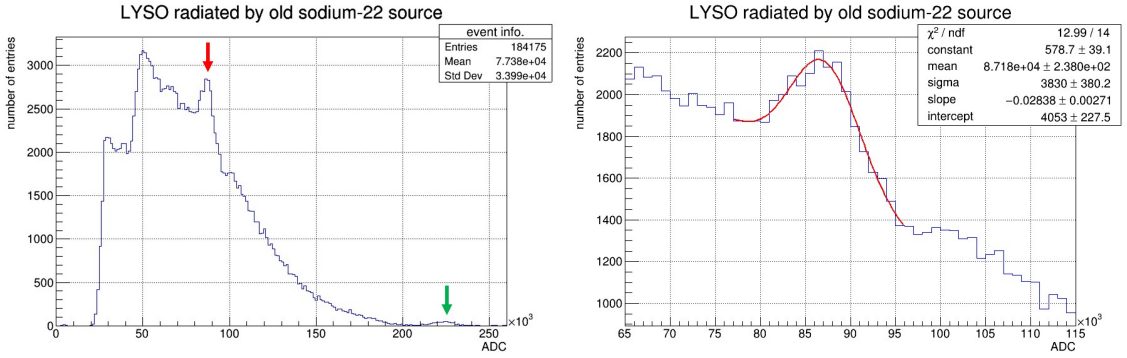

Figure 4.11: The light yield measurement by old Sodium-22 source. The left figure points out the (511, 1275 keV) peaks by arrows. The right figure is fitting to get the light yield of LYSO at 511 keV.

The above examples from a successive test show the light yield results by two Sodium-22 source are consistent. However, the high activity of new Sodium-22 can make the scintillation spectrum less affected by LYSO intrinsic spectrum and can accumulate more data in the same time. I will use the new Sodium-22 as the external radioactive source to study the light yield of LYSO at 511 keV.

doi:10.6342/NTU202300991

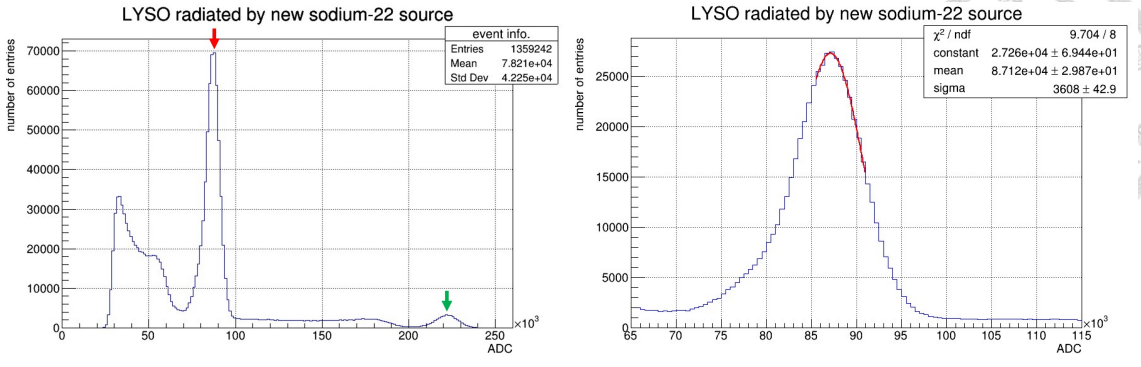

Figure 4.12: The light yield measurement by new Sodium-22 source. The left figure points out the (511, 1275 keV) peaks by arrows. The right figure is fitting to get the light yield of LYSO at 511 keV.

4.4 The light yield measurement

In this section, I will introduce the light yield of LYSO obtained from the standard measurement process I designed. This standard measurement process is decided after a series of systematic tests. I will first introduce what these systematic items can be improved or how they will affect the light yield, and finally light yield of our LYSO sample under the standard measurement process.

I try my best to make the measurements of the same group of systematic items on the same day, but due to the limited time of day, different groups of systematic items will be measured on different days. Therefore, I will perform LED calibration before the start of each experiment, and calculate the light yield based on the calibration result. My formula for calculating light yield:

$$\begin{aligned} &\text{Spectrum peak (number of photoeletron)} = \\ &\text{Spectrum peak (ADC)} \div \text{single photoelectron (ADC/photoelectron)} \\ &\times \text{high voltage factor} \end{aligned} \tag{4.1}$$

doi:10.6342/NTU202300991

How to obtain single photoelectron and high voltage factor has been explained in Sec. 3.3.1 and 3.3.2 respectively. I will use the number of photoelectrons to express light yield in Sec. 4.4.1 to Sec. 4.4.3 and convert to the number of photons at the end of Sec. 4.4.5.

4.4.1 Cross section

Many references show that many crystals have significant self-absorption, because the scintillation light may interact in the crystal before reaching the light output surface. In the test of [10], a LYSO sample with size 13 mm × 13 mm × 30 mm is used for the light yield measurement. The light yield results by setting two kinds of the area as output cross-section, which are 13 mm × 13 mm and 13 mm × 30 mm, can reach a 48% difference. This shows that when the long side of the crystal is aligned with the radioactive source, the scintillation light can be generated farther away from the output cross-section, and it is more likely to be self-absorbed and cause the light yield decline.

The light yield measured by the naked crystal is too small, so I measure under the conditions of being wrapped with four layers of seal tape without optical grease. Fig. 4.13 shows the difference between the small cross-section and the large cross-section for the LYSO I used, which size is 3 mm × 3 mm and 3 mm × 20 mm. It can be seen that the light yield at 511 keV of the small cross-section case is smaller than the large cross-section case. If I repeat five times measurement with seal tape rewrapping, the different cross-section results are recorded in table 4.1. The light yield difference between them can reach 86.58%. This makes the short side should be used for the longitudinal side of PMT window that makes the light loss from self-absorption becomes smaller, so large cross-section should be used as the light output surface to contact the PMT window.

doi:10.6342/NTU202300991

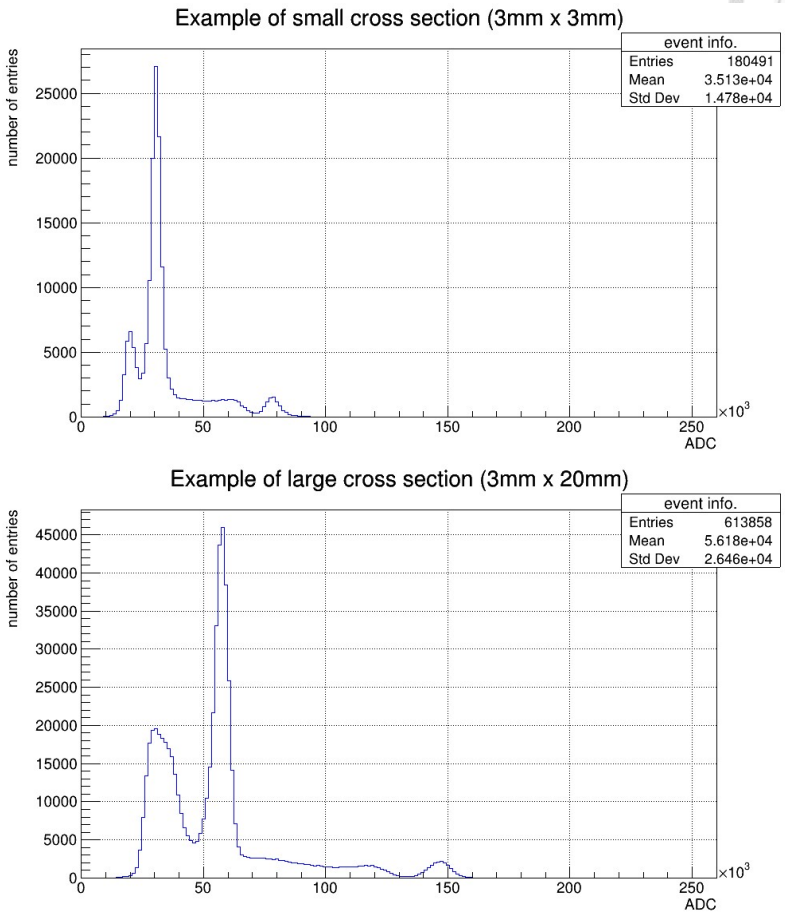

Figure 4.13: The example to demonstrate the light yield difference of small cross-section (upper figure) and large cross-section (lower figure).

Cross section	Small (3 mm × 3 mm)	Large (3 mm × 20 mm)
511 keV (number of p.e)	1208.17	2254.25
uncertainty (number of p.e)	20.00	58.69
Relative error σ/μ (%)	1.66	2.60

Table 4.1: The light yield from five times measurements of different cross-section.

doi:10.6342/NTU202300991

In addition, I have also carried out the measurement of four different large cross sections (3 mm × 20 mm) of LYSO I used, and the results are shown in Table 4.2. The light yield differences measured in the other three cross sections are all within 3% as the result of the first cross-section being the benchmark. Because all surfaces of this LYSO sample have been well polished, the light yield of four different large cross sections can be consistent. However, I will still use the same cross-section, which is the 1st cross-section in Table 4.2, for all other measurements.

Large cross section (3 mm × 20 mm)	1*st* (used for all other tests)	2*nd*	3*rd*	4*th*
511 keV (number of p.e)	2216.02	2203.13	2260.16	2272.27
%	100	99.42	101.99	102.54

Table 4.2: The light yield from four different large cross-section measurements.

4.4.2 Seal tape

A good covering material should reflect more scintillation light that except the light-emitting surface and has high reflectivity at near 400 nm wavelength for LYSO. There are some candidates for covering materials before deciding to use seal tape as the covering material, and I put them in Append. A.5. Their performance is not significantly better than seal tape, and considering the convenience of wrapping the crystal, I finally choose seal tape as the covering material.

To decide how many layers of seal tape should be used to wrap the crystal, I measure the reflectivity of the three sets of seal tapes we have, which are most of the seal tapes used

doi:10.6342/NTU202300991

in this thesis. Fig. 4.15 is their appearance, and Fig. 4.16 is their reflectivity respectively. It can be seen that both of the wavelength decreases and the number of layers increases, and the reflectivity increases, which consists with the characteristics of PTFE that are mentioned in [11]. The significant change region of reflectivity is from one layer to three layers. The reflectivity at nearly 400 nm is all about 90% or above for the three layers above.

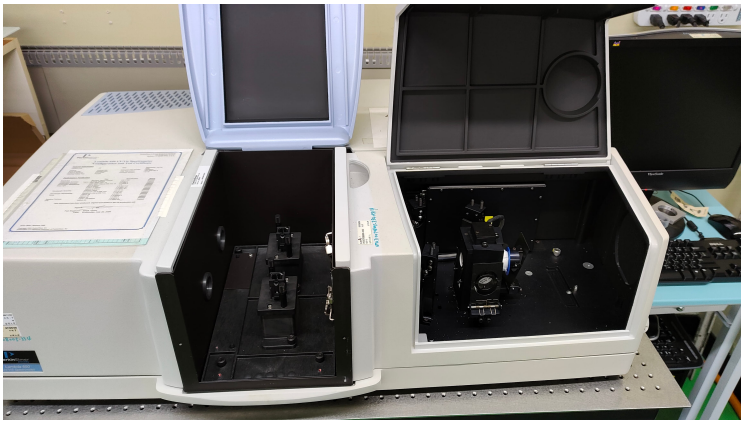

Figure 4.14: The spectrometer lambda 650 from PerkinElmer.

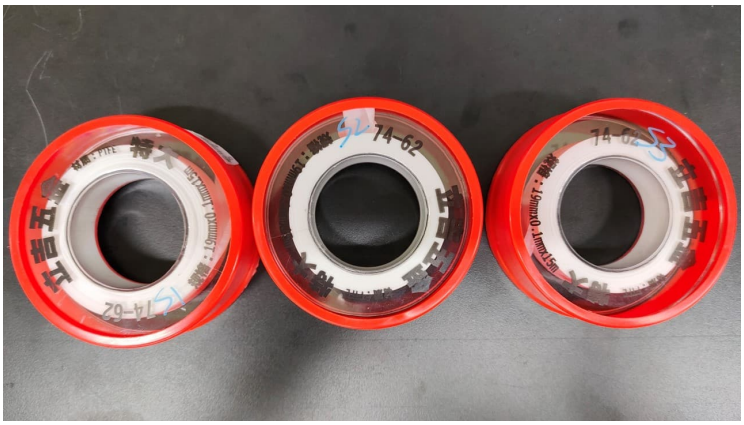

Figure 4.15: Three rolls of seal tapes were used in most of the measurements in this thesis. Mark S1, S2, and S3 respectively from left to right.

If I repeat five times experiments for each number of wrapping layers from one to six, the results are recorded in Table 4.3. The light yield increases as the number of wrapping layers increases, and the increase in light yield slows down significantly as the three layers above (Fig. 4.17). Although a high number of wrapping layers can still increase the light

doi:10.6342/NTU202300991

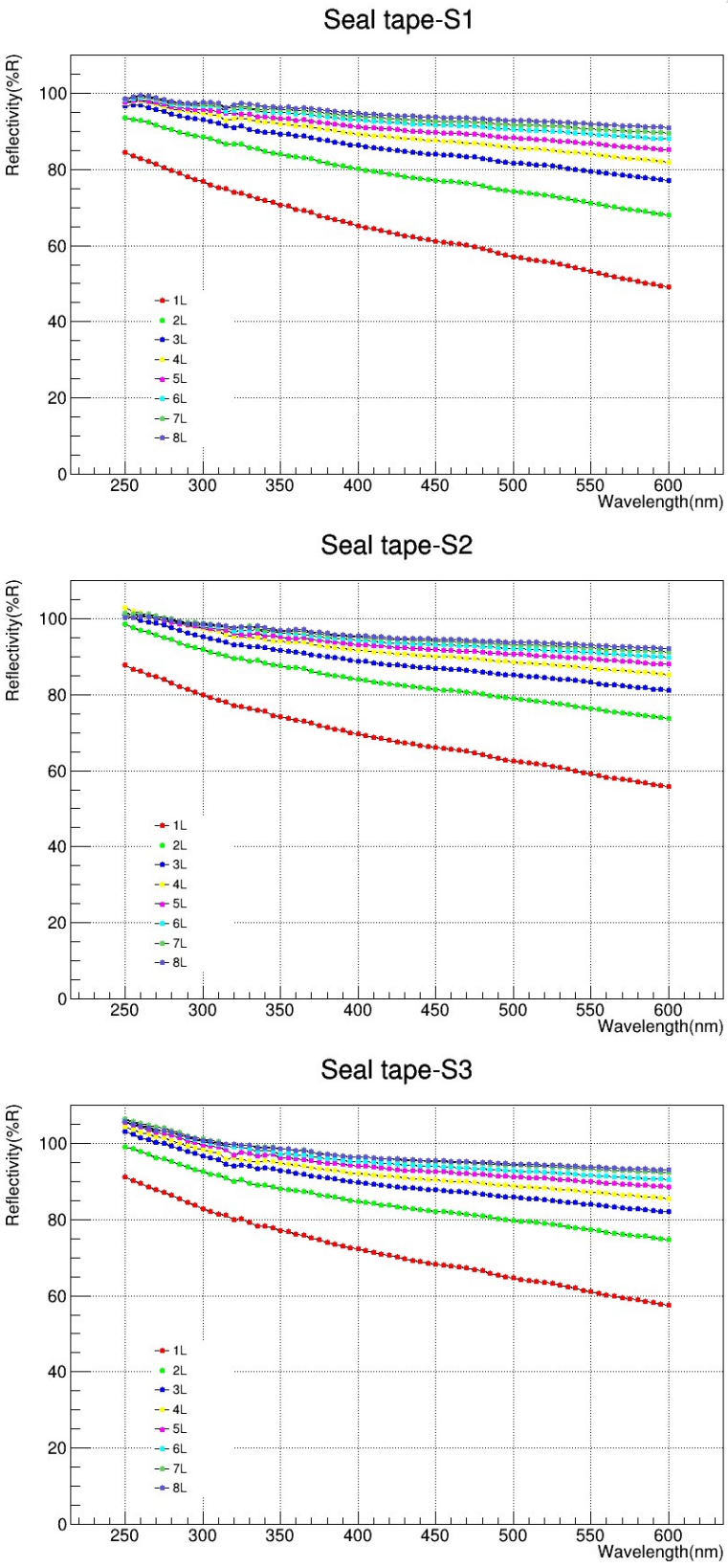

Figure 4.16: The reflectivity from one layer to eight layers of the three rolls of seal tapes. The title name corresponds to the mark of each seal tape.

doi:10.6342/NTU202300991

yield, the benefit is limited and the uncertainty becomes larger. Combined with the results of reflectivity, I finally choose "four layers" as the number of wrapping layers of seal tape in the standard measurement process.

Wrapping layers	1	2	3	4	5	6
511 keV (number of p.e)	1877.73	2002.44	2179.28	2254.25	2273.97	2291.19
uncertainty (number of p.e)	85.63	123.20	66.27	58.69	56.61	140.76
Relative error σ/μ (%)	4.56	6.15	3.04	2.60	2.49	6.14

Table 4.3: The light yield from the five times measurements of different layers of seal tape wrapping.

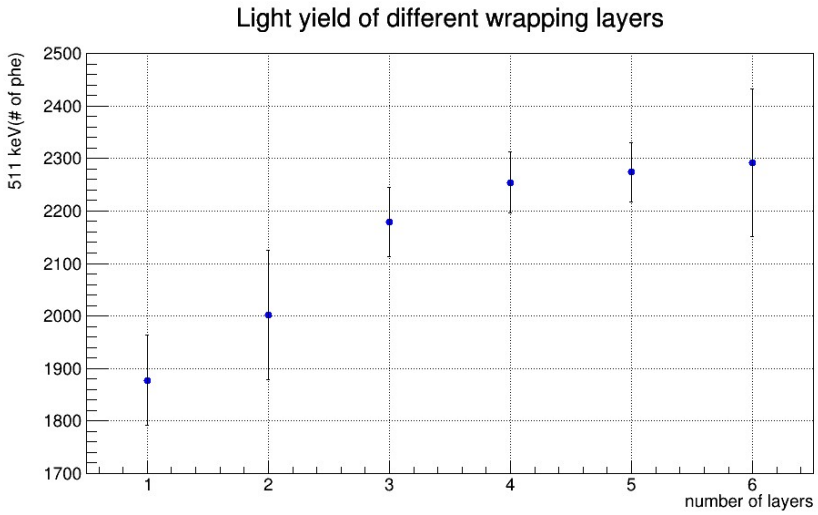

Figure 4.17: The plot of light yield and uncertainty from Table 4.3.

doi:10.6342/NTU202300991

4.4.3 Optical grease

Fig. 4.18.a shows various possible light paths between the scintillation light and photocathode of PMT [12]. The use of optical grease between the scintillator and the detector interface has several advantages. It makes scintillation light can exit the crystal with a larger angle of refraction than in the case of the scintillator-air interface, which reduces the light trapping in the scintillator and leads to light losses by self-absorption (Fig. 4.18.b). It also makes the photons can enter the PMT window with a larger angle than in the case of the air-glass interface, which may lead to the light trapping in the window-photocathode substrate (Fig. 4.18.c), and the multiple interactions with photocathode can enhance *QE*. The basic information of the optical grease I used is mentioned in Sec. 4.2.3.

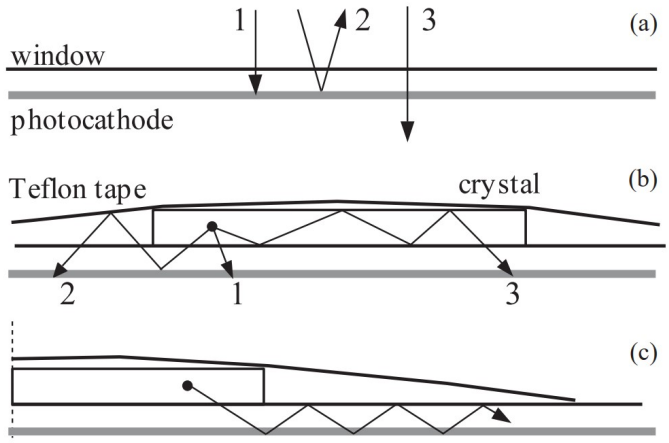

Figure 4.18: (a) The incident (1), reflected (2) and transmitted light (3) at a photocathode. (b) Direct absorbed (1), back reflected (2) and trapped (3) scintillation light. (c) Multiple internal reflected light in window/photocathode substrate.

Fig. 4.19 shows the difference between the use of optical grease or not. It can be seen that the light yield at 511 keV of the case not using optical grease is smaller than the case using optical grease. If I repeat five times measurements with four layers of seal tape wrapping, the results of using optical grease or not are recorded in Table 4.4. The light

doi:10.6342/NTU202300991

yield difference between them can reach 35.18%. This shows that it is necessary to use optical grease for optical coupling in the light yield measurement of LYSO.

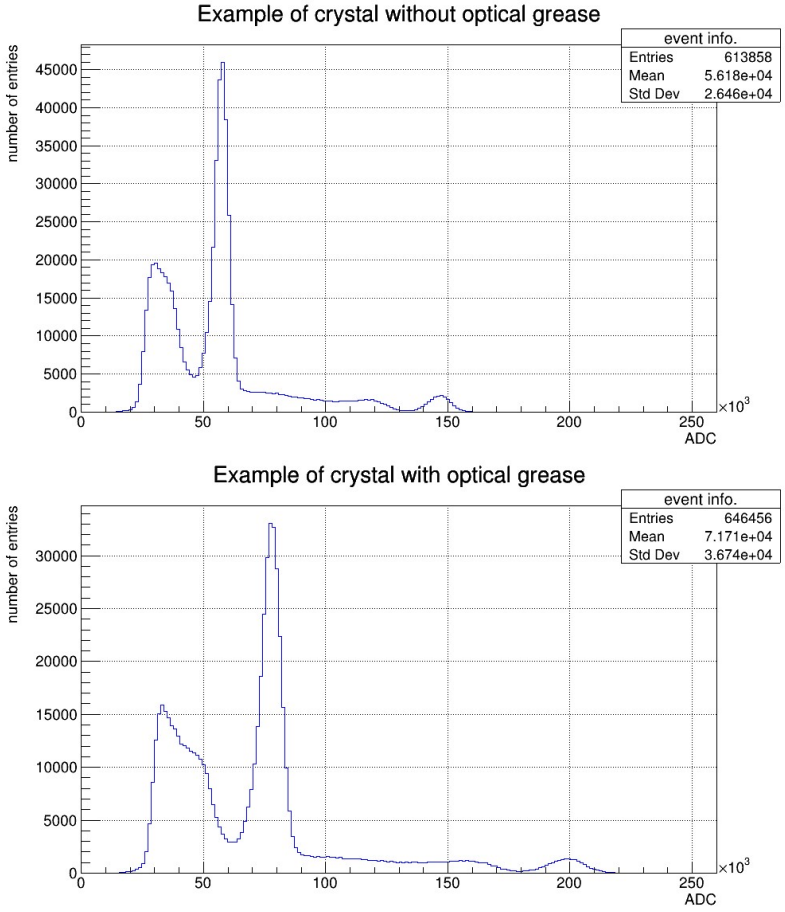

Figure 4.19: The energy spectrum to demonstrate the light yield difference of not using optical grease (upper figure) or using optical grease (lower figure).

4.4.4 Change over time

During the experiments, I also found that the measured light yield will gradually decrease with PMT operation. All the measurements in this subsection is 4 hours, and taken every 5 minutes as a data point. Each data point will plot at the end time of each data (i.e $0 \sim 5$ minutes plot at 5 minutes, $25 \sim 30$ minutes plot at 30 minutes), and set the result of $0 \sim 5$ minutes as 100%.

doi:10.6342/NTU202300991

Optical grease	Without	With
511 keV (number of p.e)	2254.25	3047.34
uncertainty (number of p.e)	58.69	147.13
Relative error σ/μ (%)	2.60	4.83

Table 4.4: The light yield from five times measurements of using optical grease or not.

Start with the unbaked case, which means start measuring immediately after turning on PMT to the working voltage. A total of four different measurements are shown in Fig. 4.20. We can see all of them indicate the light yield keeps decreasing with time and the decline magnitude getting smaller with time. To check the light yield decrease is not caused by LYSO, I also tried a high light level result by LED. Fig. 4.21 is the peak value of a high light level result every 5 minutes for a total of four hours. The light intensity by LED also keeps decreasing with time and the decline magnitude is getting smaller with time.

Based on the experience of some seniors, I try to ”bake” the PMT, that is, turn on the working voltage with a dark room condition for a while before starting measurements. If I bake the PMT more than 30 minutes, then carry out the same process mentioned above. A total of four different measurements are shown in Fig. 4.22. This time we can see except for the early time such as the first 10 minutes, the light yield is almost stable in the long time. This confirms the light yield drop caused by the PMT operation will be gradually stabilizing with the power-on time. The above three cases are all without optical grease. However, if I carry out the case with bake also applied with optical grease, then measure the same process mentioned before. A total of four different measurements are shown in Fig. 4.23. The light yield decreases with time, and the decline magnitude seems closer

doi:10.6342/NTU202300991

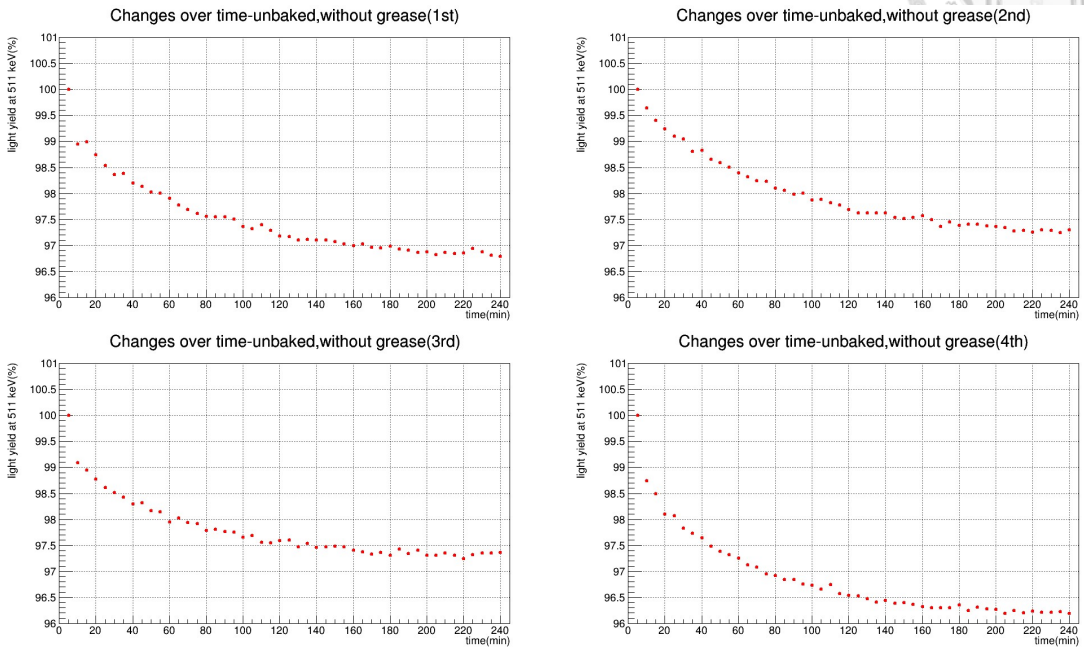

Figure 4.20: The different four times measurements of the light yield change over time under the unbaked condition without optical grease.

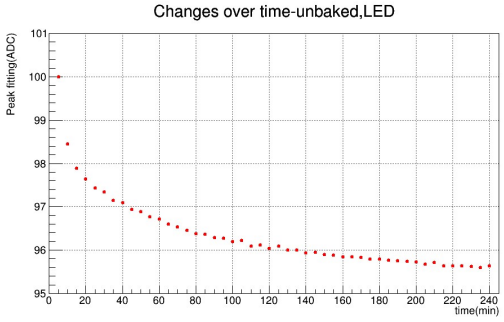

Figure 4.21: The peak value of a high light level result change over time

doi:10.6342/NTU202300991

to the linear relationship. The possible reason is that optical grease ”infiltrates” the seal tape, making the seal tape more transparent and reducing reflectivity (Fig. 4.24).

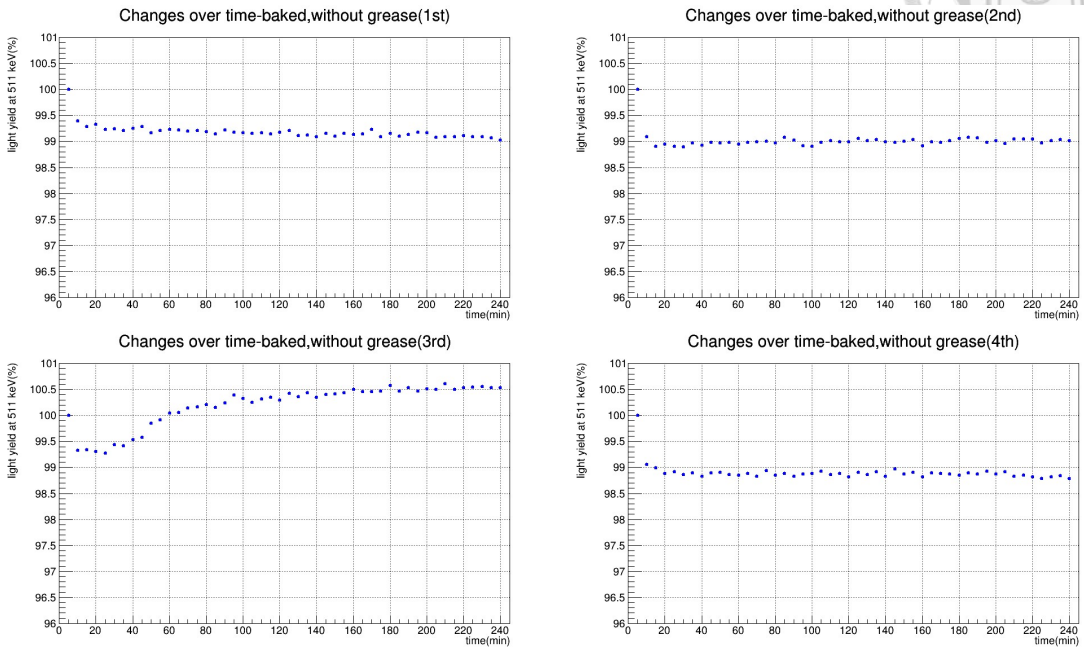

Figure 4.22: The different four times measurements of the light yield change over time under the baked condition without optical grease.

In addition to the light yield decrease over time, another important thing is to know that PMT is most unstable when it turns on to the working voltage. No matter what kind of case, the first period, that is, 0 to 5, or even 10 minutes, is the interval where the result changes most drastically. In summary, for any measurements, we should bake PMT for enough time, and wait for a while not too long after the PMT is turned on to the working voltage. These can reduce the effect of light yield changes over time. My suggestion is that the baking time and waiting time are both 30 minutes, and I quote 1% of the systematic error in the light yield at 511 keV results of the standard measurement process.

doi:10.6342/NTU202300991

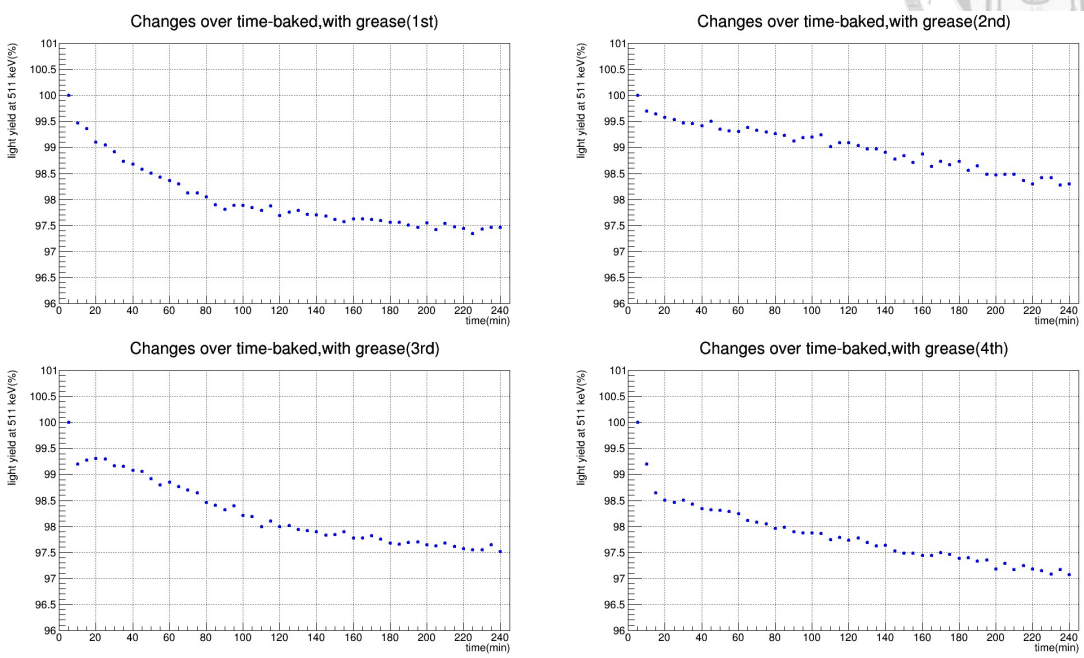

Figure 4.23: The different four times measurements of the light yield change over time under the baked condition with optical grease.

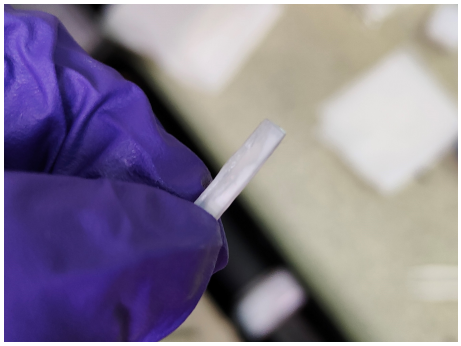

Figure 4.24: The photo that optical grease infiltrates seal tape.

doi:10.6342/NTU202300991

4.4.5 Standard process

From Sec. 4.4.1 to Sec. 4.4.4, we understand the light yield difference caused by these systematic items. Therefore, I design the following standard process to measure the light yield of our LYSO sample:

(1) Place LED calibration setup. Turn on the high voltage to 2500 V, then short time test to find the proper setting of the standard low light level result and high light level result.

High voltage = 2500 V is the working voltage I use to measure single photoelectron. How to adjust the setting to reach the standard low light level result has been mentioned in Sec. 3.3.1. In terms of the high light level, I choose to take the results that "statistical mean around 20000 ADC", which represents the light intensity of about 10 photoelectrons.

(2) Baking PMT for 30 minutes. Low light level measurement for 5 minutes, then high light level measurement for 5 minutes.

(3) Down to high voltage at 1500 V, wait for 5 minutes then high light level measurement for 5 minutes.

High voltage = 1500 V is the working voltage I use to measure the light yield of LYSO. Waiting for 5 minutes is to make sure the high voltage supply output is stabilized.

(4) Turn off high voltage. Place light yield measurement setup, then turn on the high voltage at 1500 V, waiting for PMT for 30 minutes.

(5) LYSO light yield measurement under the conditions that wrap four layers of seal tape, use cross section 3.0 mm $\times$ 20.0 mm, and applied optical grease to contact the PMT

doi:10.6342/NTU202300991

window.

Each measurement from a standard measurement process can give out a group of results, including ”single photoelectron”, ”high voltage factor”, ”light yield of LYSO at 511 keV” to calculate the ”light yield of LYSO per keV in the number of photoelectrons”. After establishing the standard measurement process, I accumulated ten groups of results. Each of them is separated by a week or longer, and the total period is nearly three months. Table 4.5 is the mean and statistical error of single photoelectron, high voltage factor, and light yield of LYSO at 511 keV obtained by each standard measurement process. Table 4.6 is the mean, uncertainty, and relative error of the above items calculated from these ten groups of results. The relative error of single photoelectron, high voltage factor, and light yield of LYSO at 511 keV are calculated by the uncertainty divided by the mean. The relative error of light yield of LYSO in the number of photonelectrons per keV use the total error divided by mean. The total error $\sigma_{total} = \sqrt{\sigma_{sys.}^2 + \sigma_{stat.}^2}$, where $\sigma_{sys.}$ is the systematic error and $\sigma_{stat.}$ is the uncertainty divided by $\sqrt{10}$, and use the uncertainty of these three items to become the source of systematic error. It can be seen that the relative error of all measured items is within 5%. I think these results show that the standard measurement process is reliable and stable enough.

We know that the difference between number of photons and number of photoelectrons comes from quantum efficiency, so the formula derived from 4.1:

$$\begin{aligned}&\text{Spectrum peak (number of photon)} = \\ &\text{Spectrum peak (number of photoelectron)} \div \text{QE (photoelectron/photon)}\end{aligned} \tag{4.2}$$

. Most of the information shows that the LYSO emission maximum is at 420 nm, but the overall wavelength distribution I found seems not narrow (Fig. 4.25) [13]. Based on

doi:10.6342/NTU202300991

Day	1*st*	2*nd*	3*rd*	4*th*	5*th*
Single p.e (ADC)	1856 ± 10.19	1933 ± 4.03	1820 ± 9.80	1845 ± 5.14	1837 ± 11.88
HV factor (a.u.)	73.60 ± 0.15	72.03 ± 0.15	73.65 ± 0.15	73.27 ± 0.15	73.15 ± 0.15
511 keV (ADC)	74270 ± 15.59	76990 ± 14.93	69660 ± 12.29	74330 ± 14.39	72940 ± 13.67
Day	6*th*	7*th*	8*th*	9*th*	10*th*
Single p.e (ADC)	1792 ± 12.07	1830 ± 12.49	1792 ± 12.70	1827 ± 11.22	1861 ± 9.47
HV factor (a.u.)	73.23 ± 0.15	73.38 ± 0.14	74.64 ± 0.16	72.62 ± 0.14	74.74 ± 0.16
511 keV (ADC)	76110 ± 14.61	76100 ± 13.10	75510 ± 14.66	73550 ± 23.27	75600 ± 17.9

Table 4.5: Each piece of information under the standard measurement process on different days.

	Single p.e (ADC)	HV factor (a.u.)	511 keV (ADC)	Number of photoelectrons per keV
Mean	1839.30	73.43	74506	5.82
Uncertainty	40.25	0.82	2119.37	0.07
Systematic error				0.24
Relative error (%)	2.19	1.11	2.84	4.10

Table 4.6: The mean, uncertainty, and relative error among these ten groups of results.

doi:10.6342/NTU202300991

this distribution, I take the emission intensity every 10 nm with an accuracy of 1 a.u and give an estimate of 0.5 a.u. I took the quantum efficiency of R329-02 (Fig. 3.3) every 10 nm with an accuracy of 1% and gave an estimate of 0.5%. By the weighted average of emission intensity and quantum efficiency from 350 nm to 650 nm, I get quantum efficiency $= 19.5 \pm 0.5\%$, and this means the number of photons will be 5.13 ± 0.13 times the number of photoelectrons. The light yield of our LYSO sample in my measurement is 29.86 ± 0.97 photons per keV, and this is only 0.47% different from the 30 photons per keV recorded in standard LYSO. However, there is a difference of 9.52% between the 33 photons per keV recorded in the datasheet of Taiwan Applied Crystal Company [8] (also the manufacturer that provides emission intensity distribution [13]).

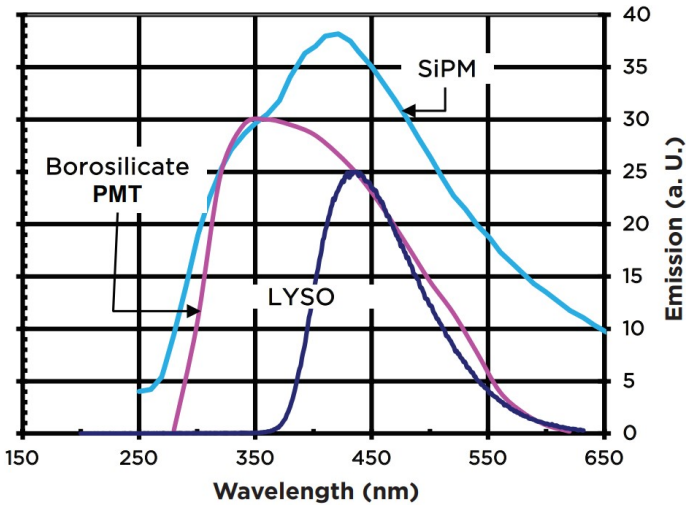

Figure 4.25: The scintillation wavelength distribution of LYSO (Borosilicate PMT and SiPM in this figure have nothing to do with my experiment) [13].

4.4.6 Discussion

For my current system, there are still several issues that will cause light loss or difference when converting the light yield in the number of photons. First, I mentioned in Sec. 4.4.1 that light loss from self-absorption comes from the thickness (length of the lon-

doi:10.6342/NTU202300991

gitudinal side to the PMT window). For the large cross-section case, the sample still has a thickness of 3 mm, resulting in a small amount of self-absorption. A possible solution is to measure several samples with the same output cross-section but different thicknesses, and use extrapolation to infer the light yield of thickness = 0 mm case. Second, I give the reason why four layers are finally selected as enough wrapping layers in Sec. 4.4.2. However, the light yield still increases for five and six layers shows the seal tape is still not collecting the maximum amount of reflected light. If we can find the details for the higher uncertainty of high number of layers and reduce them, then light yield can slightly increase by the high number of layers measurement. Then, there is still a significant gap between the refractive index = 1.46 of the optical grease I used and the refractive index = 1.7 of LYSO. Using a higher refractive index of optical grease can further improve the light yield in theory, or need to try several refractive indexes to find out the best solution. Finally, the scintillation wavelength distribution of LYSO and the quantum efficiency distribution of PMT are both from the datasheet. They might be different from the real situation, resulting in different quantum efficiency than my system.

Even the combination of the new Sodium-22 source and large size LYSO still cannot scintillate enough light amount that is visible in a dark room, we need a higher activity external radioactive source to produce more scintillation light if we want to measure the scintillation wavelength distribution of LYSO by a spectrometer. Although the center of the sample and external source are aligned with the center of the PMT window, the quantum efficiency to wavelength of our PMT, and even the contribution by the different photon incident positions need to be measured. There are some measurements about quantum efficiency and photocathode uniformity of PMT I found in [14] and related literature, and I will introduce its main content in Append. A.6.

doi:10.6342/NTU202300991

These may be the factors that light yield in my measurement cannot agree with the nominal value, and completing these works will be improved for the future research on absolute light yield measurement.

doi:10.6342/NTU202300991

Chapter 5

Setup & Measurements on polarized single photon

5.1 Introduction

In Chap. 3, we introduced how to obtain low light level results through the combination of PMT and LED, which is very likely to be a single photon candidate. In this chapter, I will start with the concept of LED calibration setup to build another setup for the extension study of polarized single photon.

5.2 Setup

Fig. 5.1 shows the polarized single photon setup. From left to right in the figure above, they are LED, two polarizers, and finally PMT. They are all built on a support and placed in a black box. The function generator, high voltage power supply, and digitizer are all the same. The following subsections will explain the operation and usages of the

doi:10.6342/NTU202300991

components different from the LED calibration setup.

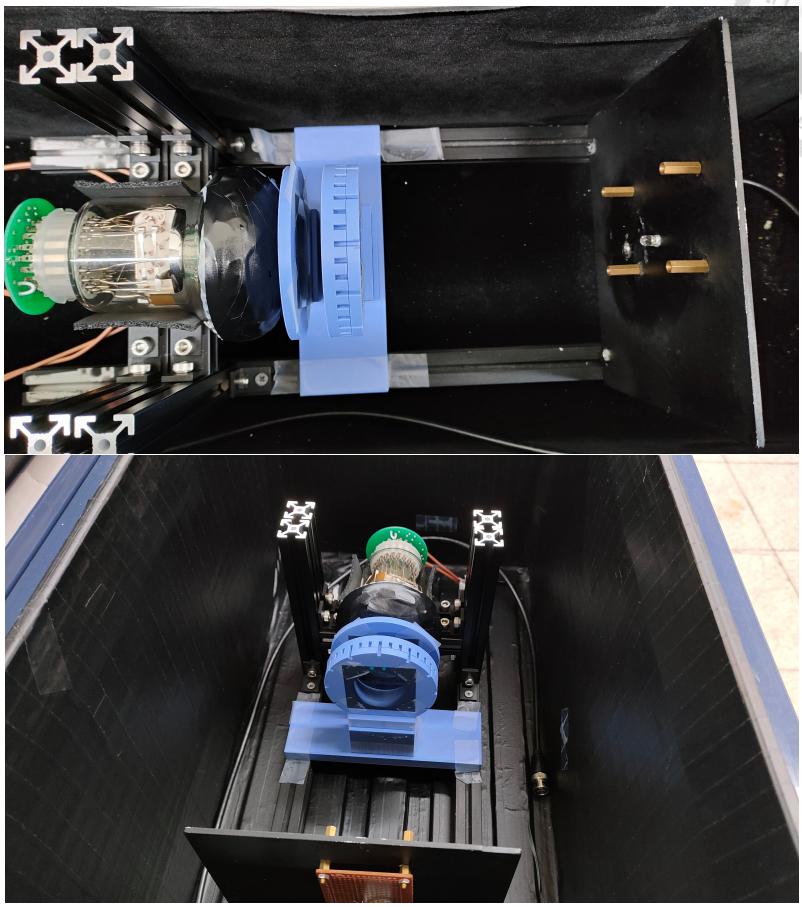

Figure 5.1: The polarized single photon setup, from different perspectives.

5.2.1 Light sensor-HZC XP72B20

Because I want to calculate the exact light amount during the measurement. The PMT used for polarized single photon study needs to have better photoelectron resolution. This means that the peaks of several photoelectrons representing single, double, triple... in low light level spectrum must be more obvious and narrower. On the other hand, there is no geometry restriction of the PMT window.

HZC XP72B20 showed better photoelectron resolution in tests and was selected as the light sensor in the polarized single photon study. The basic size and appearance infor-

doi:10.6342/NTU202300991

mation of XP72B20 is shown in Fig. 5.2. The wavelength response, gain to high voltage curve, and some sensitivity information is shown in Fig. 5.3.

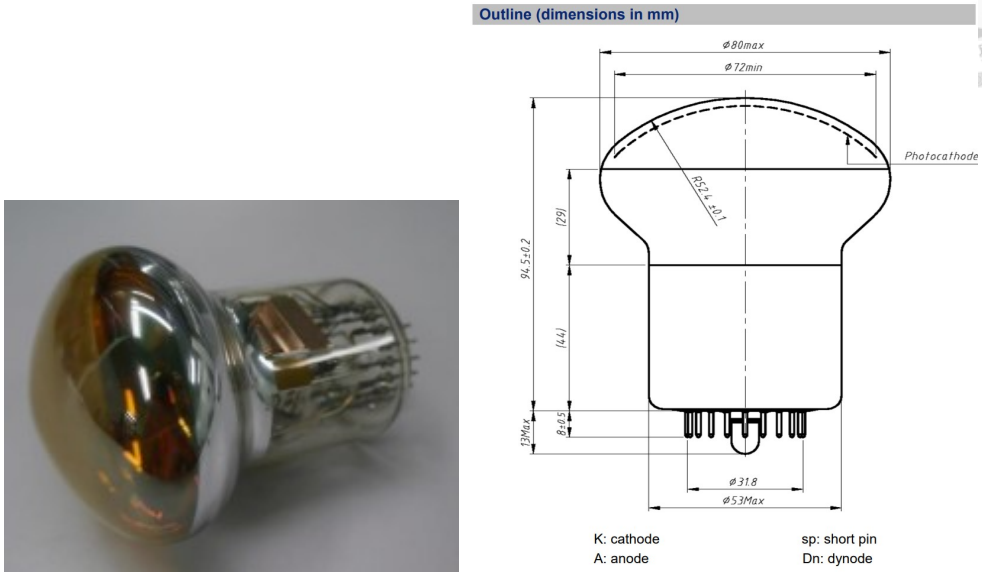

Figure 5.2: The appearance and dimensional outline of XP72B20.

To make sure the photon must pass through the combination of polarizers and then incident into PMT, the surface of XP72B20 will be wrapped with black tape until the exposed area is smaller than the area of the polarizers, as shown in Fig. 5.4.

5.2.2 Polarizers and other components

To produce polarized photon, I imitate the classical polarization experiment, a combination of a non-rotatable polarizer and a rotatable polarizer also called analyzer. Fig. 5.5(a) shows two polarizers pasted on the plate and placed on the base. 5.5(b) demonstrate how to rotate the angle of the analyzer. The plate of the analyzer and the base have several teeth as the angle basis, and the resolution $= 10°$.

To fit the size of the components I used, I made a stand to place LED, polarizers and PMT, as shown in Fig. 5.6(a). The size of the stand is 38.0 cm $\times$ 15.5 cm $\times$ 17.0 cm. I

doi:10.6342/NTU202300991

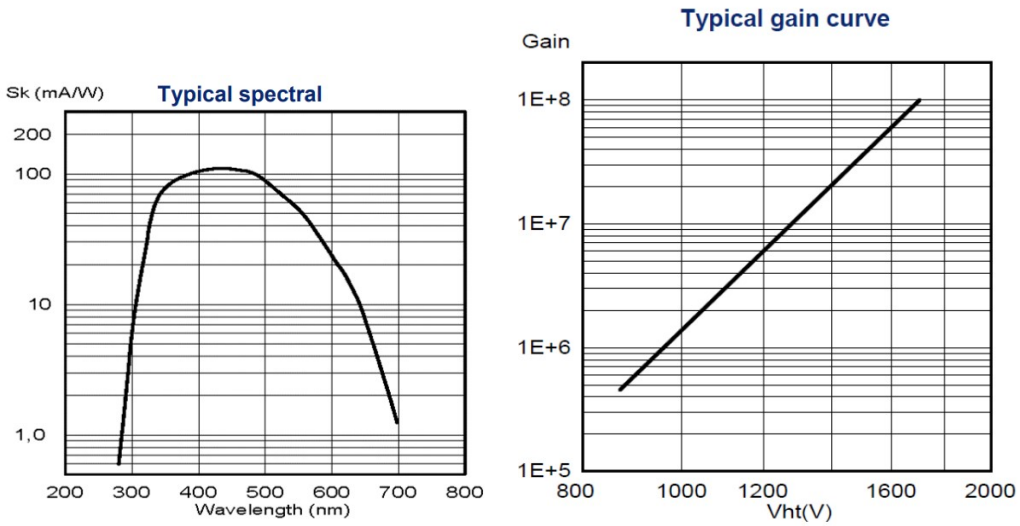

Photocathode characteristics	Min	Typ	Max	Unit
Spectral range:		290-700		nm
Maximum sensitivity at		404		nm
Sensitivity:				
Luminous		110		μA/lm
Blue *	10	12		μA/lmF
Quantum Efficiency, at 404 nm	25	28		%
Quantum Efficiency, at 470 nm	18	20		%

Figure 5.3: The spectral response to wavelength, gain to supply voltage, and some sensitivity information of XP72B20.

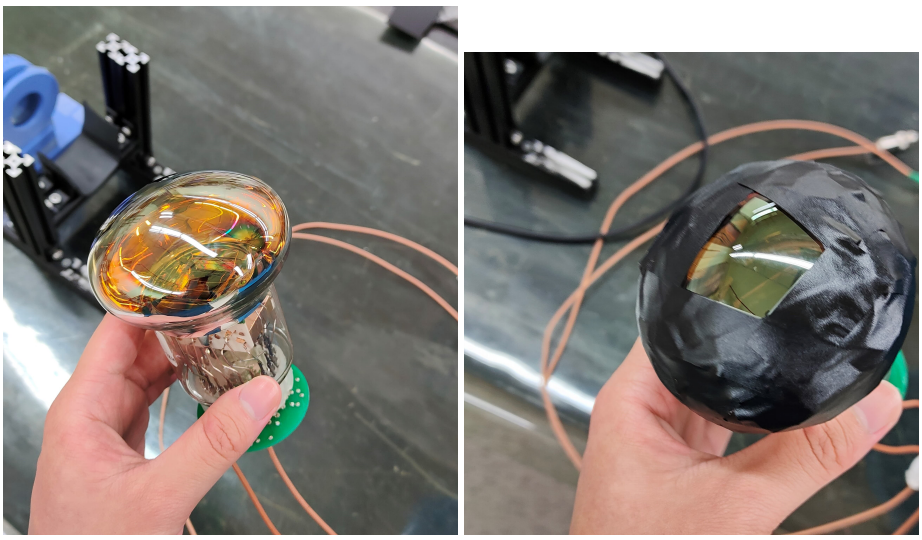

Figure 5.4: Wrap the light-sensing area of the PMT surface with black tape to be smaller than the area of polarizers.

doi:10.6342/NTU202300991

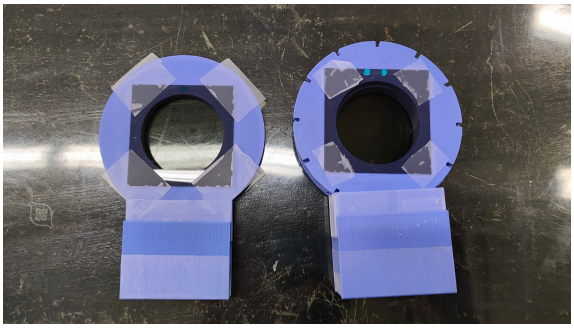

(a) The polarizer (left one, non-rotatable) and the analyzer (right one, rotatable).

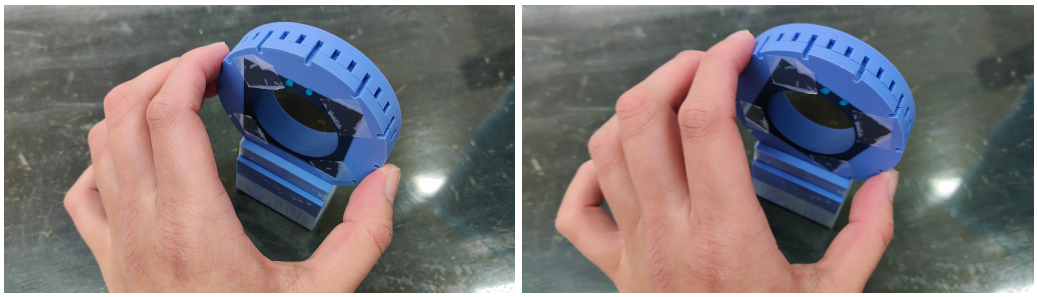

(b) The example figures of how to rotate the analyzer by 20°.

Figure 5.5: The polarizers and their operation.

also need a black box to place our stand, as shown in 5.6(b). The size of the black box is 58.0 cm × 33.5 cm × 35.0 cm, with several layers of black tape paste inside to prevent light leakage and drill a hole in a corner of the box (5.6(c)) to let cables can pass through the black box. To match the maximum quantum efficiency of PMT XP72B20 for better photoelectron conversion, I choose a 400 nm LED fixed on this stand as the light source (Fig. 5.7).

5.3 Results of polarized photon

In the polarized single photon study, I produce two kinds of results: extremely low light level and low light level. In extremely low light level results, I observe whether the very weak light intensity can still change with polarization angle, and evaluate the rationality of intensity change. In low light level results, I use the intensity change with

doi:10.6342/NTU202300991

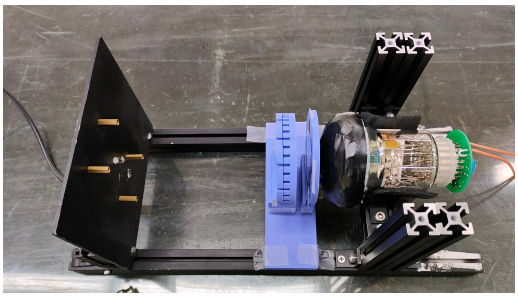

(a) The appearance of each component is place on the stand.

(b) The appearance of the black box.

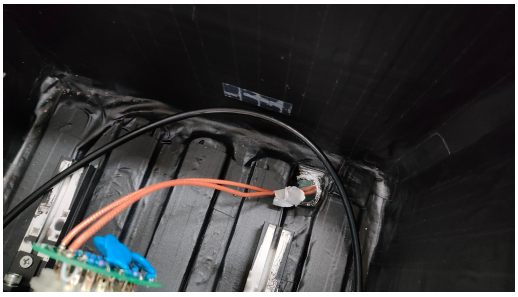

(c) The drilled hole to let cable pass through the black box.

Figure 5.6: Instructions for use of the black box.

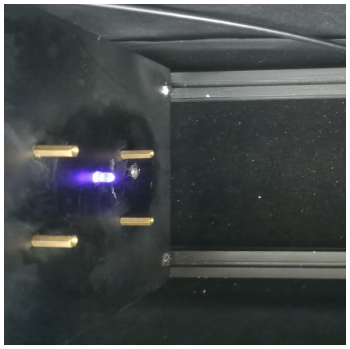

Figure 5.7: The example of LED lighting (not the case during the experiment).

doi:10.6342/NTU202300991

polarization angle to confirm the photon intensity model of LED described in Chap. 2, and that makes us can quickly obtain the low light level intensity.

In my setup, I do not know the absolute angle between the polarizer and the analyzer, so all the recorded angle θ is the angle of the analyzer compared to its base in the clockwise direction. I will measure the results under the analyzer at several different angles θ and refer to the classical model: $\cos^2\theta$ to get the light amount fitting function:

$$P(\theta) = p_0 \cdot \cos^2(\theta - p_1) + p_2 \tag{5.1}$$

, where p_0 is scale coefficient, p_1 is phase constant, and p_2 is shift constant. I will check whether the total amount of light received during the experiment conforms to this fitting function under several methods.

5.3.1 Extremely low light level

The extremely low light level result is the special case of low light level result that only single photoelectron peak can be seen. Fig. 5.8 shows the extremely low light level spectrum I measured in several different angles under the same LED setting. It can be seen that the peak intensity is smaller as close to 90°, and larger as close to 0° or 180°. This consists with the trend of $\cos^2\theta$ in the classical mode. Determining the light intensity at different polarization angles requires calculating the total light amount received during the measurement, and I did this in two ways.

The first way is to define single to quadruple photoelectron value and their resolution, and I will use the same method in LED calibration to take a standard low light level spectrum (Fig. 5.9) and use four Gaussians fitting result to define the mean: Q_1, Q_2, Q_3, Q_4

doi:10.6342/NTU202300991

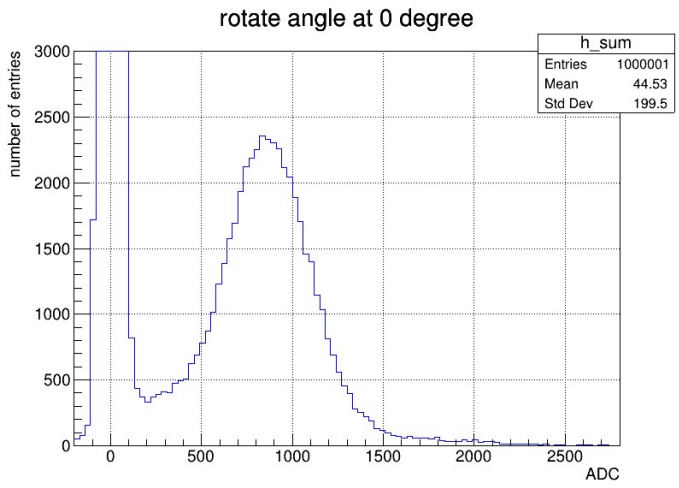

(a) analyzer angle = 0°

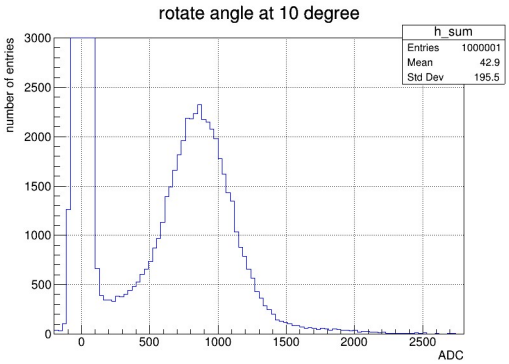

(b) analyzer angle = 10°

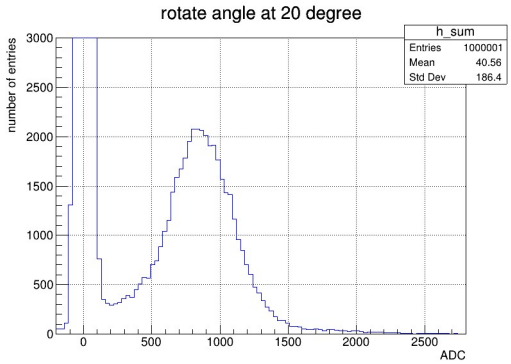

(c) analyzer angle = 20°

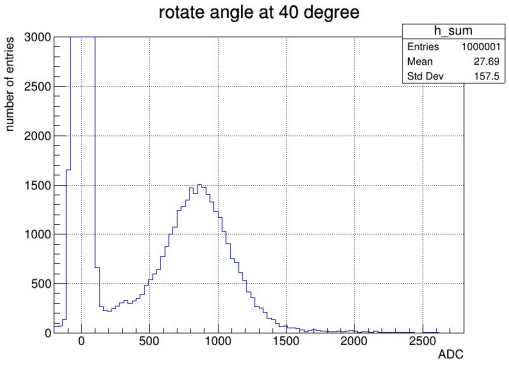

(d) analyzer angle = 40°

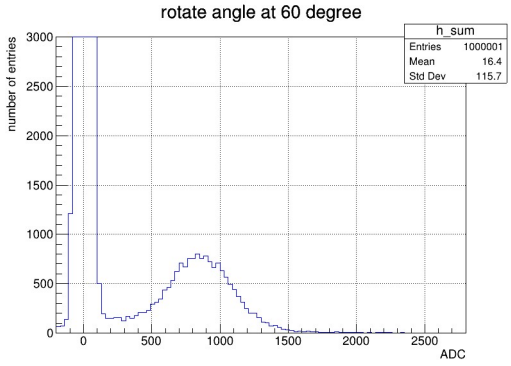

(e) analyzer angle = 60°

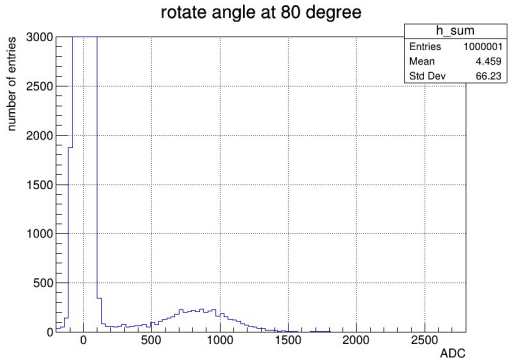

(f) analyzer angle = 80°

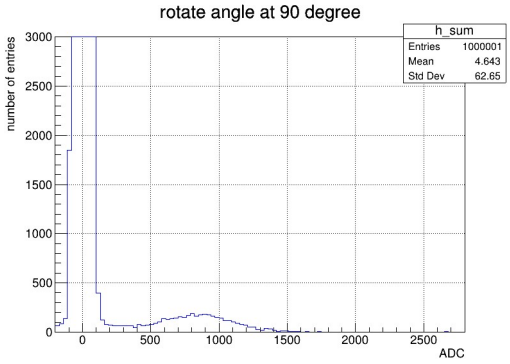

(g) analyzer angle = 90°

doi:10.6342/NTU202300991

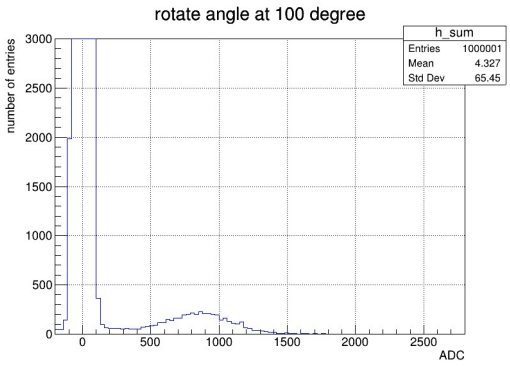

(h) analyzer angle = 100°

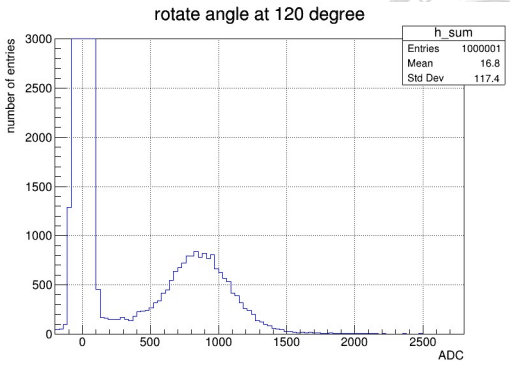

(i) analyzer angle = 120°

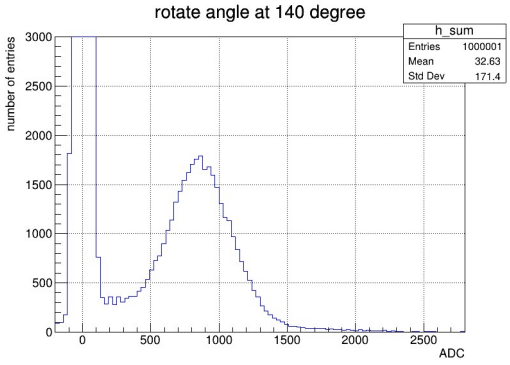

(j) analyzer angle = 140°

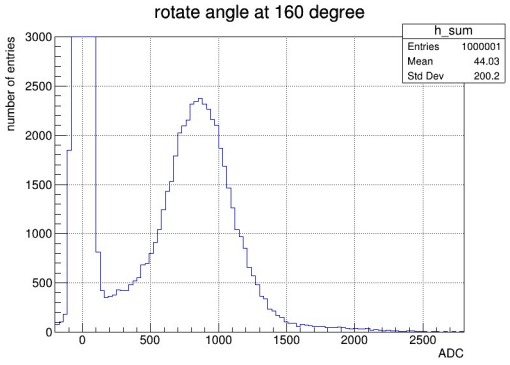

(k) analyzer angle = 160°

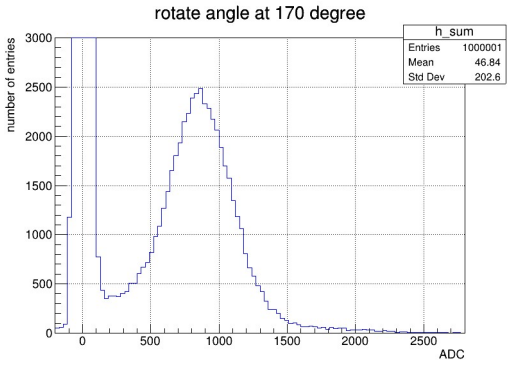

(l) analyzer angle = 170°

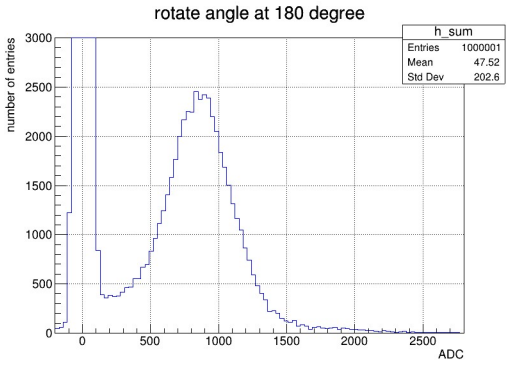

(m) analyzer angle = 180°

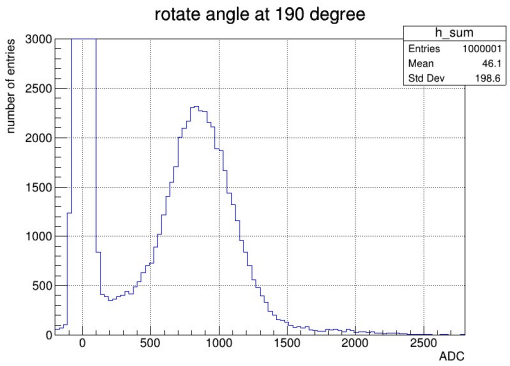

(n) analyzer angle = 190°

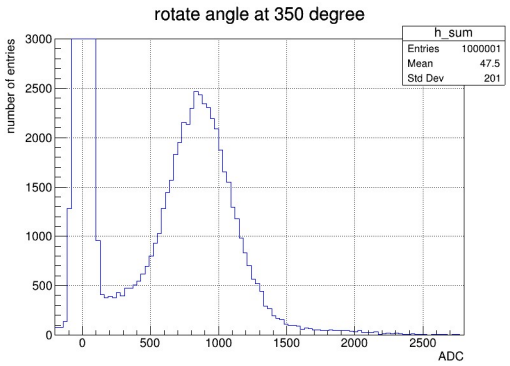

(o) analyzer angle = 350°

Figure 5.8: The extremely low light level spectrum of several polarization angles I have measured.

doi:10.6342/NTU202300991

and sigma: σ_1, σ_2, σ_3, σ_4 of each Gaussian. Perform histogram integral in each range, integrate each Gaussian within the range of three sigma (the characteristics of Gaussian), multiply the corresponding number of photoelectrons, and then summation:

$$\text{light amount (number of p.e)} = \sum_{n=1}^{4} (n \times \int_{Q_n-3\times\sigma_n}^{Q_n+3\times\sigma_n}) \tag{5.2}$$

. Fig. 5.10 is the plot of the total number of phototelectrons calculated by the first ways versus angle and fit by Eq. 5.1. It can be seen that the light amount does have a $\cos^2\theta$ relationship to the polarization angle. However, the first way to calculate the light amount has some drawbacks. First, it does not remove the contribution of the second type background of PMT. Then, the integral range of each Gaussian has overlaps since I perform the histogram integral.

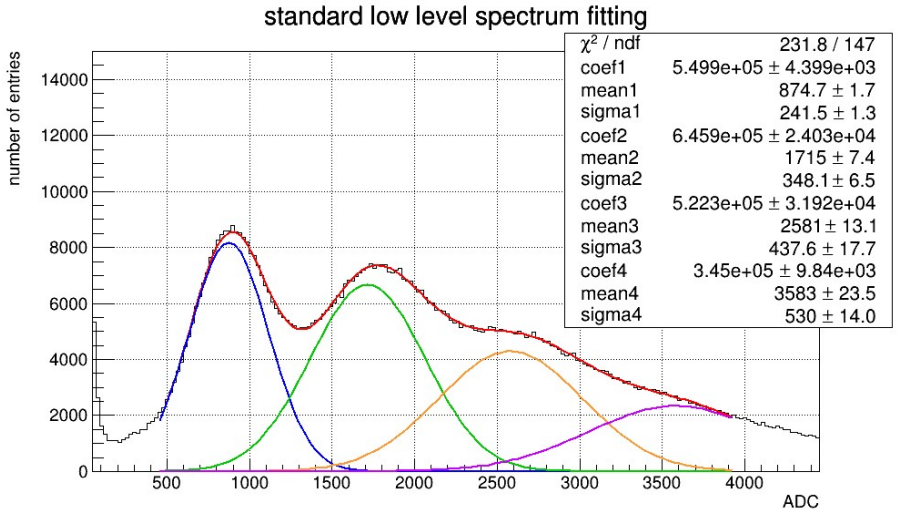

Figure 5.9: The standard low light level spectrum fitting on PMT XP72B20 at high voltage = 1500 V.

I also calculate the light amount by the second way, that is, fit two Gaussians plus an exponential decay function to each spectrum to directly obtain the contribution of single photoelectron, double photoelectrons, and second type background in each result. Fig. 5.11 shows the fitting results of each spectrum. The blue line and green line represent

doi:10.6342/NTU202300991

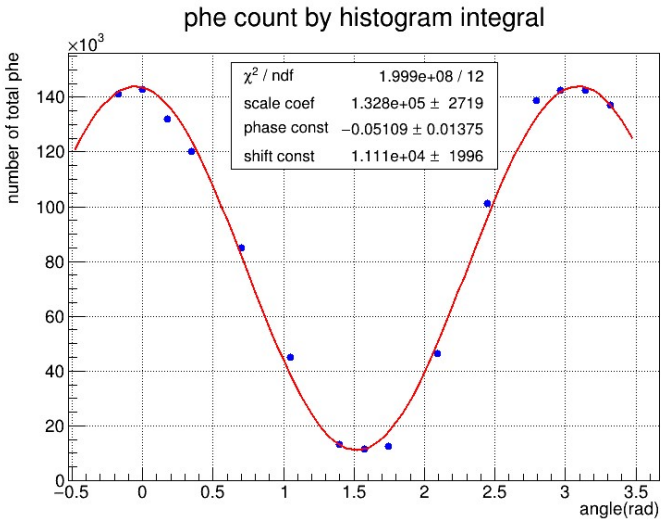

Figure 5.10: The plot of the number of photoelectrons by the first method versus angle.

the Gaussian function of the single photoelectron and double photoelectrons respectively, and the pink line represents the exponential decay function of the second background. Integrate these two Gaussian fitting functions, multiply the corresponding number of photoelectrons, and then summation (in arbitrary units):

$$\text{light amount (a.u.)} = \sum_{n=1}^{2} (n \times \int_{Q_n - 3\times\sigma_n}^{Q_n + 3\times\sigma_n}) \tag{5.3}$$

. Fig. 5.12 is the plot of the total light amount calculated by the second way versus angle and fit by Eq. 5.1. It can be seen that the amount of incident light conforms to $\cos^2\theta$ relationship.

By the light amount change with polarization angle in the extremely low light level results, we see the polarization can still work on this kind of single photon source candidate.

doi:10.6342/NTU202300991

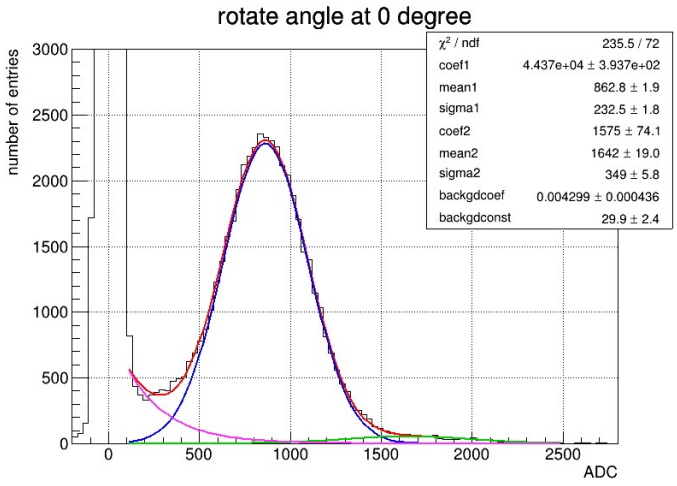

(a) analyzer angle = 0°

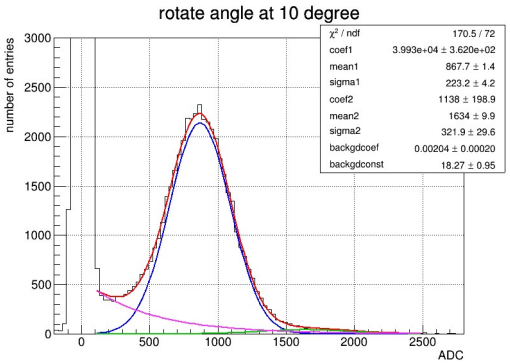

(b) analyzer angle = 10°

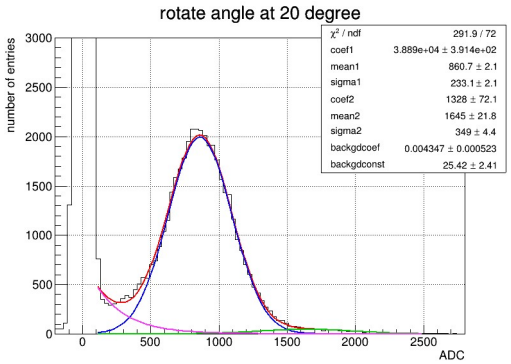

(c) analyzer angle = 20°

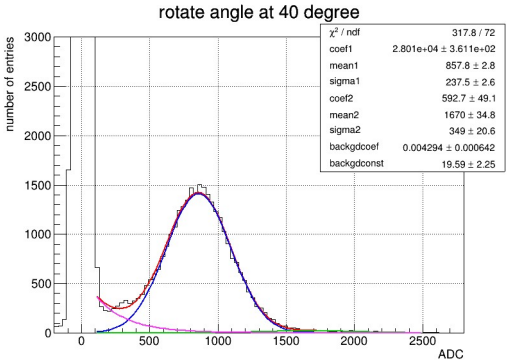

(d) analyzer angle = 40°

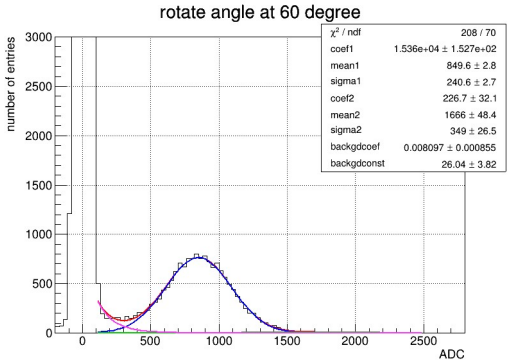

(e) analyzer angle = 60°

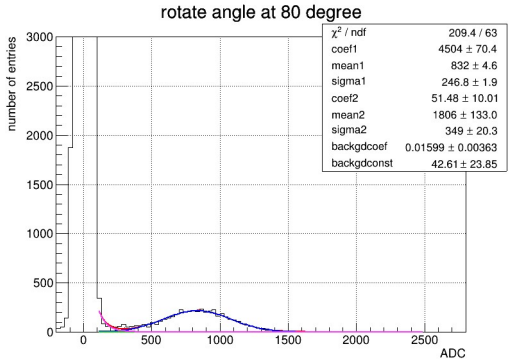

(f) analyzer angle = 80°

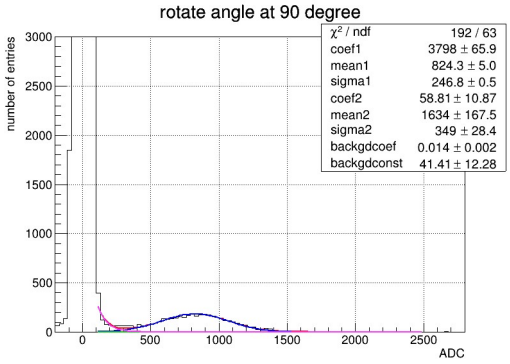

(g) analyzer angle = 90°

doi:10.6342/NTU202300991

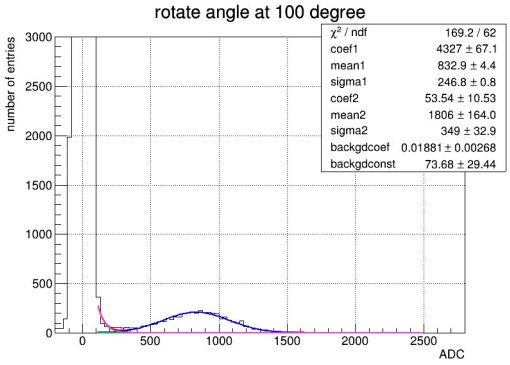

(h) analyzer angle = 100°

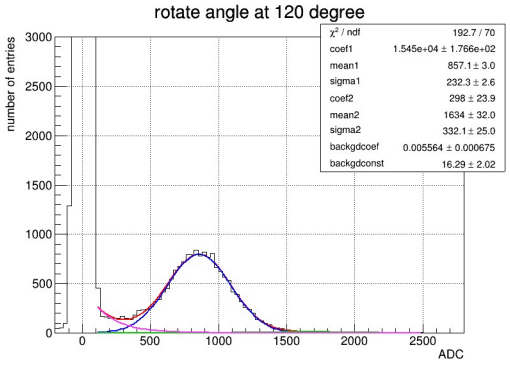

(i) analyzer angle = 120°

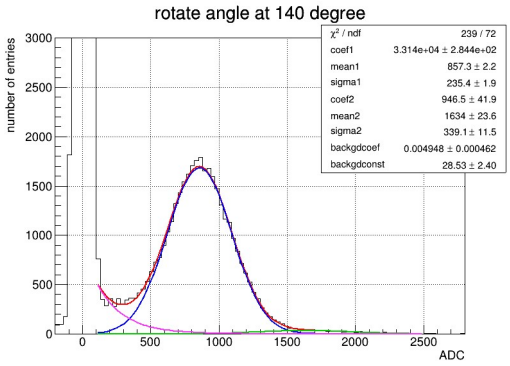

(j) analyzer angle = 140°

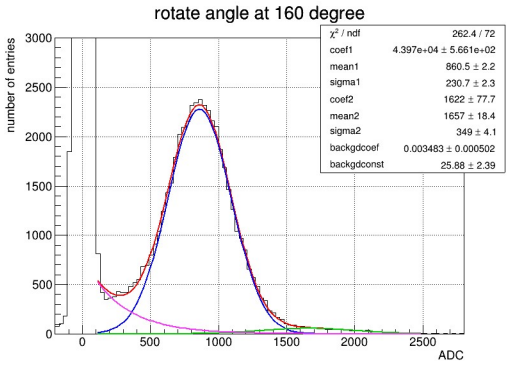

(k) analyzer angle = 160°

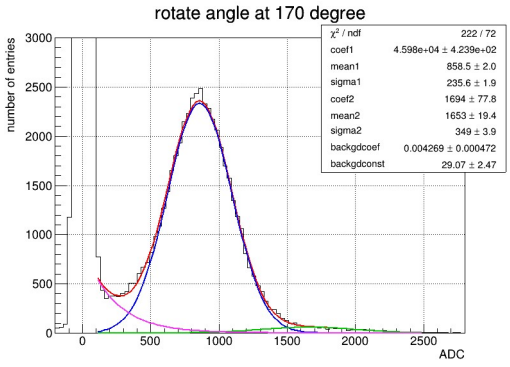

(l) analyzer angle = 170°

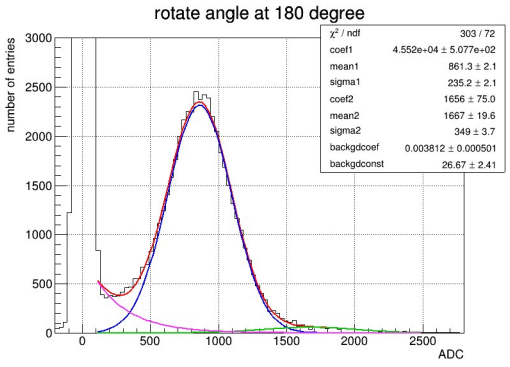

(m) analyzer angle = 180°

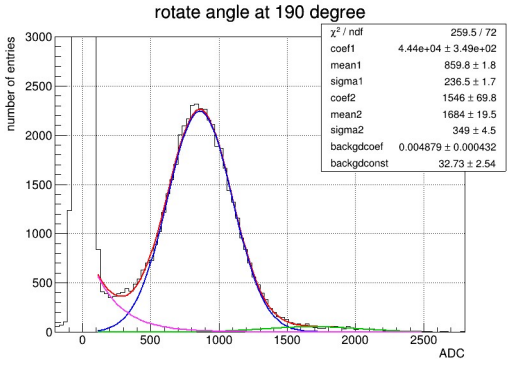

(n) analyzer angle = 190°

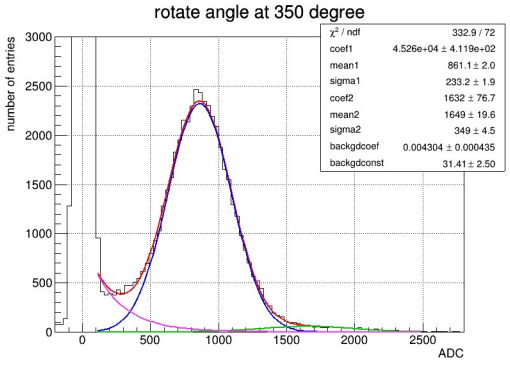

(o) analyzer angle = 350°

Figure 5.11: The fitting of all the extremely low light level spectrum in Fig. 5.8.

doi:10.6342/NTU202300991

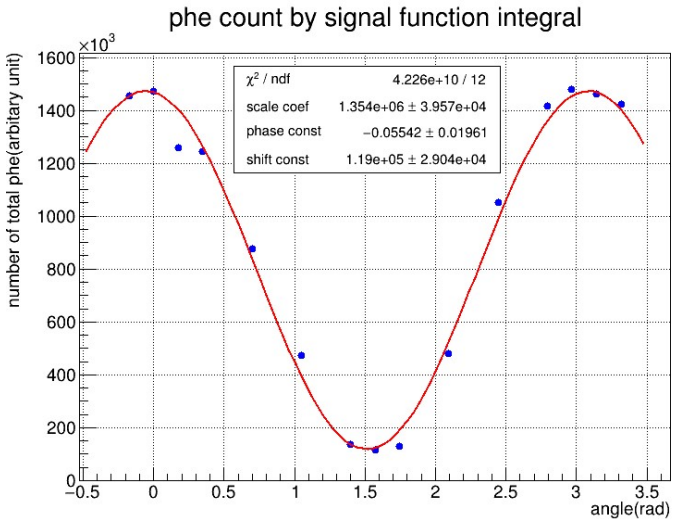

Figure 5.12: The plot of the total amount of light (in arbitrary units) calculated by the second method versus angle.

5.3.2 Low light level

In Sec. 5.3.1, to define the range of different numbers of photoelectron, I measured a standard low light level result, which is Fig. 5.9. I have a discovery on this spectrum. Even if the fitting parameters are appropriately enlarged, σ_2/σ_1 will still be maintained at about $\sqrt{2}$, as the theoretical prediction mentioned in Sec. 2.3. This cannot be seen on the spectrum of R329-02, and make me try whether I can perform a fitting function closer to the theoretical model on the low light level spectrum of XP72B20.

Fig. 5.13 shows the low light level spectrum with an appropriate light intensity I set when the analyzer rotates at 0°. This spectrum shows that the resolution of XP72B20 can clearly distinguish even the third photoelectron peak. If I use an equation closer to the theoretical model for fitting:

$$S(x) = B \cdot e^{-\alpha x} + C \cdot \sum_{n=1}^{\infty} \frac{\mu^n e^{-\mu}}{n!} \frac{1}{\sigma_1 \sqrt{2\pi n}} e^{\frac{(x-nQ_1)^2}{2n\sigma_1^2}} \tag{5.4}$$

doi:10.6342/NTU202300991

, where B is the background constant, α is the background coefficient, μ is the mean number of photoelectrons, C is the signal coefficient, and Q_1, σ_1 are the same as before. This fitting function means the distribution of the number of photoelectrons is controlled by only a single Poisson function, and the mean number of photoelectrons μ represents the light intensity. This condition is not like the case in the LED calibration study, where the intensity of each photoelectron can be free. Fig. 5.14 is the fitting result of Fig. 5.13 by Eq. 5.4. The red line is the total function, the pink line represents the exponential decay function of the second type background, and the blue, green, ⋯line represents the Gaussian function of the each number of photoelectrons respectively. It can be seen that the fitting function can roughly describe the entire spectrum by only 6 free parameters, while the signal part by only 4 free parameters.

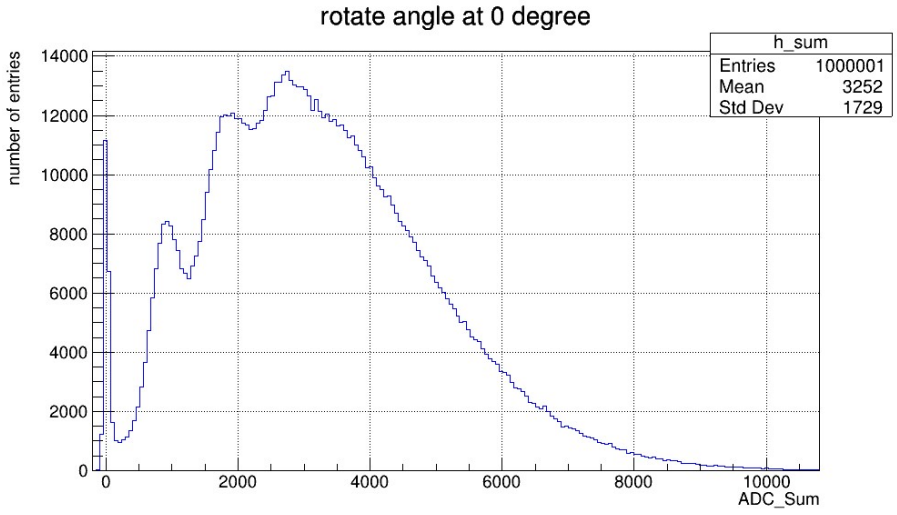

Figure 5.13: The low light level spectrum with appropriate intensity as analyzer = 0°.

Fig. 5.15 is the spectrum results of several different polarization angles I have measured, and each of them fit with Eq. 5.4. Compared with the extremely low light level spectrum, the change of low light level spectrum is more obvious. It can be seen that as the angle changes from 0° to 90° and then to 180°, the peaks representing the second or third photoelectron gradually disappear and then reappear. The situation of all fitting results is

doi:10.6342/NTU202300991

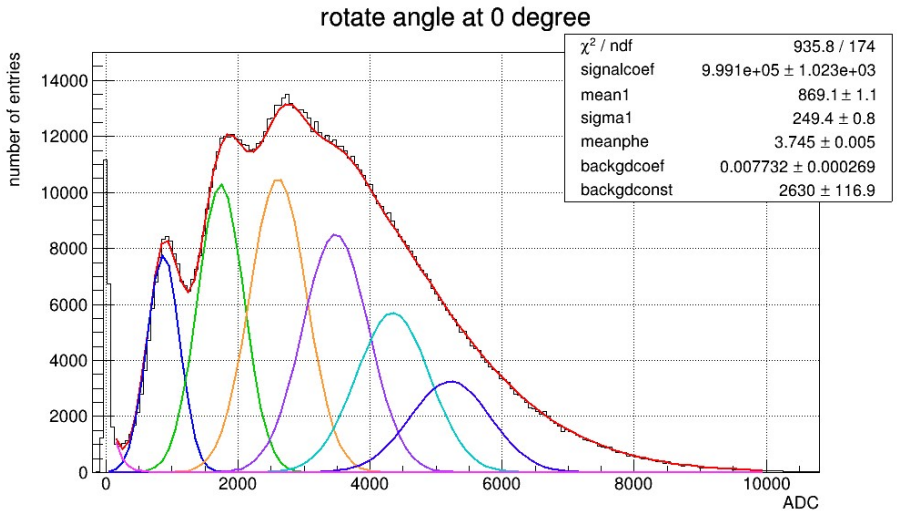

Figure 5.14: Fig. 5.13 fit by Eq. 5.4 .

not perfect, but the function can generally cover the spectrum distribution. Fig. 5.16 is the mean number of photoelectrons versus angle by each result. It can be seen that the mean number of photoelectrons shows a good relationship with $\cos^2\theta$.

Since the change of received light intensity due to the polarization angle does not depend on the setting of the pulse signal, which means the change in the mean number of photoelectrons at different polarization angles is consistent with the change in the mean number of photons. Thus, the fitting results of different polarization angles to prove the number of photons emitted by LED at low light levels does follow the Poisson distribution.

The photon distribution followed by the Poisson distribution might also explain why the asymmetry of the high light level spectrum mentioned in Sec. 3.3.2 becomes less obvious as light intensity increases (Fig. 5.17). However, as mentioned in Sec. 2.4, I currently have not been able to find an appropriate model that can describe high light level spectrum based on Poisson distribution to be consistent. How to find a model that correctly describes the photoelectron distribution of the high light level result has become a future topic.

doi:10.6342/NTU202300991

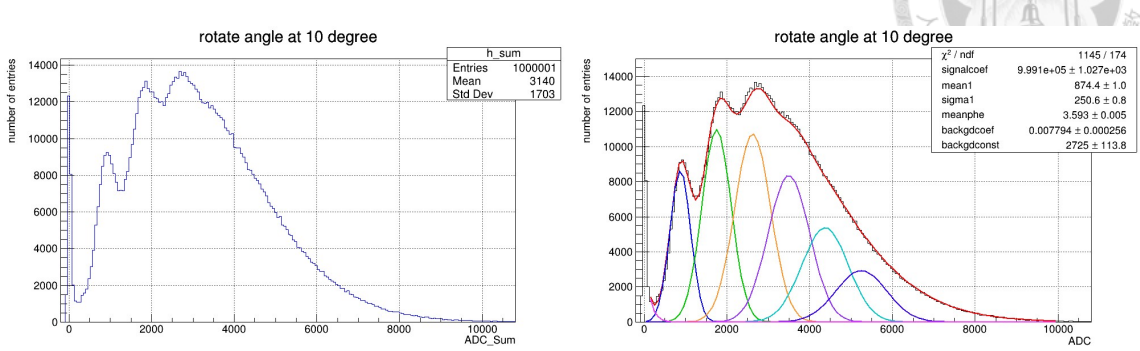

(a) analyzer angle = 10°

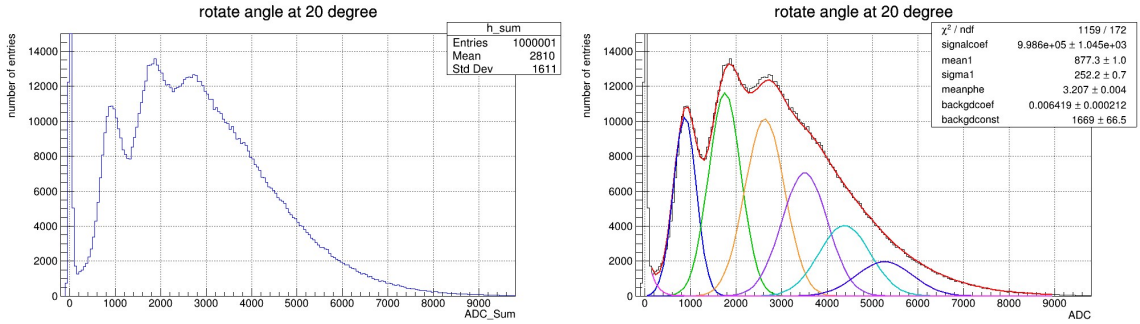

(b) analyzer angle = 20°

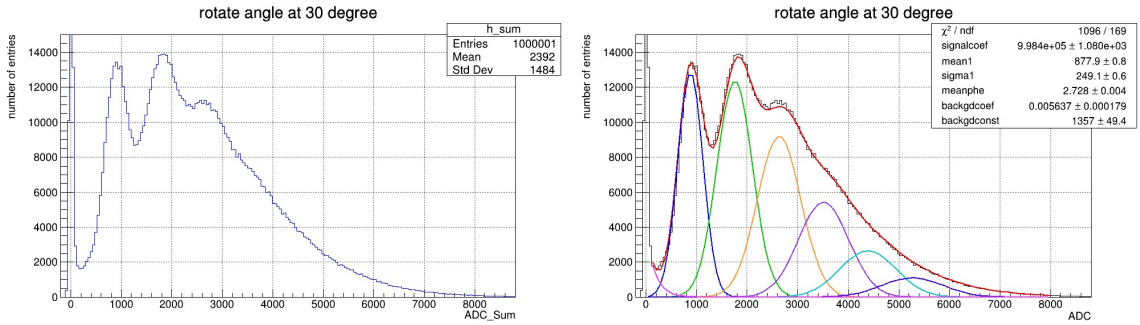

(c) analyzer angle = 30°

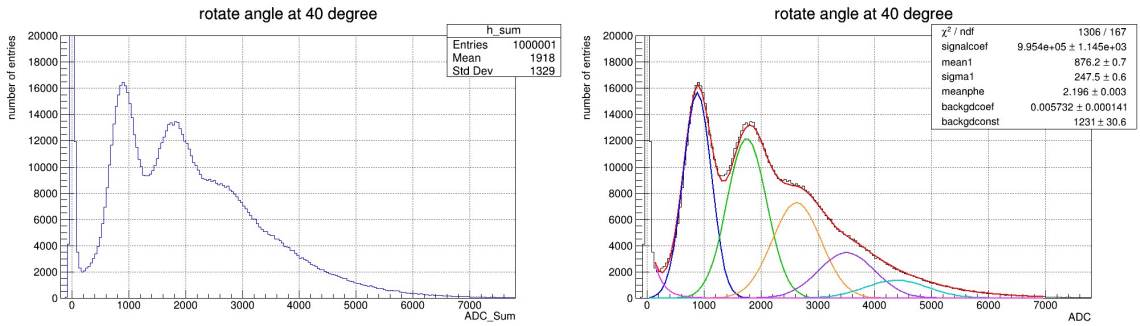

(d) analyzer angle = 40°

doi:10.6342/NTU202300991

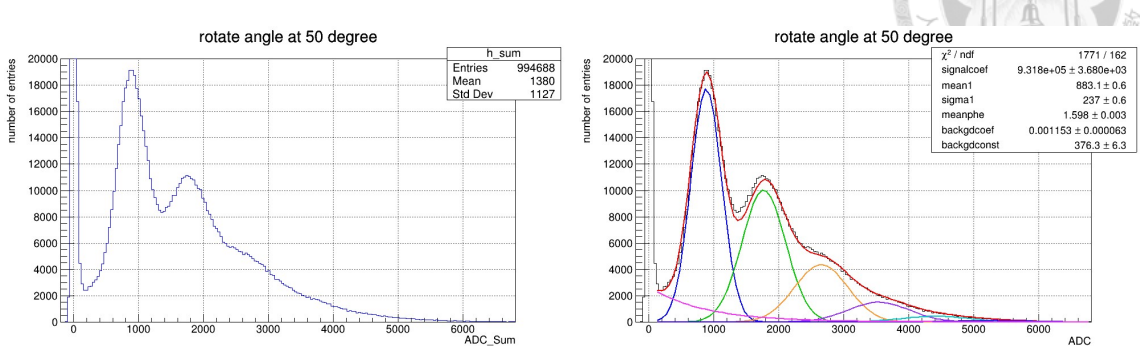

(e) analyzer angle = 50°

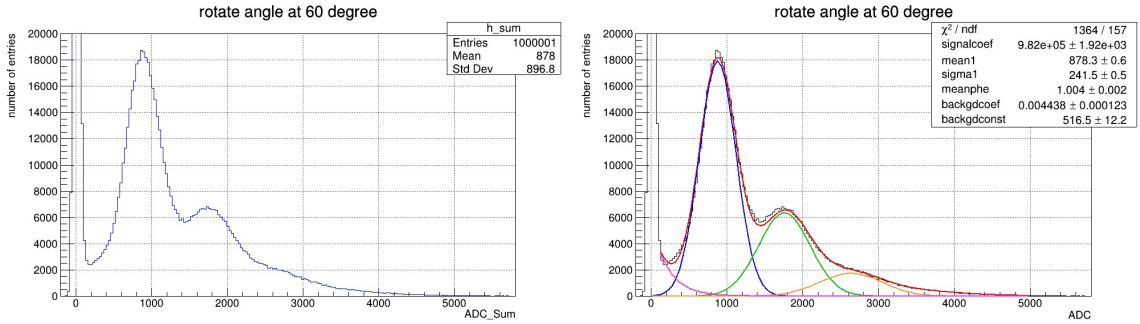

(f) analyzer angle = 60°

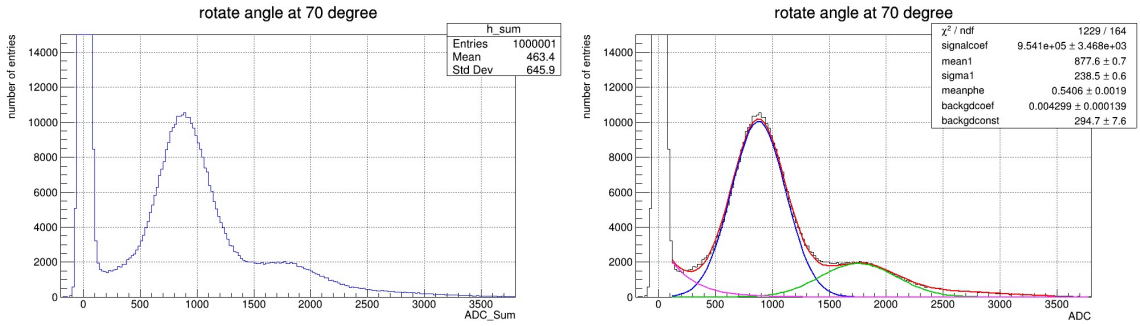

(g) analyzer angle = 70°

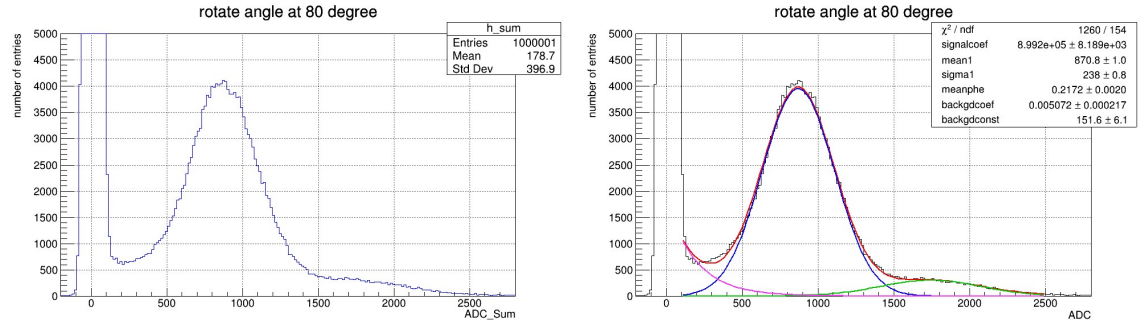

(h) analyzer angle = 80°

doi:10.6342/NTU202300991

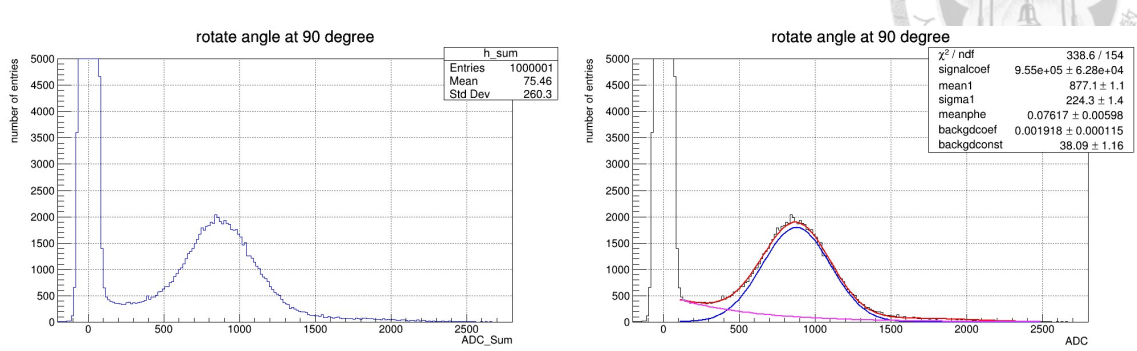

(i) analyzer angle = 90°

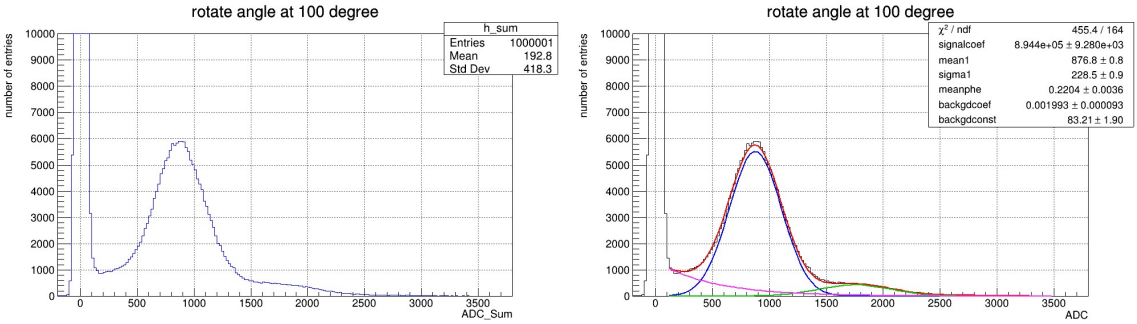

(j) analyzer angle = 100°

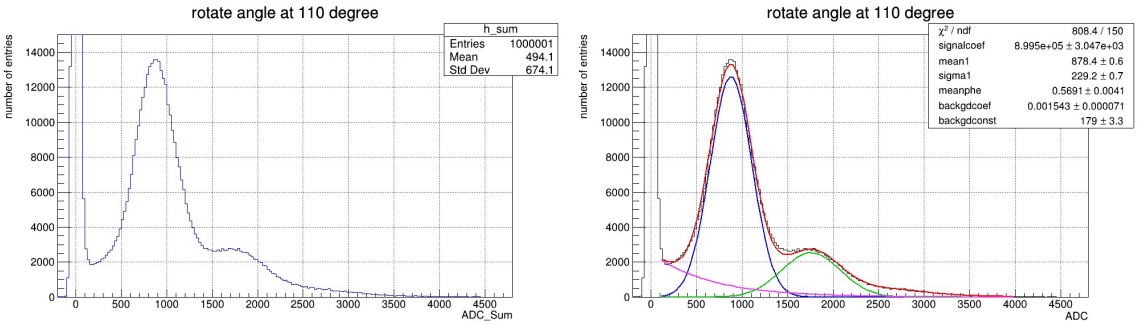

(k) analyzer angle = 110°

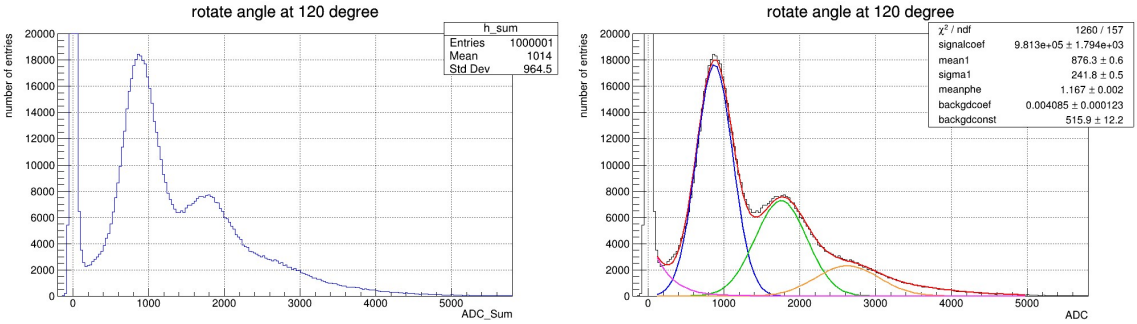

(l) analyzer angle = 120°

doi:10.6342/NTU202300991

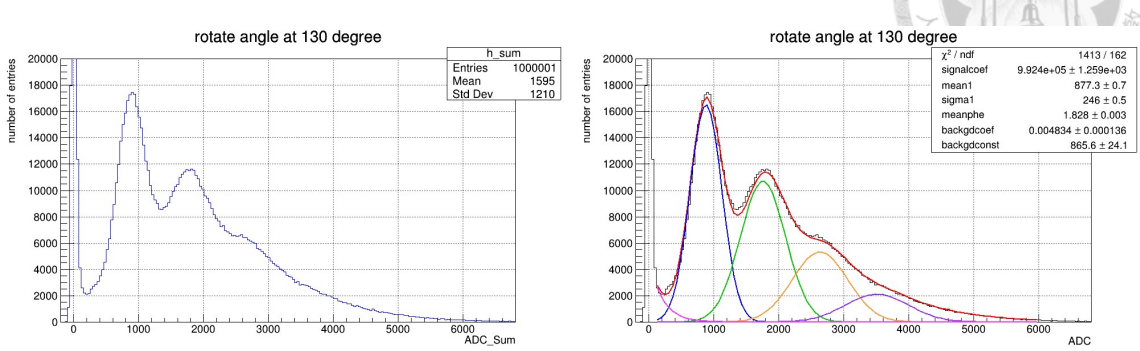

(m) analyzer angle = 130°

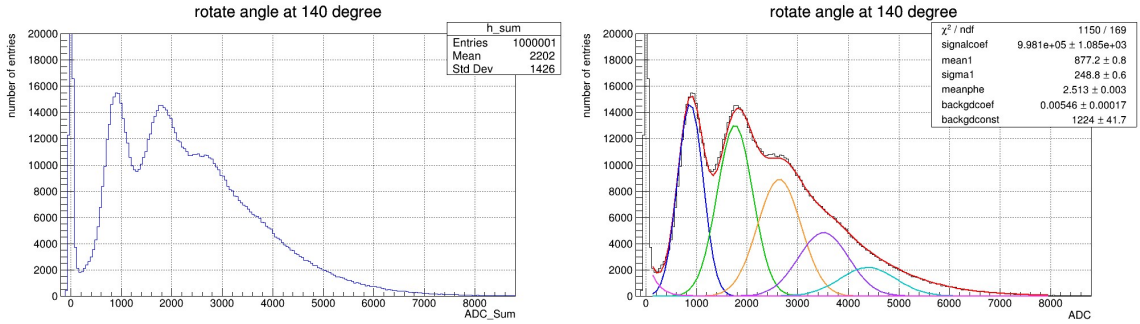

(n) analyzer angle = 140°

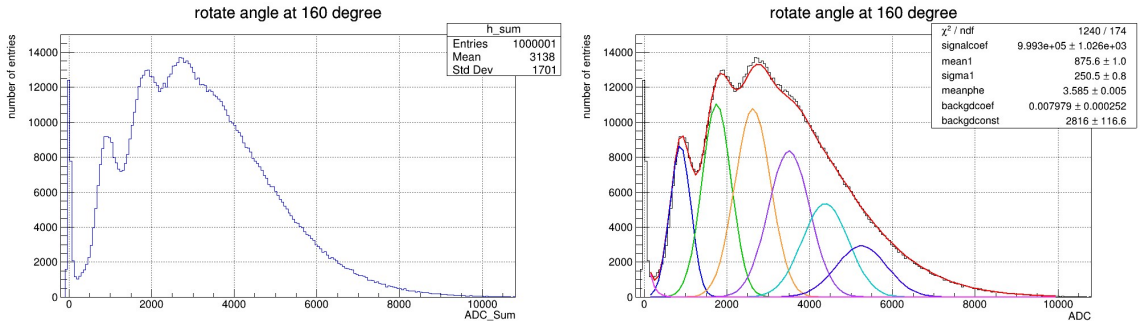

(o) analyzer angle = 160°

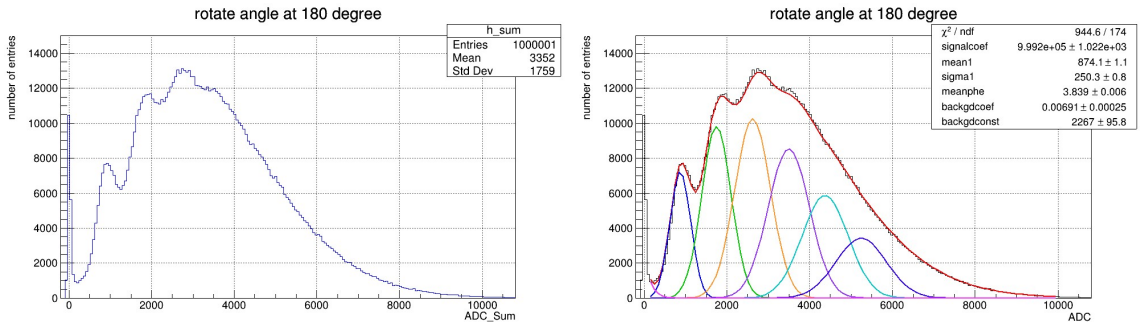

(p) analyzer angle = 180°

doi:10.6342/NTU202300991

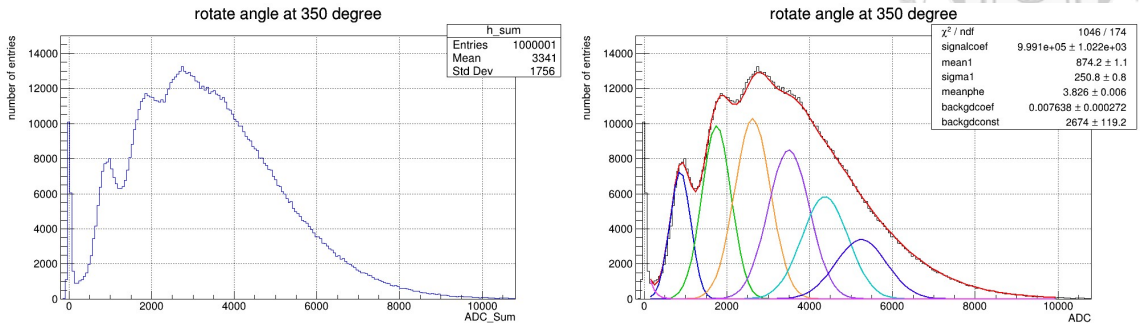

(q) analyzer angle = 350°

Figure 5.15: The low light level results of several polarization angles I have measured. The left figure of each column is the spectrum, and the right figure is their fitting by Eq. 5.4.

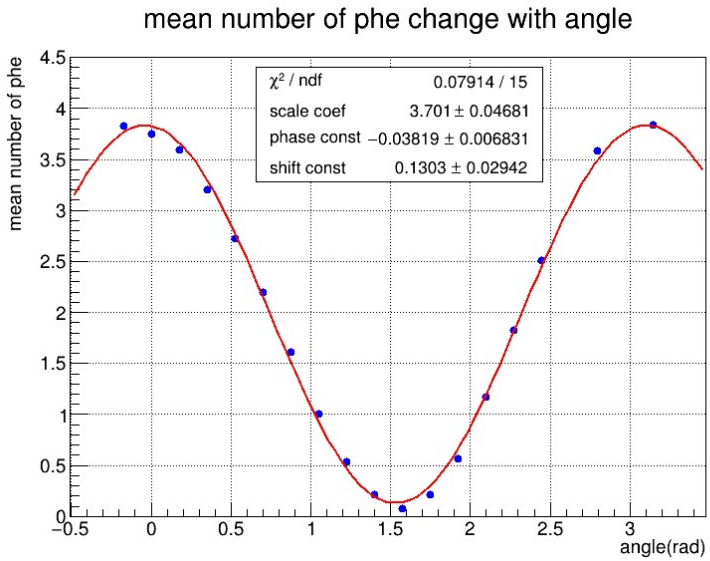

Figure 5.16: The plot of the mean number of photoelectrons by fitting results versus angle.

doi:10.6342/NTU202300991

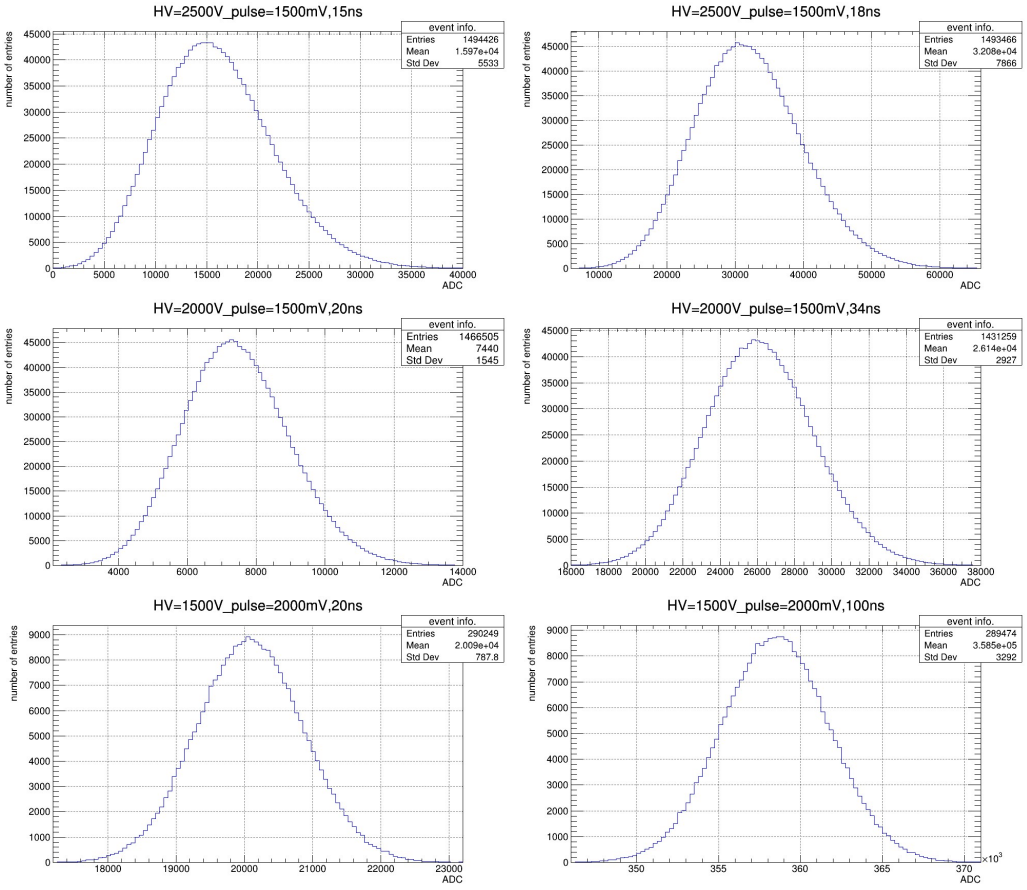

Figure 5.17: The asymmetry of spectrum in high light level results. The order of figures follows the light intensity stronger.

doi:10.6342/NTU202300991

Chapter 6

Conclusion

As a scintillator commonly used in modern PET systems, LYSO has several advantages that make it a good candidate for detecting 511 keV annihilation photons. The property of comparable light output becomes our motivation in the LYSO study, so I design a set of procedures to measure the light yield of LYSO.

In LED calibration, I used LED to complete the single photoelectron calibration of PMT and understood the light-emitting mechanism of LED driven by a fast pulse signal. In light yield measurement of LYSO, I confirmed the characteristics of LYSO intrinsic spectrum and radioactive source Sodium-22 spectrum and established a standard measurement process to measure the light yield of LYSO sample reliable and stable though there are still some issues in absolute light yield. In polarized single photon, I check the single photon source candidate can still be polarized and prove LED photon distribution consistent with the theory in weak light conditions.

With these results so far, we know that LED could be a cheap and convenient single photon source candidate, and very useful for future scientific research or demonstration.

doi:10.6342/NTU202300991

Our future projects will conduct other experiments to further confirm the reliability of this kind of single photon source, such as double-slit or measured by other single photon detectors. We may also develop the experimental setup into a manufacturable model, hoping the polarized single photon source we designed can be used for some scientific education.

doi:10.6342/NTU202300991

Appendix A

Appendix

A.1 Introduction about PET system

This section is the introduction to the PET system, which is the most famous application of LYSO [15]. PET system trace amounts of short-lived radioactive molecules, which are injected into the bloodstream, to map functional processes in the body. When the material undergoes radioactive decay, it emits a positron, and soon collides with an electron to produce two gamma rays with the same energy but travel in 180 degrees opposite directions from each other (Fig. A.1).

The scanner consists of a ring of detectors that surround the patient (Fig. A.2). The detectors contain crystals that scintillate in response to gamma rays, which is where LYSO comes in handy (Fig. A.3). When two detectors exactly opposite from each other on the ring simultaneously detect a gamma ray, a computer hooked up to the scanner records this as a coincidence event. The computer records all of the coincidence events that occur during the imaging period and then reconstructs this data to produce cross-sectional images, used to construct a 3D volume (Fig. A.4).

doi:10.6342/NTU202300991

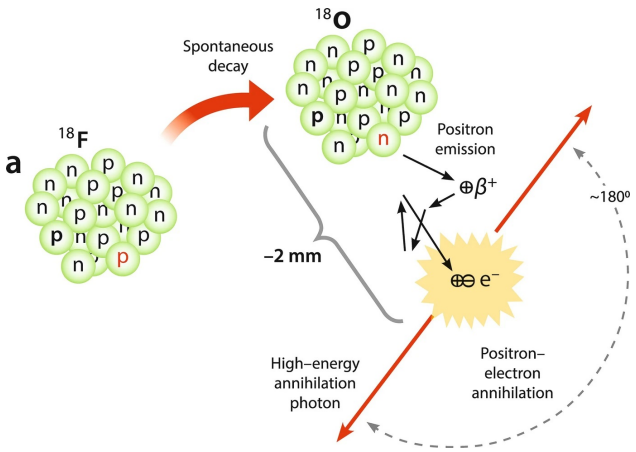

Figure A.1: The process of positron-electron annihilation where emitted 180° to each other [16].

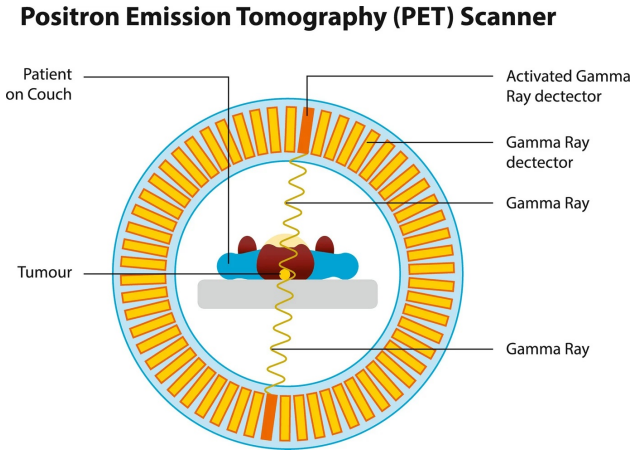

Figure A.2: The basis of the PET image acquisition [16].

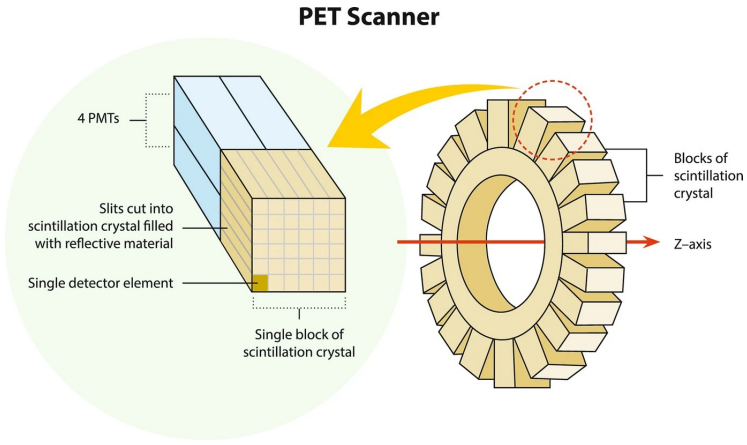

Figure A.3: An example of the composition of photodetectors in a PET system [16].

doi:10.6342/NTU202300991

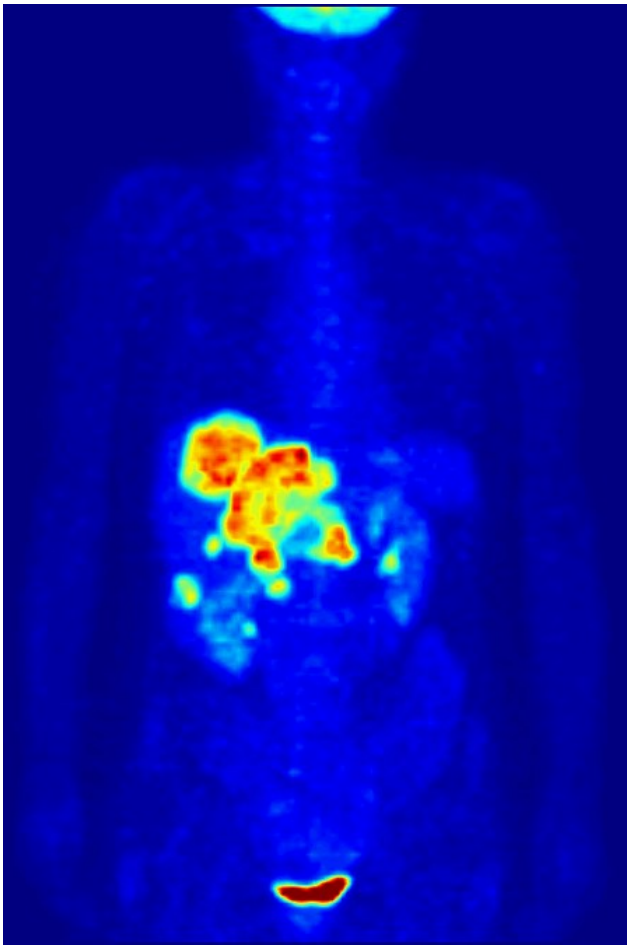

Figure A.4: An example of 3D Volume picture by PET scan.

doi:10.6342/NTU202300991

A.2 Introduction about three common distributions

This section is the introduction of the three common distributions: Binomial, Poisson, and Gaussian used in Sec. 2.2. These distributions are used to describe the signal response of PMT obtained after each working process in theory.

The Binomial distribution gives the probability of finding exactly the number of n successes in a positive integer number of N trials. The success trial, with probability p, where $0 \leq p \leq 1$, and the failure trial, with probability $1-p$. The probability of obtaining n number of successes:

$$P(n) = \frac{N!}{n!(N-n)!} p^n (1-p)^{N-n} \tag{A.1}$$

for values of n ranges from 0 to N, and the expectation value to number of n successes:

$$\bar{n} = \sum nP(n) = Np \tag{A.2}$$

.

The Poisson distribution gives the probability of finding exactly n events in a given length of time t(and/or space) if the events occur independently at a constant rate f and expectation value $\mu = ft$:

$$\begin{aligned} P_\mu(n) &= \frac{N!}{n!(N-n)!} (\frac{\mu}{N})^n (1-\frac{\mu}{N})^{N-n} \\ &= \frac{\mu^n}{n!} \frac{N(N-1)\dots(N-n+1)}{N^n} (1-\frac{\mu}{N})^N (1-\frac{\mu}{N})^{-n} \\ &\to \frac{\mu^n}{n!} \cdot 1 \cdot e^{-\mu} \cdot 1 = \frac{\mu^n}{n!} e^{-\mu} \end{aligned} \tag{A.3}$$

The standard deviation of Poisson is $\sigma = \sqrt{\mu}$, and it is an important feature.

doi:10.6342/NTU202300991

The Gaussian is a well-known distribution with the probability function of observing x independent events:

$$P(x) = \frac{1}{\sqrt{2\pi}\sigma} e^{-\frac{(x-\mu)^2}{2\sigma^2}} \tag{A.4}$$

where the expectation value is μ and the standard deviation is σ.

A.3 Notices of the pedestal calculation

This section is to introduce the problems I encountered in data processing. In each event window, I divide the period into two intervals: baseline window and signal window, as shown in Fig. A.5. I will set the trigger point to make sure the signal window is long enough to accommodate the signal waveform. There will be no signal before this time, and I will use the average of the ADC value during this period as my baseline for this event. This baseline makes me can calculate the "self-pedestal" of an event by event. The problems come from the self-pedestal calculation and will affect the light yield result. The following divide the problems into two parts: pedestal width and pedestal deviation.

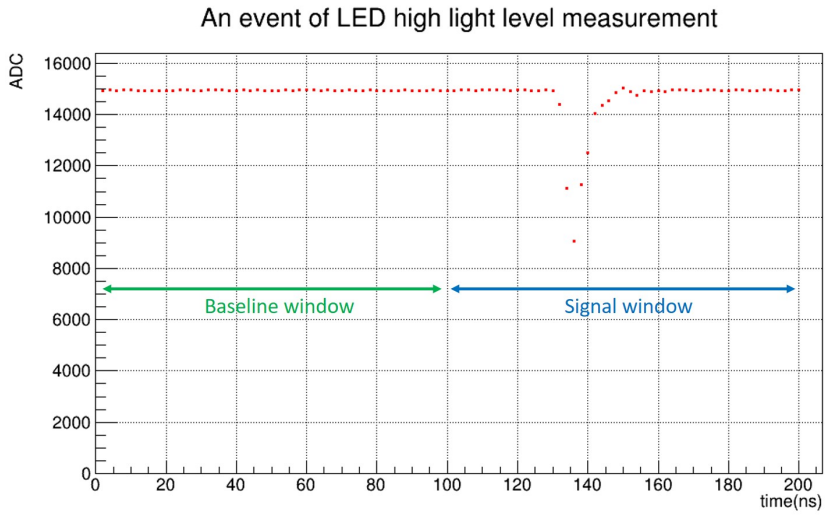

Figure A.5: The example of an event window, which can be divided into a baseline window and a signal window.

doi:10.6342/NTU202300991

For a signal window with a fixed interval, the length of the baseline window will affect the ”pedestal width”. Take PMT R239-02 and signal window = 100 ns as an example, which is the case in the LED calibration study. When there is no LED light signal, the measured results can be regarded as pedestal distribution. Fig. A.6 shows that when the baseline window = 20, 40, 60 ns is selected, the standard deviation of pedestal distribution will decrease with the baseline window increase, and the decline magnitude will slow down when the baseline window increase to = 80, 100 ns. This shows that for a signal window, we need a long enough baseline window to reduce the width of the pedestal distribution. A wide pedestal will reduce the single photoelectron resolution, and even interfere with the appearance of the single photoelectron peak. Fortunately, for high voltage = 1500 V and = 2500 V, the standard deviation of each pedestal is similar under the same baseline window (Table A.1), and finally, I choose baseline window = 100 ns in my measurements.

baseline window (ns)	20	40	60	80	100
without HV (ADC)	48.19	34.34	32.73	27.34	26.32
HV = 1500 V (ADC)	49.63	34.12	32.91	27.34	26.55
HV = 2500 V (ADC)	48.38	33.39	29.38	26.71	26.14

Table A.1: The standard deviation of pedestal distribution to baseline window under three high voltage conditions.

Since the voltage signal of our digitizer record is in the form of ADC, its value must be an integer. If we still use the integer variable to deal with data, the ”pedestal deviation”

doi:10.6342/NTU202300991

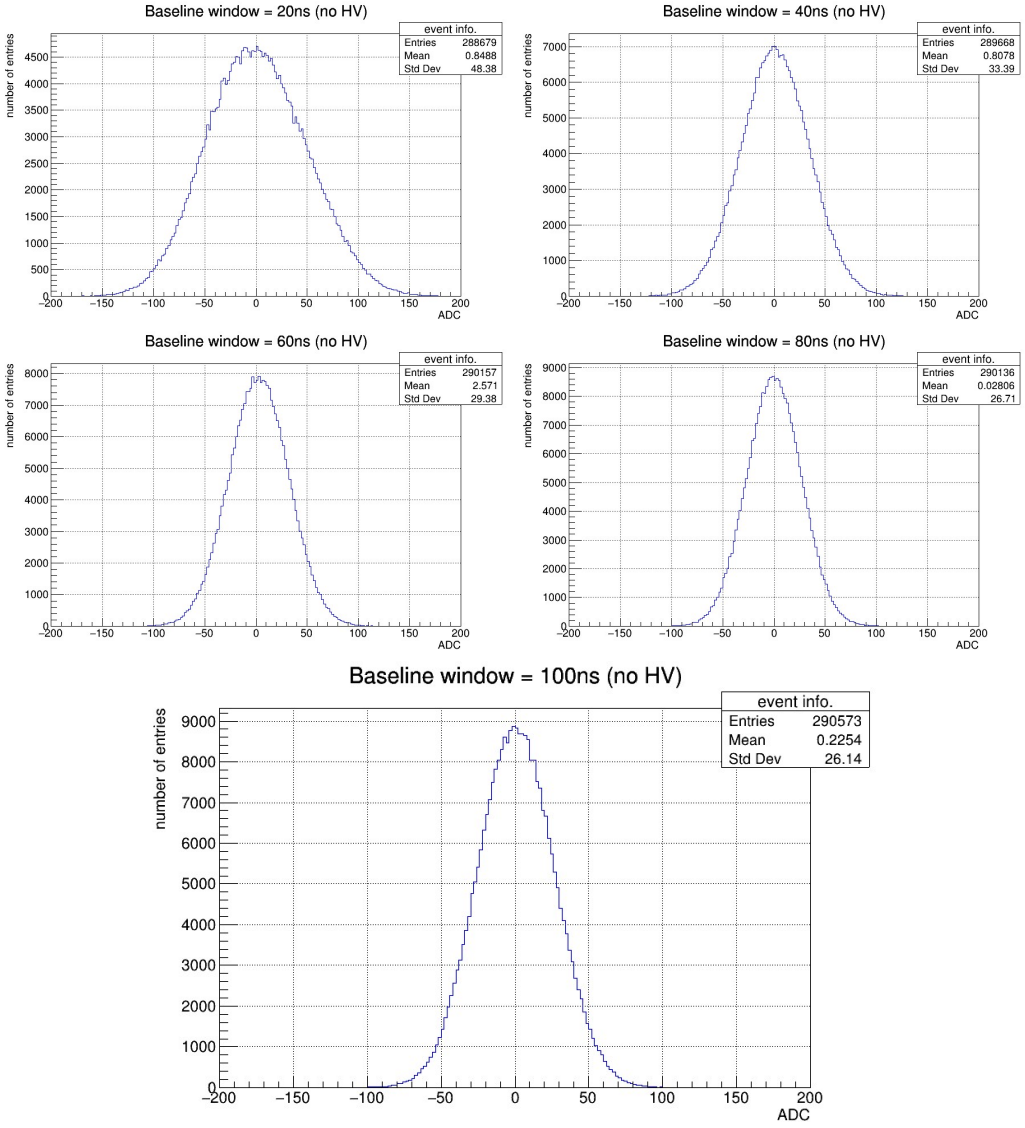

Figure A.6: The pedestal distribution change with different baseline windows.

doi:10.6342/NTU202300991

will happen. Because the analysis software ROOT is based on C++, it will unconditionally discard all decimal places when performing integer division, and this will cause the calculated average value to be smaller than the correct average value. Since our signal polarity is negative, the pedestal will be shifted to a higher value. It will make each sample point smaller by $0 \sim 1$ ADC, and the overall deviation will depend on how long the "signal window" is used. In the case of LED calibration, the signal window $= 100$ ns, that is, 50 sample points of each event since the sample rate $= 500$ MS/s. The pedestal deviation will be between $0 \sim 50$ ADC, and this will have a strong impact on the results with smaller ADC orders. Fig. A.7 shows the difference in peak value of high light level results at HV $= 2500$ V with or without pedestal deviation. It can be seen that there is only a bias of about 30 ADC for the peak value, which cause a difference of -0.15%. Fig. A.8 shows the difference of peak value high light level results at HV $= 1500$ V with or without pedestal deviation by the same group of results above. The bias is still about 30 ADC, but this time the peak value has a large difference of -8.87%. If five groups of high light level results are taken from the standard measurement results (Table A.2), the average high voltage factor with pedestal deviation is 9.84% higher than the correct value. This is why the light yield results in our earlier reports were higher than now.

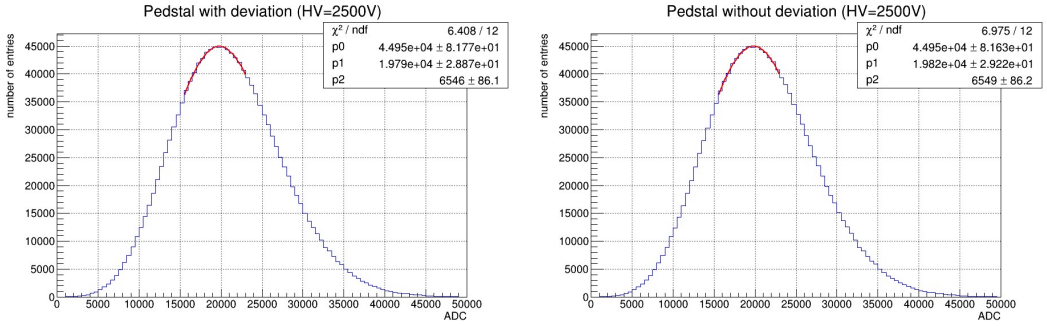

(a) with pedestal deviation (b) without pedestal deviation

Figure A.7: The effect of pedestal deviation at high voltage $= 2500$ V.

doi:10.6342/NTU202300991

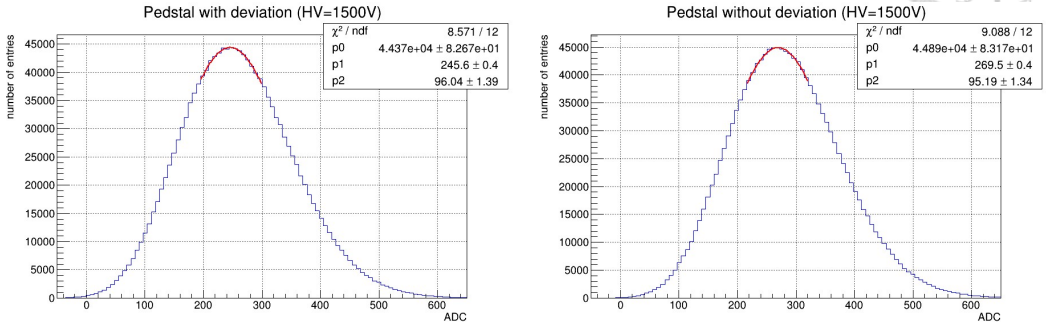

(a) with pedestal deviation (b) without pedestal deviation

Figure A.8: The effect of pedestal deviation at high voltage = 1500 V.

With deviation (a.u.)	80.57	80.71	80.66	80.68	79.67
Without deviation (a.u.)	73.60	73.65	73.15	73.27	72.62
%	9.48	9.59	10.28	10.12	9.71

Table A.2: The difference of the pedestal deviation or not to the results of high voltage factor. Take each high voltage factor without deviation as 100 %.

doi:10.6342/NTU202300991

A.4 The Poisson model in the high light level results

It has been mentioned many times in this thesis that the theory uses the Poisson model to assume the distribution of a number of photons emitted by LED, and it is proved in Sec. 5.3.2 that consists with the Poisson model in low light level. However, Sec. 2.4 have also mentioned that the Poisson model is not consistent for the high light level results. This section is the introduction of the Poisson model in the high light level results.

As mentioned in Sec. 2.4, we use Eq. 2.16 to approximate the fitting equation of the Poisson model in the high light level spectrum. Taking the first set of high light level results in the standard measurements as an example, perform the Poisson model fitting on both high voltage = 1500 V and 2500 V, and the results are shown in Fig. A.9. There is an obvious difference 11.14% between $Q_1 = 2068$ ADC obtained by Poisson model and $Q_1 = 1856$ ADC obtained by single photoelectron calibration (Table 4.5) at high voltage = 2500 V, and high voltage = 1500 V cannot make single photoelectron calibration so it cannot be compared. If five groups of high light level results are taken from the standard measurement process (Table A.3), it can be found that the mean number of photoelectrons of each group between 1500 V and 2500 V has a significant difference of average -11.93%. Unable to explain the same light intensity but will get the different mean number of photoelectrons under the Poisson model, which eventually became the main reason for abandoning the Poisson model to describe high light level spectrum.

doi:10.6342/NTU202300991

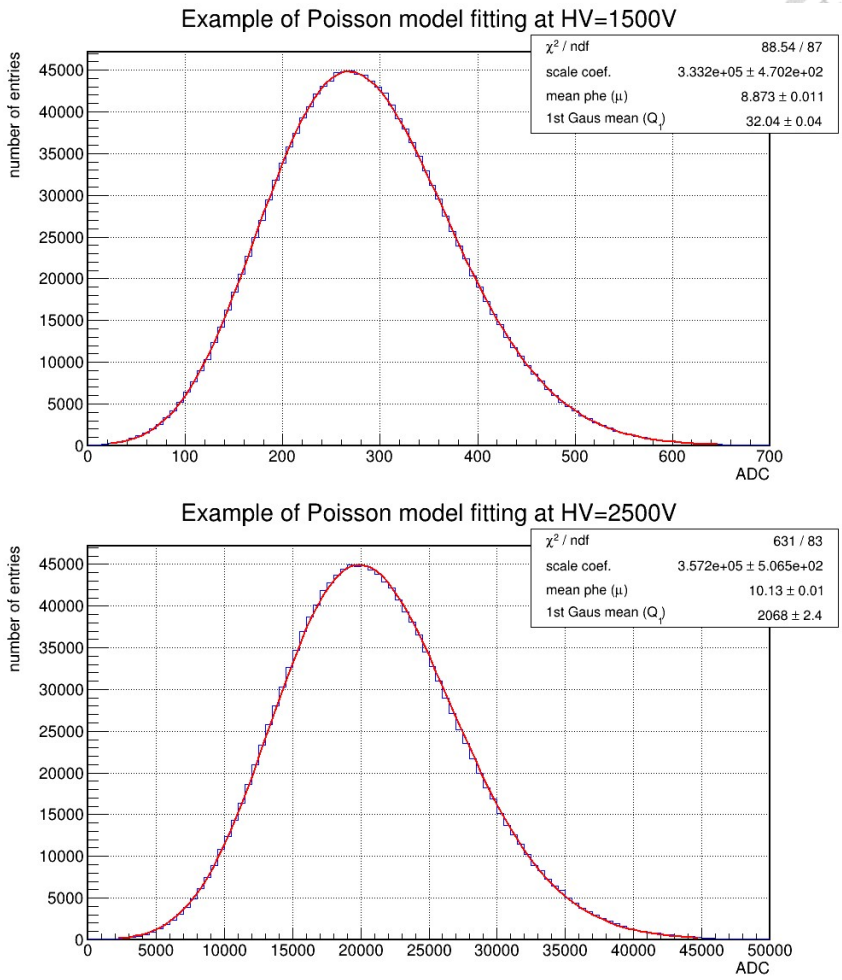

Figure A.9: The example of high light level spectrum fitting by Poisson model at high voltage = 1500 V and 2500 V

HV = 1500 V (mean number of p.e)	8.55	8.86	9.08	8.87	9.01
HV = 2500 V (mean number of p.e)	9.69	9.97	10.22	10.13	10.37
%	−11.74	−11.16	−11.15	−12.41	−13.16

Table A.3: The difference of the mean number of photoelectrons by the Poisson model fitting between 1500 V and 2500 V. Take each result of 2500 V as 100%.

doi:10.6342/NTU202300991

A.5 The candidate covering materials

This section is about the candidates for the reflective material I have tested before deciding to choose seal tape as the reflective material of our LYSO sample. They include MgO, Teflon sheet, and Tyvek paper. The following are their reflectivity versus wavelength measured by Lambda 650 spectrometer (Fig. 4.14), which range from 650 nm to 250 nm with 5 nm per step.

MgO is in the form of a crucible, and its appearance is shown in the Fig. A.10. Fig. A.11 is the reflectivity of different parts of the MgO crucible, including bottom, long side, short side, and the cap of the crucible.

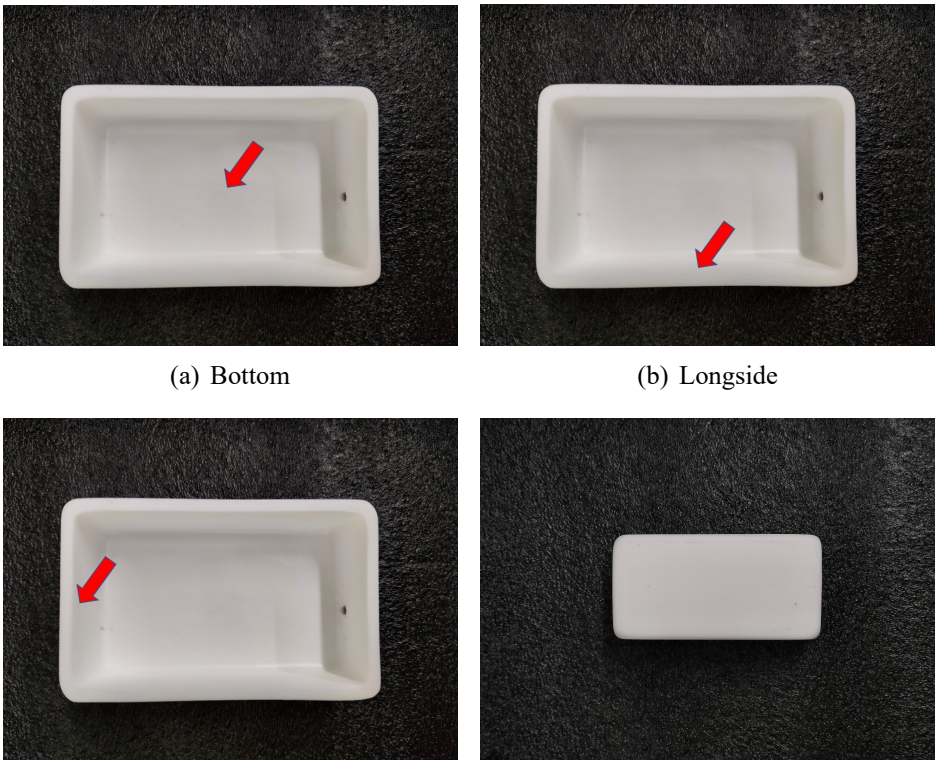

(a) Bottom (b) Longside

(c) Shortside (d) Cap

Figure A.10: The appearance of different parts of the MgO crucible

There are three kinds of thickness of Teflon sheet: 0.05 mm, 0.1 mm, and 0.3 mm.

doi:10.6342/NTU202300991

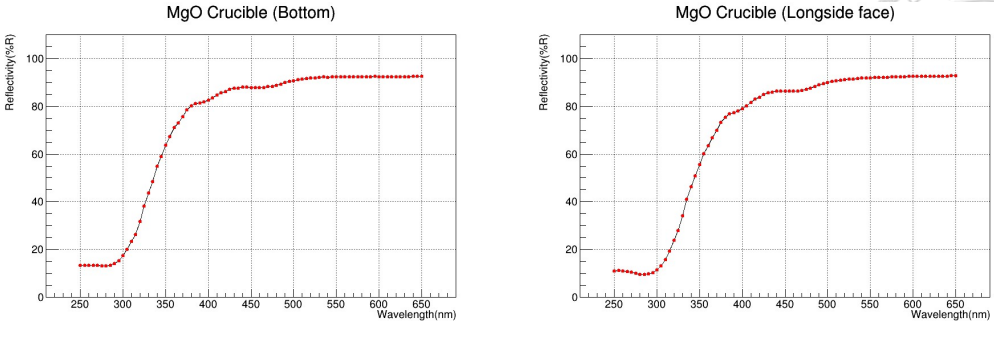

(a) Bottom

(b) Longside

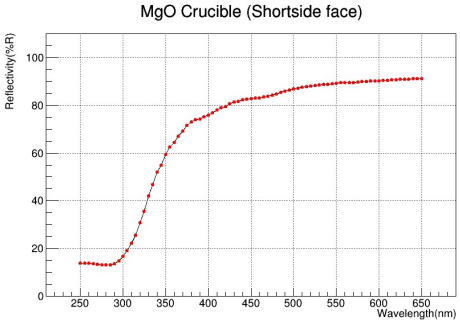

(c) Shortside

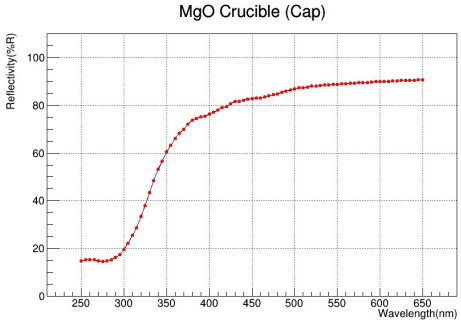

(d) Cap

Figure A.11: The reflectivity results of different parts of the MgO crucible.

The appearance of 0.1 mm is shown in Fig. A.12. The reflectivity results are shown in Fig. A.13. The reflectivity increase with thickness and decrease with wavelength, which conforms to the trend of Teflon mentioned in Ref. [11].

Figure A.12: The appearance of the 0.1 mm Teflon sheet.

The thickness of Tyvek paper is about 0.1 mm, and the appearance is shown in Fig. A.14. Fig. A.15 is the reflectivity one to three layers. The reflectivity of the three different layers of Tyvek paper is similar, which is in line with the thickness insensitivity mentioned

doi:10.6342/NTU202300991

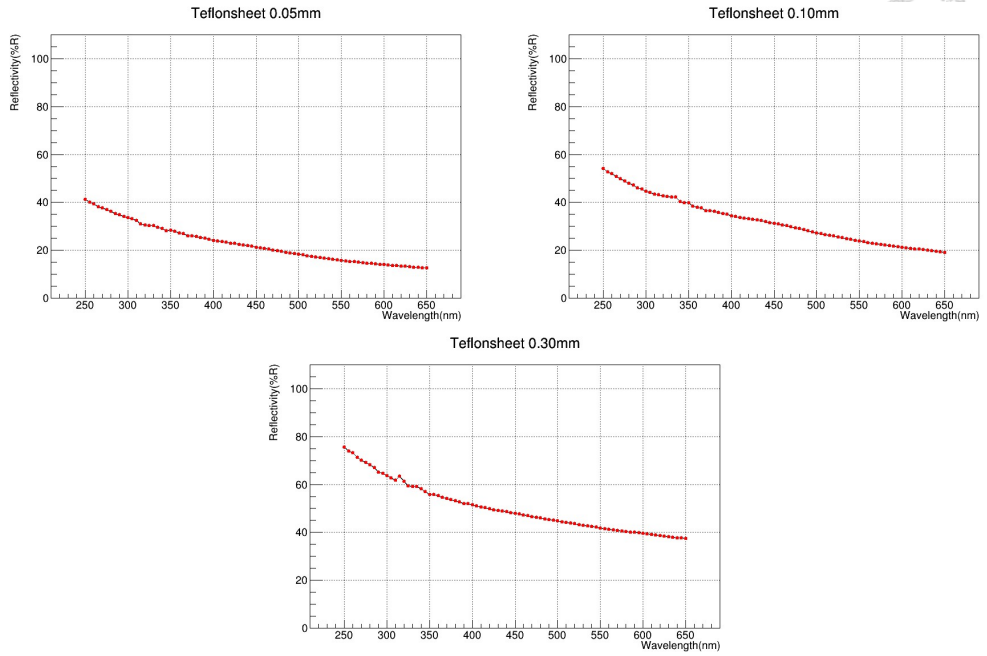

Figure A.13: The reflectivity results of different thickness of Teflon sheet.

in Ref. [11].

Figure A.14: The appearance of the Tyvekpaper.

The reflectivity results of seal tape have mentioned in Sec. 4.4.2 (Fig. 4.16). It can be seen that Tyvek paper has the highest reflectivity in the candidate covering materials at near 400 nm. However, there is no obvious advantage in the results of LYSO intrinsic spectrum (Fig. A.16), so in the end I still choose seal tape as the reflective material for wrapping the crystal.

doi:10.6342/NTU202300991

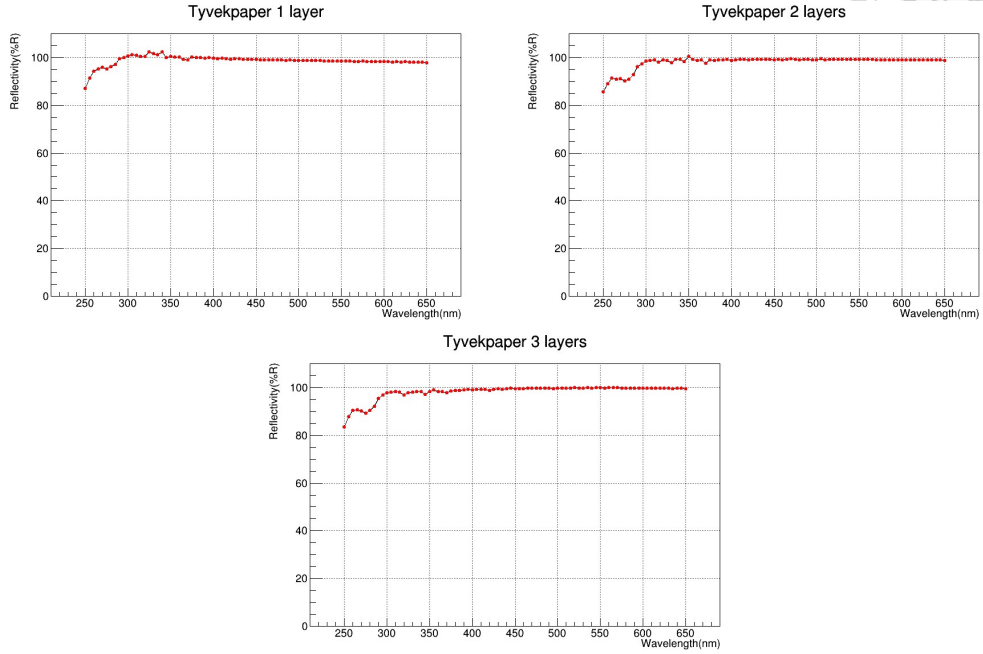

Figure A.15: The reflectivity results of different layers of Tyvekpaper.

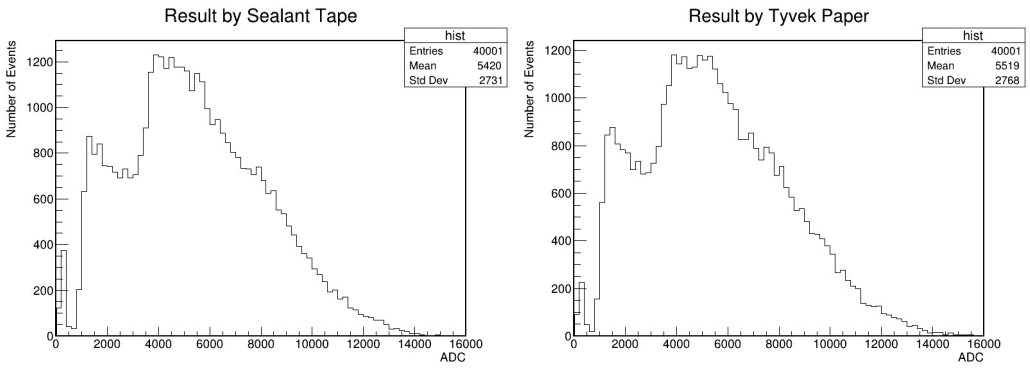

Figure A.16: The LYSO intrinsic spectrum of using seal tape (left figure) or Tyvek paper (right figure) under the same experimental conditions.

doi:10.6342/NTU202300991

A.6 The measurements about quantum efficiency and photocathode uniformity of PMT

The following is an introduction about evaluate the performance of the PMT system from Ref. [14]. I think its method is intuitive, but unfortunately, I do not have enough time and instruments to build the setup and complete these measurements currently.

There are two different methods to measure the quantum efficiency. One is measured with a reference photodetector, and the other one is direct measurement. In the relative measurement, we need to send both the unknown PMT and reference photodetector, then get quantum efficiency by

$$QE_{unknown} = QE_{ref} \cdot \frac{I_{unknown}}{I_{ref}} \tag{A.5}$$

, where $I_{unknown}$ and I_{ref} are the cathode current of the known PMT and reference photodetector respectively. Ref. [14] recommends using photodiode as a reference since it has high collection efficiency and good uniformity compared to PMT. In the direct measurement, we need a powermeter to directly calibrate the light intensity that illuminates the unknown PMT. Through radiant sensitivity

$$S = \frac{I_{unknown}}{I_{light}} \tag{A.6}$$

where I_{light} is the incident light intensity, the quantum efficiency will be

$$QE_{unknown} = \frac{S \cdot h \cdot c}{\lambda \cdot e} \tag{A.7}$$

, where h is Planck constant, λ is the wavelength of incident light, c is the light velocity

doi:10.6342/NTU202300991

in vacuum, and e is the electron charge. To make sure all photoelectrons emitted from the photocathode are collected, the current plateau must appear in the photocurrent versus voltage curve (Fig. A.17), and the corresponding current value should be used to the quantum efficiency calculation. Ref. [14] gives their measurements at 410 nm of three PMT by these two methods, and find their results are consistent with the other (Fig. A.18). To measure the quantum efficiency of different wavelengths, we need a monochromator which can send specific wavelength light in a wide range to cover the sensitivity region of unknown PMT.

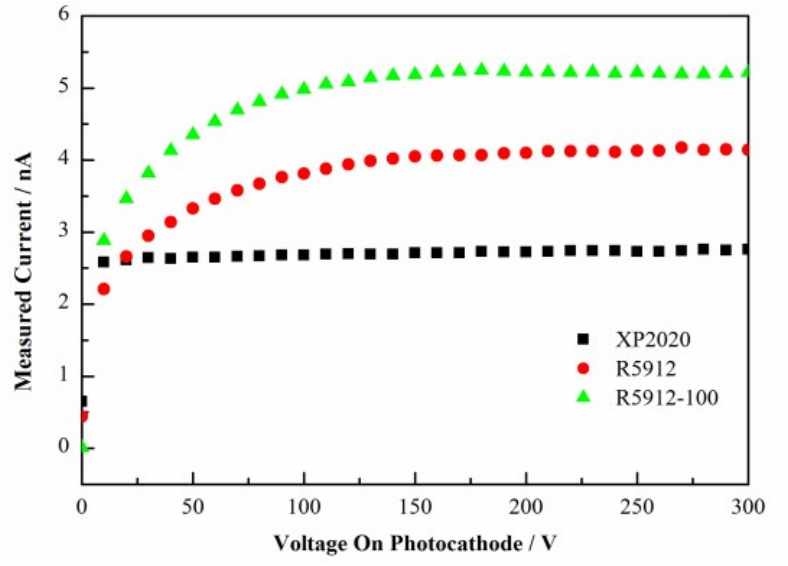

Figure A.17: Measured current versus voltage curves for different PMT models at 410 nm (from [14]).

Product Model	Relative QE / %	S / mA/W	Direct QE / %
Reference PD S2744	Reference value: 71.0	234.5	70.9
PMT XP2020	23.4	76.5	23.1
PMT R5912	24.7	82.1	24.8
PMT R5912-100	34.6	112.6	34.1

Figure A.18: Measured quantum efficiency at 410 nm by relative and direct methods (from [14]).

To measure the photocathode uniformity, we need to build a setup that light source

doi:10.6342/NTU202300991

can scan the complete PMT window, and Ref. [14] provides two kinds of solutions to the two types of PMT window respectively (Fig. A.19). Two-dimensional one is used for a plane window, which PMT is fixed on the support while the light source is installed on a movable platform. Three-dimensional one is used for a spherical window, in which light source is fixed on the support while the PMT is installed on a rotatable device around a horizontal or a vertical axle. This makes light source scanning along both the latitude and longitude of the PMT surface, and the distance to the PMT window will be a constant distance to avoid angular effect. This two kind of setups can obtain photocathode uniformity, that is the quantum efficiency of certain wavelengths to different positions of the PMT window. The position resolution will be determined by the light spot, and Fig. A.20 and Fig. A.21 are example of results from Ref. [14].

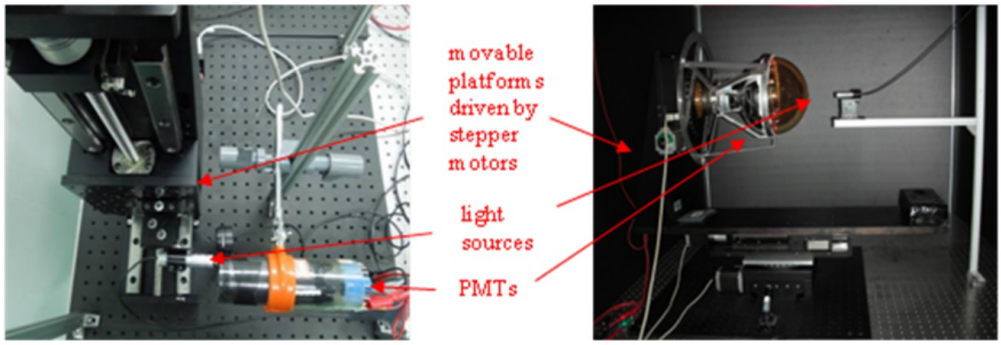

Figure A.19: The examples of photocathode uniformity setups for plane window (left) and spherical window (right) (from [14]).

In addition to quantum efficiency and photocathode uniformity, there are many factors for evaluating PMT system performance mentioned in Ref. [14] and the related literatures. Knowing more detailed PMT system performance can be more accurate in the calculation of light output, and even obtain more accurate weak light intensity when performing single photon measurements (Chap. 5) in the future.

doi:10.6342/NTU202300991

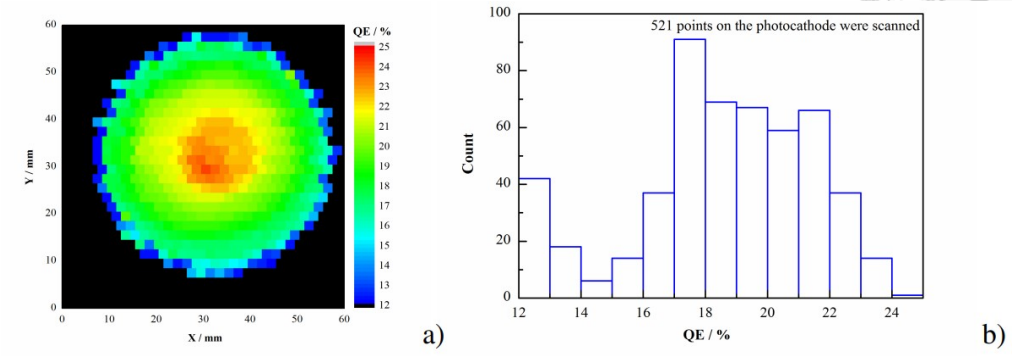

Figure A.20: Quantum efficiency of a PMT with plane window at 410 nm: a) the position distribution of *QE*, b) the statistic of *QE* of all measured points on the photocathode (from [14]).

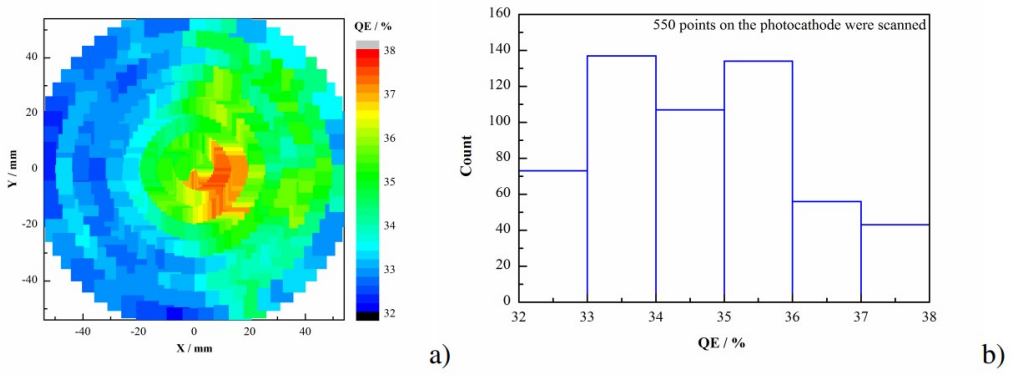

Figure A.21: Quantum efficiency of a PMT with spherical window at 410 nm: a) the position distribution of *QE* (projected onto the equatorial plane), b) the statistic of *QE* of all measured points on the photocathode (from [14]).

doi:10.6342/NTU202300991

Appendix A. Appendix

doi:10.6342/NTU202300991

Bibliography

[1] S.H. Byun. Chapter 4 scintillation detectors. https://www.science.mcmaster.ca/radgrad/images/6R06CourseResources/4R6Notes4_ScintillationDetectors.pdf.

[2] H Alva-Sánchez, A Zepeda-Barrios, V D Díaz-Martínez, T Murrieta-Rodríguez, A Martínez-Dávalos, and M Rodríguez-Villafuerte. Understanding the intrinsic radioactivity energy spectrum from 176lu in LYSO/LSO scintillation crystals. *Sci. Rep.*, 8(1):17310, November 2018.

[3] Glenn F Knoll. *Radiation Detection and Measurement*. John Wiley & Sons, Chichester, England, 4 edition, August 2010.

[4] D L Fried. Noise in photoemission current. *Appl. Opt.*, 4(1):79, January 1965.

[5] R Foord, R Jones, C J Oliver, and E R Pike. The use of photomultiplier tubes for photon counting. *Appl. Opt.*, 8(10):1975–1989, October 1969.

[6] E H Bellamy, G Bellettini, J Budagov, F Cervelli, I Chirikov-Zorin, M Incagli, D Lucchesi, C Pagliarone, S Tokar, and F Zetti. Absolute calibration and monitoring of a spectrometric channel using a photomultiplier. *Nucl. Instrum. Methods Phys. Res. A*, 339(3):468–476, February 1994.

doi:10.6342/NTU202300991

[7] Chig Pao Chang. The single photon measurement by using the front-end readout system of neutrino telescope. Master's thesis, National Taiwan University, 2011.

[8] Taiwan applied crystal. https://www.tacrystal.com/.

[9] The sodium-22 spectrum. https://www.ld-didactic.de/software/524221en/Content/Appendix/Na22.htm.

[10] R A Ramirez, Wai-Hoi Wong, Soonseok Kim, H Baghaei, Hongdi Li, Yu Wang, Yuxuan Zhang, Shitao Liu, and Jiguo Liu. A comparison of BGO, GSO, MLS, LGSO, LYSO and LSO scintillation materials for high-spatial-resolution animal PET detectors. In *IEEE Nuclear Science Symposium Conference Record, 2005*. IEEE, 2006.

[11] M Janecek. Reflectivity spectra for commonly used reflectors. *IEEE Trans. Nucl. Sci.*, 59(3):490–497, June 2012.

[12] J T M de Haas, P Dorenbos, and C W E van Eijk. Measuring the absolute light yield of scintillators. *Nucl. Instrum. Methods Phys. Res. A*, 537(1-2):97–100, January 2005.

[13] The scintillation wavelength of lyso. https://www.crystals.saint-gobain.com/sites/hps-mac3-cma-crystals/files/2021-08/LYSO-Material-Data-Sheet.pdf.

[14] J Xia, S Qian, W Wang, Z Ning, Y Cheng, Z Wang, X Li, M Qi, Y Heng, S Liu, and X Lei. A performance evaluation system for photomultiplier tubes. *J. Instrum.*, 10(03):P03023–P03023, March 2015.

doi:10.6342/NTU202300991

[15] Positron emission tomography. https://multimodalneuroimaging.wordpress.com/2015/04/28/c-positron-emission-tomography/.

[16] Sikandar Shaikh. *PET-CT in infection and inflammation*. Springer Nature, Cham, Switzerland, December 2020.

doi:10.6342/NTU202300991